



## Antineutrino Anomalies and Right-Handed Currents

CARL H. ALBRIGHT<sup>\*</sup> and ROBERT E. SHROCK  
Fermi National Accelerator Laboratory<sup>†</sup>, Batavia, Illinois 60510

### ABSTRACT

We analyze the predictions of several gauge theory models for inclusive charged-current (anti)neutrino reactions on isoscalar, proton, and neutron targets. In particular, we calculate  $y$ - and  $W$ -distributions, average  $y$ ,  $B$ -parameters, and cross section ratios. Gauge models incorporating right-handed quark transitions of the type  $u \rightarrow b$  and  $d \rightarrow x$  are considered, where the heavy quarks  $b$  and  $x$  have charges  $-1/3$  and  $-4/3$ , respectively. The effects of varying both the quark masses and the physical thresholds are examined. Experimental cuts and flux-averaging, where appropriate, are applied to the model predictions for the Fermilab counter and bubble chamber experiments. We find that with reasonable choices of parameters, five- or six-quark models with valence strength right-handed currents can fit most of the present experimental data to within one standard deviation accuracy.

---

<sup>\*</sup>Permanent address: Department of Physics, Northern Illinois University, DeKalb, Illinois 60115; work supported in part by National Science Foundation Grant No. PHY 75-05467.



## I. INTRODUCTION

There is currently evidence for new particle production in high energy deep inelastic charged-current neutrino reactions. The available high energy data come from the Harvard-Penn-Wisconsin-Fermilab<sup>1</sup> (HPWF) and Caltech-Fermilab<sup>2</sup> (CF) counter experiments and from several experiments using the 15' Fermilab bubble chamber. The latter include the Berkeley-Fermilab-Hawaii-Michigan<sup>3</sup> ( $\nu H_2$ ), Argonne-Carnegie Mellon<sup>4</sup> ( $\bar{\nu} H_2$ ), Wisconsin-Berkeley-CERN-Hawaii<sup>5</sup> ( $\nu(H_2 + Ne)$ ), Fermilab-IHEP-ITEP-Michigan<sup>6</sup> ( $\bar{\nu}(H_2 + Ne)$ ) and the Columbia-Brookhaven-Fermilab<sup>7</sup> ( $\nu(H_2 + Ne)$ ) groups. The evidence for new particle production lies in the observation of multilepton events and nonscaling behavior in the differential and total cross sections.

The HPWF collaboration<sup>1</sup> finds that as  $E$ , the (anti)neutrino energy increases beyond about 30 GeV,  $d^2\sigma^{\bar{\nu}N}/dx dy$  changes from the approximate  $(1-y)^2$  shape observed at low energy and acquires a flat component especially noticeable at high  $y$ . This effect is largely, but not exclusively, localized in the small  $x$  region,  $x \lesssim 0.15$ . Correspondingly,  $\langle y \rangle^{\bar{\nu}N}$  and  $R_{ch} = \sigma^{\bar{\nu}N}/\sigma^{\nu N}$  both increase substantially. Moreover, the distribution in invariant hadronic mass  $W$  for antineutrinos exhibits an enhancement at high  $W$ . The CF data<sup>2</sup> are consistent with HPWF on  $R_{ch}$  values. In both the HPWF and CF data,  $d\sigma^{\nu N}/dy$  is consistent with being roughly flat and  $\sigma^{\nu N}$  is observed to rise linearly with energy.<sup>1</sup> The Fermilab  $\nu H_2$  bubble chamber experiment confirms<sup>3</sup> these two results. However, the  $\bar{\nu} H_2$

experiment<sup>4</sup> and the most recent results of the  $\bar{\nu}(H_2 + Ne)$  experiment<sup>6</sup> do not show any pronounced anomalous  $y$  distributions.

In view of the variety of experiments bearing on the question of new particle production and the excitation of new quark transitions, we have undertaken a detailed comparison of the existing data, from both counter and bubble chamber groups, with the prediction of several types of gauge models. Specifically, we consider the standard Weinberg-Salam theory,<sup>8</sup> and three models with right-handed charged-current quark transitions including  $u \rightarrow b$  and  $d \rightarrow x$ , where  $x$  is a  $Q = -4/3$  charge quark. The effects of asymptotic freedom corrections at the energies of interest have been found in previous studies<sup>9</sup> to be small and are therefore neglected here. We have focussed on the question of whether, when one takes into account the cuts and detailed flux spectrum appropriate for each individual experiment, models with valence strength right-handed transitions can fit both the counter and bubble chamber data.<sup>10</sup>

Results are presented for the quantities  $d^2\sigma/dx dy$ ,  $d\sigma/dy$ ,  $d\sigma/dW$ ,  $\langle y \rangle$ ,  $B$ ,  $\sigma/E$ , and  $R_{ch} = \bar{\sigma}/\sigma^{\nu}$ . An analysis is made of the effects of various cuts on the theoretically calculated quantities cited above. We find that models with right-handed currents connecting valence quarks  $u$  or  $d$  with heavy quarks with charge  $-1/3$  and  $-4/3$ , respectively, are able to account for the anomalous  $y$  distribution and growth in  $\langle y \rangle$  and  $R$  observed in the HPWF experiment. The same models yield slightly flatter  $y$  distributions than are found in the  $\bar{\nu}H_2$  and  $\bar{\nu}(H_2 + Ne)$  experiments.

The outline of this paper is as follows. In Sec. II we discuss our choice of gauge models for which predictions are compared with the data. In Sec. III we describe the calculations and in particular the nature of slow rescaling as governed both by effective quark masses and physical hadronic thresholds. The results are presented in Sec. IV first with no cuts and then with cuts and flux-averaging appropriate to each experiment. Conclusions from our study are given in Sec. V.

## II. GAUGE MODELS

We shall consider several models of weak and electromagnetic interactions based on the gauge group  $SU(2) \times U(1)$ . It would be out of place to discuss these models in detail here; for this purpose we refer the reader to the original papers. The  $\nu_\mu - \mu$  coupling is the same in all of these models. As regards the quarks, we shall restrict ourselves to models which have only doublet and singlet quark multiplets. Table I shows the doublet structure of the models studied here.

The first and simplest model considered is that of Weinberg and Salam,<sup>8</sup> with the necessary GIM mechanism<sup>11</sup> to suppress strangeness-changing neutral currents. As is well known, in this model there are four flavors of (three-colored) quarks arranged in two left-handed doublets (and four right-handed singlets). The notation used in Table I is standard:

$$d_{\theta} = d \cos \theta_C + s \sin \theta_C \quad (2.1)$$

$$s_{\theta} = -d \sin \theta_C + s \cos \theta_C$$

where  $\theta_C$  is the Cabibbo angle.

The other models considered all involve valence-strength transitions between right-handed quarks. Since the u and d contributions are dominant, in order to classify the models it is convenient to adopt the labeling<sup>12</sup>  $(2(I_3)_{u_R}, 2(I_3)_{d_R})_N$  where  $(I_3)_{u_R}$  and  $(I_3)_{d_R}$  are the third components of weak isospin for the right-handed up and down quarks respectively, and N denotes the total number of quark flavors. Inasmuch as we are trying to account for an anomaly in antineutrino scattering, we select models which have transitions from an up or down quark to a heavy quark with charge one unit lower. The minimal models of this type<sup>13</sup> are  $(1, 0)_5$  and  $(0, 1)_5$  which involve single right-handed doublets,  $(u_{\phi}, b)_{\mathbf{R}}$  and  $(d_{\phi}, x)_{\mathbf{R}}$ , respectively, where we have allowed mixing between singlets and doublets, i. e. the quarks appearing in the doublets are

$$u_{\phi} = u \cos \phi + c \sin \phi \quad (2.2)$$

and

$$d_{\phi} = d \cos \phi + s \sin \phi$$

in the two different models. (Of course the angle  $\phi$  is in general different for different models.) We shall study the effects of a  $u_{\mathbf{R}} \rightarrow b_{\mathbf{R}}$  quark transition in isolation and present some results for the  $(1, 0)_5$  model.

Six-quark models with two right-handed doublets have been discussed by a number of authors.<sup>14</sup> For definiteness and continuity with our earlier work, we choose to consider the (B) version of the Gürsey-Sikivie  $E_7$  model, which is of the  $(1, 0)_6$  type. The two right-handed doublets are shown in Table I, with the notation

$$\begin{aligned} b_\phi &= b \cos \phi + b' \sin \phi \\ b_{\phi'} &= -b \sin \phi + b' \cos \phi \end{aligned} \quad (2.3)$$

For reference, another  $(1, 0)_6$  model<sup>15</sup> contains the heavy  $b$  and  $b'$  quarks entirely in doublets according to  $(u, b_\phi)_R$  and  $(c, b'_{\phi'})_R$ . This model yields essentially the same predictions as the  $E_7$  model above, differing only by the (small)  $SU(3)$ -symmetric sea contribution arising from the  $s \rightarrow c$  transitions in the latter model.

Whereas the  $(1, 0)_5$  and  $(1, 0)_6$  models discussed above single out the  $(u \rightarrow b)_R$  transition as the source of the  $\nu$ -anomaly, it is also of interest to consider a model of the  $(0, 1)_6$  type which contains the right-handed doublets  $(d_\phi, x)_R$  and  $(s_\phi, y)_R$  as shown in Table I. This model incorporates two "exotic" quarks  $x$  and  $y$  of charge  $-4/3$ . Compared to the  $(1, 0)_6$  model based on  $E_7$ , this model gives very similar predictions for isoscalar targets; however, its predictions for proton or neutron targets are quite different. These differences will be analyzed in some detail in Sec. IV.

Neither the  $(1, 0)_5$  nor the  $(1, 0)_6$  models have a weak neutral current which naturally conserves all quark flavors. At the present time it is

not known definitely whether the neutral current is diagonal in  $Q = 2/3$  quark flavors; however, as is well known, the smallness of strangeness-changing neutral current processes requires it to be diagonal in s and d flavors to the level  $G_F \propto (m_c/m_w)^2$ . As discussed by Glashow and Weinberg,<sup>16</sup> the necessary and sufficient conditions for the GIM mechanism to be natural is that quarks of the same charge and chirality (a) have the same value of weak  $\vec{T}^2$  and  $I_3$  and (b) receive their masses either from a gauge-invariant bare mass term or from their couplings to a single neutral Higgs field (but not both). The exotic model of type  $(0, 1)_6$  cited above does satisfy these criteria.<sup>17</sup>

The four gauge models considered by us, namely the Weinberg-Salam model, the simple  $(1, 0)_5$  model, the  $(1, 0)_6$  model based on  $E_7$  and the  $(0, 1)_6$  model with charge  $-4/3$  heavy quarks, are all in reasonable accord with the neutral-current data on the inclusive reactions, the elastic  $\nu + p \rightarrow \nu + p$  and  $\bar{\nu} + p \rightarrow \bar{\nu} + p$  scatterings, and the purely leptonic reactions  $\bar{\nu}_e + e^- \rightarrow \bar{\nu}_e + e^-$ ,  $\nu_\mu + e^- \rightarrow \nu_\mu + e^-$  and  $\bar{\nu}_\mu + e^- \rightarrow \bar{\nu}_\mu + e^-$  given the presently limited statistics on the two-body reactions.<sup>18, 19</sup> None of these models fares well with the parity-violation results observed in atomic physics experiments on  $\text{Bi}_{83}^{126}$ , but these results are not yet decisive.<sup>20</sup> Since gauge models of the type  $(1, -1)_6$  with three sets of left-handed and right-handed doublets have pure vector neutral currents and are already ruled out by the inclusive and elastic reactions, we do not consider them here.<sup>21</sup>

## III. CALCULATIONS

The neutrino reactions to be considered are

$$\nu(\bar{\nu}) + T \rightarrow \mu^{\mp} + X \quad (3.1)$$

where  $T = N, p, n$  for isoscalar, proton, or neutron targets, respectively. For reference, to a good approximation, the HPWF and CF experiments<sup>1,2</sup> and heavy neon bubble chamber experiments<sup>7</sup> use isoscalar targets, the BFHM and ACM experiments<sup>3,4</sup> have a hydrogen target, and the WBCH and FIIM experiments<sup>5,6</sup> have a light neon-hydrogen mixture,<sup>22</sup> with  $p/n = 1.4$ .

The differential cross section for the reaction of Eq. (3.1) with  $T = N$  can be written

$$\frac{d^2\sigma(\nu, \bar{\nu})N}{dx dy} = \frac{G^2 ME}{\pi} \left[ xy^2 F_1(\nu, \bar{\nu})N + (1-y)F_2(\nu, \bar{\nu})N \right. \\ \left. \mp y(1 - \frac{y}{2})xF_3(\nu, \bar{\nu})N \right] \quad (3.2)$$

where  $x = Q^2/(2M\nu)$  and  $y = \nu/E$  are the usual scaling variables,  $q^2 = -Q^2$  is the momentum transfer squared,  $E(E')$  is the energy of the incident (scattered) lepton, and  $\nu = E - E'$  is the energy transfer in the lab frame. The same equation applies, with appropriate changes in the  $F_i$ , for the  $p$  and  $n$  reactions. At intermediate energies the structure functions  $F_i$  are observed to scale approximately, that is, to depend only on  $x$  rather

than  $Q^2$  and  $\nu$  separately. In the parton model this behavior is predicted as a result of the fact that the current scatters elastically off free quarks with negligible masses.

A field theoretic analysis of deep inelastic inclusive lepton production in quantum chromodynamics also predicts approximate Bjorken scaling, with scaling deviations of the form<sup>23</sup>

$$\int_0^1 F_i(x, Q^2) x^n dx \propto (\log Q^2)^{-a_n^{(i)}}, \quad i = 1, 2, 3 \quad (3.3)$$

where the  $a_n^{(i)}$  are calculable constants. The effect of these asymptotic freedom scaling deviations is to reduce the effective parity violation in  $\nu(\bar{\nu})$  scattering, since

$$\lim_{Q^2 \rightarrow \infty} \int_0^1 x F_3(x, Q^2) dx = 0 \quad (3.4a)$$

whereas

$$\lim_{Q^2 \rightarrow \infty} 2 \int_0^1 x F_1(x, Q^2) dx = \lim_{Q^2 \rightarrow \infty} \int_0^1 F_2(x, Q^2) dx \sim \text{const} . \quad (3.4b)$$

In terms of the  $y$ -distribution this implies that

$$\lim_{Q^2 \rightarrow \infty} \frac{d\sigma^{\nu N}}{dy} = \lim_{Q^2 \rightarrow \infty} \frac{d\sigma^{\bar{\nu} N}}{dy} \propto 1 + (1 - y)^2 . \quad (3.5)$$

Thus, asymptotic freedom corrections to Bjorken scaling will contribute to a rise in  $d\sigma^{\bar{\nu}}/dy$  at high  $y$  and a consequent increase in  $\langle y \rangle^{\bar{\nu}}$ . However, this effect has been studied<sup>9</sup> and has been found to be rather small at the accelerator energies presently available. In the analysis of Zee, Wilczek, and Treiman in ref. 9, for example, a Mellin inversion of the moment integrals was used to determine the structure functions. These were then integrated over  $x$  to obtain  $y$  distributions. A scaling fit assuming purely  $V-A$  currents was taken to be  $(\pi/G^2ME)d\sigma_o^{\bar{\nu}N}/dy = 0.5(1-y)^2$ . It was found that at  $E = 200 M \approx 188$  GeV,

$$\left(\frac{\pi}{G^2ME}\right)\left(\frac{d\sigma^{\bar{\nu}N}}{dy} - \frac{d\sigma_o^{\bar{\nu}N}}{dy}\right)\Bigg|_{y=0.9} \approx 0.06\left(\frac{\pi}{G^2ME}\right)\frac{d\sigma_o}{dy}\Bigg|_{y=0}. \quad (3.6)$$

For lower energies the effect is commensurately smaller (since it depends on  $Q^2$  and  $\langle Q^2 \rangle \sim E$ ). Given these results, we believe that it is reasonable to concentrate on a careful analysis of the effects of right-handed currents alone, without asymptotic freedom corrections.

When heavy quarks are produced in the reaction  $q_i + W^\pm \rightarrow q_j$  the dependence of the structure functions on the kinematic variables is not as simple as the Bjorken scaling form.<sup>24</sup> Let us note first that we shall consider only transitions from light to heavy quarks. This is a reasonable approximation since the content of heavy quarks in the nucleon, as measured by their quark distribution functions, is considerably smaller than that of the light quarks, in particular the valence quarks. This statement is,

of course, dependent upon the value of  $Q^2$  and the mass of the heavy quark considered; as  $Q^2 \rightarrow \infty$  only the flavor singlet part of the structure functions will contribute, so that the corresponding parton distributions will be SU(N)-symmetric, where N is the number of quark flavors. Clearly the approach to flavor symmetry is more rapid, the smaller the difference between the heavy quark and light quark masses.

An analysis<sup>24</sup> of the quark mass corrections to Bjorken scaling shows that much of the nonscaling behavior can be summarized in the form of an effective scaling variable

$$\xi_j \approx x + m_j^2 / (2MEy) \quad (3.7)$$

where  $m_j$  is the effective mass of the heavy quark. Since quarks presumably do not exist as physical states the quark mass cannot be defined in the usual way as the pole of the renormalized propagator. For our purposes we shall regard  $m_j$  as a phenomenological constant. Thus the parton distributions which enter in the differential cross section would be  $u_i(\xi_j)$  (and similarly for antiquarks). The actual effective scaling variable proposed in ref. 24 also involves the Nachtmann factor representing nucleon mass corrections to scaling, namely

$$\frac{2}{1 + (1 + Q^2/\nu^2)^{\frac{1}{2}}} \quad (3.8)$$

which would multiply the right-hand side of Eq. (3.7). However, this factor is close to unity for the region of large  $W$  (and hence, in general, large  $\nu$  and small  $Q^2$ ) where new particle production associated with the excitation of right-handed currents is important. For example, for  $E = 50$  GeV,  $x = 0.25$ , and  $y = 0.7$ , the factor is equal to 0.997. For this reason, and because we are primarily interested in the effects due to heavy quark thresholds rather than small nucleon mass corrections, we shall approximate the additional factor in Eq. (3.8) by unity.<sup>25</sup>

The physical region for a reaction involving heavy quark production is restricted by the condition that the invariant hadronic mass  $W$  satisfy  $W > W_j$  where  $W_j$  is the threshold value for the production of hadrons containing the heavy quark of flavor  $j$ . This constraint also affects the range of the variable  $\xi_j$ . The minimum value of  $\xi_j$  is easily determined to be

$$(\xi_j)_{\min} = \xi_j(x = 0, y = 1) = \frac{m_j^2}{2ME} \quad (3.9)$$

In order to determine the maximum value, one re-expresses  $\xi$  as a function of  $x$  and  $W$  or  $y$  and  $W$ :

$$\xi_j(x, W) = x + \frac{m_j^2}{W^2 - M^2} (1 - x) \quad (3.10a)$$

$$\xi_j(y, W) = 1 - \frac{W_j^2 - M^2 - m_j^2}{2MEy} \quad (3.10b)$$

Then, (assuming  $W_j^2 - M^2 - m_j^2 > 0$ ),

$$(\xi_j)_{\max} = 1 - \frac{W_j^2 - M^2 - m_j^2}{2ME} \quad (3.11)$$

There is a question here of how to relate  $W_j$  and  $m_j$ . We shall for the most part take

$$W_j \approx m_j + 1 \text{ GeV} \quad (3.12a)$$

which is a reasonable approximation to the mass of a heavy baryon of flavor  $j$  (except for the charmed quark, where we take  $W_c = 2.25$ ,  $m_c = 1.5$  GeV) or a final state consisting of a nucleon and heavy meson of flavor  $j$ . One could, alternatively, take the point of view that since  $m_j$  is simply a phenomenological constant one can define it so that  $(\xi_j)_{\max} = 1$ , i. e.

$$W_j = (m_j^2 + M^2)^{\frac{1}{2}} \quad (3.12b)$$

This choice does, however, have the effect of making the threshold mass quite close to the heavy quark mass if the latter is large compared to  $M$ . For example, for  $m_b = 5$  GeV, the lightest  $b$ -baryon mass is determined to be  $M_b \lesssim W_b = 5.1$  GeV.

The physical region for several different variables is shown in Fig. 1. Figs. 1(a) and 1(b) are familiar plots of the physical region in  $Q^2$  and  $\nu$ , and  $x$  and  $y$ , respectively, showing curves of constant  $W$ . The total range of  $\xi$  as a function of energy  $E$  is shown in Fig. 1(c) for both choices (3.12) of the  $m_j - W_j$  relation and three choices of  $W_j$ . Specifically,  $\alpha$ ,  $\beta$ , and  $\gamma$  denote  $W_j = 2.25, 5$  and  $7$  GeV, respectively, with the solid curves referring to  $m_j = 1.5, 4$  and  $6$  GeV and the dotted curves referring to  $m_j \approx 2.0, 4.9$  and  $6.9$  GeV. Figs. 1(d), 1(e), and 1(f) show, for  $E = 30$  GeV, the allowed range in  $\xi$  as a function of  $y$ ,  $x$ , and  $W/\sqrt{s}$ . The maximal ranges (at fixed  $E$ ) for  $\xi(y, E)$  and  $\xi(x, E)$  are reached with  $y = 1$  and  $x = 0$  respectively; for  $\xi(y = 1, E)$ , the range is equal to the total range shown in Fig. 1(c) (at  $E = 30$  GeV).

Several important kinematical features of heavy quark production are evident in these graphs. First, since the physical range of  $\xi_j$  for a given transition  $q_i(\text{light}) \rightarrow q_j(\text{heavy})$  starts at zero at the threshold beam energy  $E_{\text{Th}}$  and gradually increases, only asymptotically approaching the range  $0 < \xi_j < 1$ , the effects of this new transition on the differential and total cross section,  $\langle y \rangle^{\bar{\nu}}$ , etc. set in slowly. Thus there is gradual rescaling above heavy quark (hadron) thresholds. Secondly, the traditional view, that an effect which occurs at small  $x$  is due to sea quarks is wrong when heavy quarks (new flavors) are produced. In this case, although it is preferable, especially for  $E$  only slightly above  $E_{\text{Th}}$ , for  $x$  to be small in order to maximize  $W$ , the true momentum fraction  $\xi_j$  of the initial

quarks which can undergo the transition  $q_i(\text{light}) \rightarrow q_j(\text{heavy})$  is of valence magnitude. Since the momentum distributions of sea quarks decrease more rapidly for large  $x$  than those of valence quarks, the latter are thus more effective at producing heavy quarks. In passing, note that this would be true even if the integrals of the sea and valence quark distributions were equal; it is a statement about the local  $x$  distribution. Of course, the fact that the total momentum carried by the valence quarks is much greater than that carried by the sea quarks also renders the former more important in heavy quark production.

With the choice of the  $m_j - W_j$  connection in Eq. (3.12a) the transition first takes place at a moderately large value of  $\xi$ , viz.  $\xi_j = m_j^2 / (2ME_{\text{Th},j})$  where  $2ME_{\text{Th},j} + M^2 = W_j^2$ ; for example, for  $W_j = 5$  GeV,  $m_j = 4$  GeV, this initial value of  $\xi$  is  $\sim 0.66$ . If one chooses the  $m_j - W_j$  relation in Eq. (3.12b) the transition starts by construction, at  $\xi = 1$ . Consequently, as  $E$  increases above  $E_{\text{Th}}$  the strength of the transition will depend on the  $\xi \rightarrow 1$  behavior of  $u_i(\xi_j)$ , determined by the Drell-Yan-West relation<sup>26</sup> to be  $\sim (1 - \xi_j)^3$  or  $4$ . One uses here the fact that the parton distribution is the same function of  $\xi_j$  for a heavy  $j$  quark as it is for a light  $j$  quark.

In the case of heavy quark production the Callan-Gross relation<sup>27</sup> for the structure functions representing the individual quark transition  $q_i \rightarrow q_j$  (or  $\bar{q}_i \rightarrow \bar{q}_j$ ) is

$$F_2^{(i \rightarrow j)}(\xi_j) = 2\xi_j F_1^{(i \rightarrow j)}(\xi_j) \quad . \quad (3.13)$$

Similarly, the relation between  $F_2$  and  $F_3$  is

$$-\xi_j F_3^{(i \rightarrow j)}(\xi_j) = B_{ij} F_2^{(i \rightarrow j)}(\xi_j) \quad (3.14)$$

where

$$B_{ij} = \begin{cases} +1 & \text{for } (q_i)_L \rightarrow (q_j)_L \\ & \text{or } (\bar{q}_i)_R \rightarrow (\bar{q}_j)_R \\ -1 & \text{for } (q_i)_R \rightarrow (q_j)_R \\ & \text{or } (\bar{q}_i)_L \rightarrow (\bar{q}_j)_L \end{cases} \quad (3.15)$$

That is,  $B_{ij} = +1$  for negative helicity quarks and  $-1$  for positive helicity quarks. Thus the contribution to the differential cross section of the light to heavy quark transition  $q_i \rightarrow q_j$  is

$$\frac{d^2 \sigma^{\nu, \bar{\nu}}}{dx dy} (i \rightarrow j) = \frac{G^2 M E}{\pi} \left[ \left( 1 - y + \frac{xy^2}{2\xi_j} \right) \pm \frac{x}{\xi_j} y \left( 1 - \frac{y}{2} \right) B_{ij} \right] F_2^{(i \rightarrow j)}(\xi_j) \times \theta(W - W_j) \quad (3.16)$$

where

$$F_2^{(i \rightarrow j)}(\xi_j) = 2 \xi_j u_i(\xi_j) \quad (3.17)$$

with  $u_i(\xi_j)$  the parton probability distribution function for a quark of flavor  $i$  to have momentum  $\xi_j$ . The total cross section is obtained in the usual

way by assuming incoherent scattering and hence additivity of individual quark cross sections.

The parton distributions used in our calculations incorporate the usual valence-sea separation, with an SU(3) symmetric sea:

$$\begin{aligned}
 u(\xi) &= u_v(\xi) + \eta(\xi) \\
 d(\xi) &= d_v(\xi) + \eta(\xi) \\
 \bar{u}(\xi) &= \bar{d}(\xi) = s(\xi) = \bar{s}(\xi) = \eta(\xi) \quad .
 \end{aligned}
 \tag{3.16}$$

We have used a parton parametrization due to Field<sup>28</sup> which includes a sea distribution  $\eta(\xi) \sim \xi^{-1}(1-\xi)^7$  and gives a good fit to SLAC electroproduction data and low energy ( $E < 30$  GeV) neutrino data. The sea content, defined here as

$$\frac{\int_0^1 2\xi\eta(\xi)d\xi}{\int_0^1 \xi[u(\xi) + d(\xi)]d\xi}$$

is 6.5%. At low energy the Field parton parametrization yields  $\langle y \rangle^{\nu N} = 0.50$ ,  $\langle y \rangle^{\bar{\nu} N} = 0.30$ ,  $\langle x \rangle^{\nu N} = 0.26$ ,  $\langle x \rangle^{\bar{\nu} N} = 0.24$ ,  $\langle Q^2/E \rangle^{\nu N} = 0.24$  GeV,  $\langle Q^2/E \rangle^{\bar{\nu} N} = 0.12$  GeV, and  $\sigma^{\bar{\nu} N}/\sigma^{\nu N} = 0.40$ . For comparison we have also used the Pakvasa-Parashar-Tuan (PPT)<sup>29</sup> parametrization, which has a sea quark distribution characterized by a less rapid decrease with  $\xi$ :  $\eta(\xi) = 0.1 \xi^{-1}(1-\xi)^{3.5}$ . This gives a sea content of 10%. The u and d quark distributions are quite similar in both of these parametrizations.

The effects which we observe in the models with right-handed valence transitions are thus not sensitively dependent upon the differences between the Field and PPT parton parametrizations. The small contributions of heavy quark production off sea quarks are somewhat enhanced in the PPT parametrization.

#### IV. RESULTS

##### A. Without Experimental Cuts

In order to illustrate the general predictions of the gauge models considered, let us first present results without imposing any experimental cuts. We shall consider here the W-S,  $(1, 0)_5$ , and G-S(B)  $(1, 0)_6$  models, for the case of an isoscalar target. As will be apparent later, the cuts significantly affect the theoretical fits to the data.

It is necessary to choose the physical thresholds,  $W_j$ , then use one of the connection formulas, Eqs. (3.12a, b), to determine the effective quark masses  $m_j$ , and finally choose the value of the mixing angle in models where such an angle appears. In order to determine the  $W_j$  threshold values one would ideally identify from the experimentally measured hadronic invariant mass distribution,  $d\sigma/dW$ , the contributions of the lowest exclusive channels. However, the higher the quark mass is, the more closely spaced will the exclusive channels occur in a given region of  $W$  above thresholds. Furthermore, experimental resolution-smearing and statistical fluctuations lead to somewhat ambiguous interpretations of the  $W$  distribution.

Alternatively, of course, one may choose a connection formula relating  $m_j$  and  $W_j$  and then select  $(m_j, W_j)$  pairs which yield the best fits to the experimental data on  $d\sigma/dy$ ,  $\langle y \rangle$ ,  $B$ ,  $R_{ch}$ , etc. In the case of the charmed quark we use  $e^+e^-$  data on the  $\psi$  and  $\psi'$  to infer that  $m_c \approx 1.5$  GeV. The hadronic threshold is actually slightly different for incident neutrinos than for antineutrinos, since only the former can produce a charmed baryon:<sup>30</sup>  $W_c^\nu \approx m_{C_0} \approx 2.25$  GeV, while  $W_c^{\bar{\nu}} = (m_N + m_D) \approx 2.8$  GeV. For our calculations we shall neglect this small difference and take the lower value of  $W_c$ . Thus for the present discussion, we have selected the values (in units of GeV)

$$\begin{aligned} W_c &= 2.25 \\ W_b &= 5.0 \\ W_{b'} &= 7.0 \end{aligned} \quad (4.1)$$

and for the  $m_j$ , the two sets

$$\begin{aligned} m_c &= 1.5 \\ m_b &= 4.0 \\ m_{b'} &= 6.0 \end{aligned} \quad (4.2a)$$

corresponding to Eq. (3.12a) and

$$\begin{aligned}
 m_c &= 2.0 \\
 m_b &= 4.9 \\
 m_{b'} &= 6.9
 \end{aligned}
 \tag{4.2b}$$

corresponding to Eq. (3.12b). For ease in referring to these values in the Figures, we call Eqs. (4.1) and (4.2a) the (A) set of parameters and Eqs. (4.1) and (4.2b) the (B) set of parameters. Note that, as was mentioned before, the connection equation (3.12b) leads to heavy quark masses which are not much smaller than the corresponding invariant mass thresholds. Hence with this choice one gets an unrealistically large value for the effective charmed quark mass.

In Figs. 2 and 3 we present curves for  $d\sigma/dy(\nu(\bar{\nu}) + N \rightarrow \mu \mp + X)$  for (a)  $0 \leq x \leq 0.1$ , i. e.  $\int_0^{0.1} (d^2\sigma/dx dy) dx$ , and (b) all  $x$ , at  $E = 30$  GeV and  $E = 100$  GeV. The solid and dashed curves are the predictions of the G-S(B) model, with  $\cos^2 \phi = 0.5$  and quark masses (4.2a) and (4.2b), respectively. The dot-dashed curve in Fig. 3 is for the W-S model with  $m_c = 1.5$  GeV. In order to show better the effect of new quark transitions, we have normalized the differential cross sections by dividing by the cross section  $\sigma^{\nu N}$  arising from light quark transitions ( $d \rightarrow u$ ,  $s \rightarrow u$ ,  $\bar{u} \rightarrow \bar{d}$ ,  $\bar{u} \rightarrow \bar{s}$ ).

Let us first consider the antineutrino curves for the W-S model. In the valence quark model with purely left-handed currents  $d\sigma^{\bar{\nu}N}/dy \propto (1-y)^2$ . There is, in addition, at all energies a small flat component resulting

from the  $\bar{d} \rightarrow \bar{u}$  and  $\bar{s} \rightarrow \bar{u}$  transitions. The latter of these is negligible since it not only occurs off sea quarks but is also suppressed by the factor  $\sin^2 \theta_C$ . As  $E$  passes the threshold for charmed quark and charmed hadron production, the  $\bar{s} \rightarrow \bar{c}$  and negligible  $\bar{d} \rightarrow \bar{c}$  transitions occur, again giving a flat contribution to  $d\sigma^{\bar{\nu}N}/dy$ . The W-S model curves at  $E = 30$  GeV are very close to the dashed curves in Fig. 2; for clarity we have omitted them. The effect of the charmed quark production is more noticeable at small  $x$  since it involves sea quarks. Given the values of  $m_c \simeq 1.5$  GeV and  $W_c \simeq 2.25$  GeV this effect has already set in before  $E = 30$  GeV and does not increase very much between  $E = 30$  and 100 GeV. Because such a sea effect is rather small,  $d\sigma^{\bar{\nu}N}/dy$  retains an approximate  $(1 - y)^2$  form.

The behavior of  $d\sigma^{\bar{\nu}N}/dy$  is quite different in the G-S(B)  $(1, 0)_6$  model because of the onset of the  $u \rightarrow b$  and  $b' \rightarrow u$  quark transitions. These transitions occur off valence quarks and, neglecting small contributions due to sea quarks, for  $E$  far above threshold, they change  $d\sigma^{\bar{\nu}N}/dy$  from  $\propto (1 - y)^2$  to  $\propto [1 + (1 - y)^2]$ . In the naive valence quark model,  $\langle y \rangle^{\bar{\nu}N}$  would thus change from  $1/4$  to  $7/16$  and  $\sigma^{\bar{\nu}N}/E$  would increase by a factor of four, the  $V + A$  term contributing three times as strongly as the  $V - A$  term. Although the  $V + A$   $u \rightarrow b$  transition occurs off a valence quark, at energies not asymptotically far above threshold, it contributes mainly at small  $x$ , for the reason given above. Stated differently, the fact that the flattening of  $d\sigma^{\bar{\nu}N}/dy$  requires valence strength right-handed currents

and the fact that it occurs most strongly at small  $x$  do not together constitute a paradox. Although  $x$  is forced to be small, the real quark momentum fraction  $\xi$  is not small; indeed  $\xi_b > m_b^2 / 2MEy$ . For example, with  $m_b = 4$  GeV,  $E = 40$  GeV, and  $y = 0.6$ , one finds  $\xi_b > 0.35$ .

The striking effect of the excitation of right-handed currents is evident from a comparison of Figs. 2 and 3. In the plot of  $d\sigma^{\bar{\nu}N}/dy$  ( $x < 0.1$ ,  $E = 100$  GeV) one can easily observe a strong shoulder structure which reflects the  $\theta(W - W_j)$  factor in the differential cross section. As one would expect, the flattening of the  $y$  distribution is especially pronounced in the small  $x$  region, and is greater for the smaller choice (3.12a) of quark masses, since these masses control the rapidity of rescaling above heavy quark thresholds. As  $y \rightarrow 0$ ,  $W \rightarrow m_N$  and all heavy quark production is eliminated. Consequently, as is clear from Figs. 2 and 3, approximate charge symmetry holds at  $y = 0$ , the departures being due to nonzero Cabibbo angle and the resultant  $u \leftrightarrow s$   $\Delta I = 1/2$  transitions.

In both the W-S and G-S(B) models  $d\sigma^{\bar{\nu}N}/dy$  is roughly flat. This is a result of the fact that in neither model is there a valence strength right-handed transition which can be excited by neutrinos, such as  $d_R \rightarrow t_R$ . Even if there were such a transition, it would suffer a factor of three suppression relative to the  $d_L \rightarrow u_L$  contributions. In the former model, at low energies there is a small  $(1 - y)^2$  component arising from the  $\bar{u} \rightarrow \bar{d}$  (and negligible  $\bar{u} \rightarrow \bar{s}$ ) transitions. When charm threshold is passed

an additional flat component is added by the  $s \rightarrow c$  and  $d \rightarrow c$  transitions; both of these contributions are small, the former because it is a sea effect and the latter because it is suppressed by the Cabibbo factor  $\sin^2 \theta_C$ . In the G-S(B) model the same comments apply for the left-handed quark sector, but the right-handed  $s \rightarrow c$  transition makes a further  $(1 - y)^2$  contribution to the  $y$  distribution, as illustrated by the  $\nu$  curve in Figs. 2 and 3. Again, the associated shoulder can be seen to move in toward lower  $y$  as  $E$  increases from 30 to 100 GeV.

We have divided the  $y$ -distribution into two bins in  $x$ , viz.  $x < 0.1$  and  $0 \leq x \leq 1$ , because these correspond roughly to the divisions made by the experimentalists.<sup>1,6</sup> However, it is of considerable interest to examine the  $x$ -dependence of the differential cross sections in more detail in order to see how heavy quark production behaves as a function of  $x$ . Accordingly, we show in Figs. 4(a) and 4(b) the fully differential cross section  $d^2\sigma/dx dy$  for the G-S(B) model at  $E = 30$  and 100 GeV, respectively. The quark masses are those of Eq. (4.2a), and again the mixing angle is given by  $\cos^2 \phi = 1/2$ . In these figures the solid curves represent  $d^2\sigma^{\nu N}/dx dy$  and the dashed ones  $d^2\sigma^{\bar{\nu} N}/dx dy$ . At  $E = 30$  GeV for  $x = 0$  the  $\nu$  and  $\bar{\nu}$  curves are rather similar because of the concentration of sea quarks at small  $x$ . As one moves out from  $x = 0$  through  $x = 0.1$ , 0.3 to 0.5, the neutrino curves become progressively flatter and the antineutrino ones progressively closer to a  $(1 - y)^2$  shape. At  $E = 100$  GeV, the threshold shoulder structure is very marked indeed at  $x = 0$ , due to

the added sea quark contributions and in the case of antineutrinos, to the valence  $u \rightarrow b, b'$  transitions, which, recall, also contribute most strongly for small  $x$ . At larger  $x$ , only the antineutrino curves show strong departures from their low energy forms.

The onset of heavy quark and associated hadron production lead to total cross sections which grow more rapidly than linearly as a function of the beam energy,  $E$ . This is illustrated in Fig. 5. Because of the factor three enhancement in the contributions of  $V + A$  currents relative to those of  $V - A$  currents for antineutrinos,  $\sigma^{\bar{\nu}N}$  displays the largest growth with energy. Again, the solid and dashed curves are for the G-S(B) model with the quark mass choices of Eqs. (4.2a) and (4.2b) respectively.

In Figs. 6, 7 and 8 we show in the G-S(B) model how variations in the  $b'$  quark mass affect two important average quantities which describe the  $y$  distribution, namely the mean value of  $y$ ,  $\langle y \rangle$ , and an effective B-parameter defined here by the equation

$$\frac{1}{\sigma} \frac{d\sigma^{(\nu, \bar{\nu})N}}{dy} = \left[ 1 - y + \frac{y^2}{2} \pm y(1 - \frac{y}{2})B \right] / \left[ \frac{2}{3} \pm \frac{1}{3} B \right] . \quad (4.3)$$

We have chosen this definition of B because it is the one used by the experimentalists, who fit their measured  $y$  distributions to Eq. (4.3). It should be recalled, however, that in the presence of heavy quark production the  $y$  dependence of the differential cross section is given by Eq. (3.16) summed over all possible quark transitions and is not so simple as the

form (4.3). In particular, the  $x$  and  $y$  dependences no longer factorize, and the parton distribution functions themselves depend on  $y$ , through the variable  $\xi$ . In order to compare with experiment we have made a  $\chi^2$  fit of the calculated  $y$ -distributions to Eq. (4.3). We have set  $W_{b'}$  = 5, 7 and 10 GeV and used the connection formula (3.12a) and Eqs. (4.1) and (4.2a) for the  $c$  and  $b$  parameters with  $\cos^2 \phi = 0.5$ . It is clear from the figures that the higher mass values (7 and 10 GeV) push the onset of the  $b'$  contribution out beyond 50 GeV. Note that for both  $\langle y \rangle$  and  $B$ , the curves actually overshoot their asymptotic values (7/16 and 0 respectively). The reason for this is that one is trying to fit  $(1/\sigma) d\sigma/dy$  to the parabolic form Eq. (4.3), whereas in the presence of heavy quark production the actual  $y$  distribution is not of this form, but instead has the shoulder structure evident in Figs. 3 and 4. Because the  $\chi^2$  fit gives greater weight to the points in the shoulder region it yields a  $B$  value corresponding to a flatter parabolic shape than one would naively expect.

In Figs. 9, 10 and 11 we illustrate the effects of varying the  $b'$  mass parameters on  $\langle y \rangle$ ,  $B$  and  $R_{ch}$ .

## B. Experimental Cuts and Beams

In order to compare directly with the experimental data, we must impose the same cuts on the theoretical model predictions and flux average with the same spectra as those which were used by each experimental group. We shall discuss in detail the cuts for the HPWF counter experiment and mention briefly the cuts for the CF counter and the FIIM and ACM bubble chamber experiments.

### 1. Harvard-Pennsylvania-Wisconsin-Fermilab Experiment

The HPWF experiment<sup>1</sup> used a liquid scintillator hadron calorimeter followed by a magnetic spectrometer for the scattered muons. The data were obtained in a series of runs which used both single and double-focussing horns and a quadrupole triplet target train. In particular, most of the antineutrino events came from runs with a single horn beam (tuned to focus antineutrinos). For our flux-averaging we have utilized flux spectra for the various beams obtained from a comprehensive calculation of Fermilab neutrino spectra performed by Stefanski and White.<sup>31</sup>

The experimental cuts include first, the following restrictions on the muon energy and angle, which are used for all distributions:

$$E_{\mu} \geq 4 \text{ GeV and } \theta_{\mu} \leq 0.225 \text{ rad.} \quad (4.4)$$

It should be noted that the  $\theta$  cut represents an average. In reality, the actual cut depends on the location of the interaction vertex in the target-calorimeter; the further toward the rear of this apparatus the vertex is, the larger the acceptance angle for the muon to go through the magnet. The regions of the  $x - y$  plots affected by these cuts are shown in Fig. 14 for  $E = 50 \text{ GeV}$ . The muon energy cut causes the  $y$ -distribution to vanish beyond  $y = 4/E \text{ (GeV)}$ , while the angle cut eliminates large  $x$  events and causes the  $y$ -distribution to roll off rapidly at high  $y$ . As  $E$  increases, the effect of both cuts diminishes.

Two sets of  $y$ -distributions are given by the experimentalists corresponding to

$$\text{small } x: 0 \leq x \leq 0.15 \quad (4.5a)$$

$$\text{"all" } x: 0 \leq x \leq 0.6 \quad (4.5b)$$

The latter cut serves to eliminate the elastic events from the plotted  $y$ -distributions. The energy dependence of  $\langle y \rangle$  is obtained by applying (4.4), (4.5b) and in addition, the cut

$$Q^2 \geq 1.0 \text{ GeV}^2 \text{ or } W \geq 1.6 \text{ GeV} \quad (4.6)$$

This has the effect of eliminating small  $y$  events, in particular the quasi-elastic and  $\Delta$ -production events, which are not in the scaling region. On

the other hand, B-values are obtained by making a  $\chi^2$  fit to the experimental histograms in the y regions

$$\begin{aligned} 0.1 \leq y \leq 0.55 & \quad \text{for } 10 \leq E \leq 30 \text{ GeV} \\ 0.1 \leq y \leq 0.85 & \quad \text{for } 50 \leq E \leq 100 \text{ GeV} \end{aligned} \tag{4.7}$$

with a simple constant plus  $(1 - y)^2$  curve as discussed in Sec. III. The above y-cuts serve to diminish the effect of the  $\theta_\mu$  cut which treats different values of x differently.

The events retained after these cuts are made are then corrected for detection efficiency. In the experimental determination of the energy dependence of  $\sigma^{(\nu, \bar{\nu})N}$  and  $R = \sigma^{\bar{\nu}N} / \sigma^{\nu N}$ , the HPWF group also tried to correct for events lost because they occurred in the "blind region" where the muon missed the spectrometer. This correction necessitates the use of a theoretical model for  $d\sigma^{(\nu, \bar{\nu})N} / dy$ ; the group conservatively used the y distributions as measured at low energies. Of course the blind region shrinks as E increases so that the cuts and, in the case of  $\sigma^{(\nu, \bar{\nu})N}$  and R, the corrections applied to the data are less important at higher energies.

## 2. Caltech-Fermilab Experiment

The CF counter experiment<sup>2</sup> used a long 50' iron target-calorimeter followed by a magnetic spectrometer. The experimental acceptance criteria can be crudely represented by applying the following cuts

to the model predictions:

$$E_{\mu} \gtrsim 8 \text{ GeV} \quad \text{and} \quad \theta_{\mu} \lesssim 0.10 \text{ rad.} \quad (4.8)$$

Because of the greater length of the target and smaller radius of the magnetic spectrometer compared to the HPWF apparatus, the average muon angle cut, in particular, is more severe. The detailed dichromatic flux spectra were not available to us at the time of this writing.

### 3. Fermilab-IHEP-ITEP-Michigan Experiment

In the FIIM bubble chamber experiment,<sup>6</sup> antineutrinos were obtained from 300 GeV primary protons incident on a target used in conjunction with a double horn and plug. The plug served to reduce the admixture of high energy neutrinos in the antineutrino beam, but it also reduced the flux of high energy antineutrinos.

The energy cuts in this experiment are

$$E_{\mu} > 4 \text{ GeV} \quad (4.9)$$

$$E_{\text{had}} \equiv \nu \gtrsim 2.4 \text{ GeV} \quad (4.10)$$

The cut (4.9) ensures accurate identification of the muon, measurement of its energy, and reduction of hadron background; it has the effect of restricting  $y$  to  $y < (4 \text{ GeV}/E)$ . The cut on  $E_{\text{had}}$  is made so that the fractional correction for missing neutral hadronic energy will be small. This latter cut eliminates low  $y$  events. Antineutrino  $y$ -distributions are plotted for  $x$  values in the ranges

$$\text{small } x: 0 \leq x \leq 0.10$$

(4.11)

$$\text{all } x: 0 \leq x \leq 1.0 \quad .$$

The B-parameters are determined by applying the same cuts in the muon energy and hadron energy for each of the two x-regions.

#### 4. Argonne-Carnegie Mellon Experiment

The ACM antineutrino experiment<sup>4</sup> used the 15' bubble chamber, filled with hydrogen, exposed to antineutrinos from 300 and 400 GeV primary proton beams via single and double horns, respectively, without a plug. The only cuts applied are

$$E \geq 6 \text{ GeV} \quad (4.12)$$

and  $0.1 \leq y \leq 0.9 \quad . \quad (4.13)$

The visible energy cut helps to eliminate neutron-induced events while the cuts on y eliminate neutral-current events from the charged-current data samples.

#### C. Comparison of Model Predictions with Experiment

The effects of the cuts applied to the theoretical model predictions are illustrated for the energy dependences of  $\langle y \rangle$  and B in Figs. 15 and 16. For the purpose of this comparison of the results with and without cuts, we have used the G-S(B) model with the  $(m_j, W_j)$  masses of Eqs. (4.2b) and  $\cos^2 \phi = 1.0$ . It is clear from the figures that the effect of

the cuts is to reduce  $\langle y \rangle$  and B for both neutrino and antineutrino reactions. The average y-values are lowered since the muon angle and energy cuts eliminate proportionately more of the high y-events than the  $Q^2$  or W cuts remove low y-events. This is especially true for the approximately flat neutrino y-distribution. The B-values are lowered by the cuts since the best fits to the y-distributions with a combination of flat plus parabolic curves are slightly flatter than those obtained when the high y-part of the distributions are not eliminated. Recall that the high y-enhancement moves toward lower y as E increases.

Finally, we shall compare the gauge model predictions, including cuts and, where appropriate, flux-averaging, with experimental data. We first discuss the results for the HPWF experiment, which at present has higher statistics than any of the others. In doing so, we shall select parameters which best illustrate the features of the models and at the same time give generally the best fits to the data.

The energy dependence of  $\langle y \rangle^{\nu N}$  is shown in Fig. 17 along with the prediction of the G-S(B) model for the (A) set of mass parameters and  $\cos^2 \phi = 0.25$ . The error bars on the data points are statistical only. In this model and all others considered by us where the neutrino reaction is not enhanced by the right-handed current transitions, the actual theoretical predictions are very similar. We observe, however, that the actual experimental points at moderate energies tend to be about one standard deviation below this curve. The discrepancy is apparent in the y-distributions

themselves as one can see in Figs. 18(a) and (b) for the energy ranges 30 - 50 GeV and 50 - 100 GeV, respectively. It is difficult to pinpoint the source of the discrepancy. As noted earlier, the correction due to the cuts is a large one for the neutrino reactions, and the results indicate that it may not be large enough.

Concerning the energy dependence of  $\langle y \rangle$  for antineutrinos on isoscalar targets, it is evident from Fig. 19 that the predicted curves are in reasonable agreement with the data. The solid (dashed) curves correspond to the G-S(B) model with  $\cos^2 \phi = 0.25$  (0.50), the W thresholds of (4.1) and the quark masses of (4.2a). The experimental points in Fig. 20 indicate a decrease in the B-parameter which is somewhat slower than that indicated by the theoretical curves. This relative difference in the quality of the fit of  $\langle y \rangle$  and B to the data is a result of the fact that the fitting program for B tries to fit the shoulder in  $(d\sigma/dy)^{\bar{\nu}N}$ , as was discussed before, and thereby produces rather low values of B. In Fig. 21 we show the flux-averaged y-distributions for the HPWF data and infer from this important graph that the G-S(B)  $(1, 0)_6$  model with the  $(m_j, W_j)$  choices selected is in reasonable agreement with this data. The  $(0, 1)_6$  model yields very similar fits, (since the HPWF target is isoscalar) and hence is not shown.

The curves in Fig. 22 show that five-quark models of the type  $(1, 0)_5$  also fit the y-distributions reasonably well, especially for the choice  $\cos^2 \phi = 0.5$ , corresponding to the mixing of u and c quarks. But

$\cos^2 \phi = 1$ , corresponding to a full strength  $u \rightarrow b$  transition, leads to a poor fit. The best five- and six-quark models considered also fit the  $y$ -distributions for small  $x$  quite well, as is shown in Fig. 23, though the higher energy range 50 - 100 GeV can accommodate a somewhat flatter fit to the data.

The  $W$ -distributions for the best six- and five-quark models are given in Figs. 24 and 25, respectively, for energies in the range of 50 to 100 GeV. The  $W$ -distributions for the six-quark model exhibit a secondary peak above the  $b'$  threshold as the energy is viewed above 75 GeV. At 100 GeV, on the other hand, the  $W$ -distributions for the five-quark model exhibit only one peak occurring above the  $b$  threshold. The flux-averaged  $W$ -distributions are shown in Fig. 26 for the range 50 - 100 GeV for both models. Since the inclusive predictions average over resonances, no sharp peaks appear and the histogram is fit equally well by either model.

Next, the energy dependences of the cross section ratio is shown in Fig. 27 for the six-quark model with  $\cos^2 \phi = 0.25$  (solid curve) and  $\cos^2 \phi = 0.50$  (dashed curve). The former curve, which is the better fit to the  $y$ -distribution, yields a  $\sigma^{\bar{\nu}N} / \sigma^{\nu N}$  ratio which increases somewhat more slowly than is observed experimentally. For reference, the experimental flux normalization is determined for  $E \lesssim 60$  GeV by comparison with the quasielastic cross section and for  $E \gtrsim 60$  GeV by the Sakurai method.<sup>32, 33</sup> The latter method is based on the fact that for fixed  $W$

$\lim_{E \rightarrow \infty} d\sigma^\nu/dW = d\sigma^{\bar{\nu}}/dW$ . From Fig. 27 one may conclude that the G-S(B)  $(1, 0)_6$  model with the choices of  $(m_j, W_j)$  and  $\cos^2 \phi$  which gave good fits to the  $y$ -distributions is also, as one would expect, able to fit the observed increase in  $\sigma^{\bar{\nu}N}/\sigma^{\nu N}$ . The same statement applies for the  $(0, 1)_6$  model, which gives quite similar curves in both cases. There is some hint that the experimental cross sections ratio may rise and saturate faster than the model predictions indicate, but the data are not accurate enough at this time to draw a firm conclusion.

We turn next to the Caltech-Fermilab experiment. In Fig. 28 we give the antineutrino  $y$ -distributions; since the flux spectrum was not available to us at the time of writing, we have plotted the curves for three specific energies: 50, 145 and 195 GeV. It is clear from this figure that, even at the two highest energies (which are somewhat beyond the mean energy  $\langle E \rangle = 106$  GeV investigated by the HPWF group), the  $y$ -distributions do not become flat at high  $y$ ; rather the enhancement is much more pronounced at intermediate  $y$  with the rapid rolloff at high  $y$  due to the small muon acceptance angle,  $\phi_\mu < 100$  mrad. The  $B$ -values determined from the three curves ( $B = 0.90, 0.25$  and  $0.05$ ) correspond to values for the  $\alpha$ -parameter,  $\alpha = (1 - B)/2$  of  $0.05, 0.38$  and  $0.48$  respectively. The experimental values<sup>2</sup> at the lower two energies are  $\alpha = 0.17^{+0.13}_{-0.11}$  at 50 GeV and  $\alpha = 0.32^{+0.18}_{-0.15}$  at 150 GeV.

In the case of the Fermilab-IHEP-ITEP-Michigan bubble chamber experiment which used a light neon-hydrogen mixture (20% neon corresponding

to a ratio of 14 protons to 10 neutrons), we can contrast the  $(1, 0)_6$  and  $(0, 1)_6$  models, for which the right-handed current valence transitions are  $(u \rightarrow b_\phi)$  and  $(d_\phi \rightarrow x \text{ and } s_\phi \rightarrow y)$ , respectively. In Fig. 29 we have plotted, along with the FIIM points, the energy dependence of the B-parameter for the G-S(B) model (solid curve) and the  $(0, 1)_6$  model with exotic heavy quarks (dotted curves), for the (A) choice of parameters given in (4.1) and (4.2a) and  $\cos^2 \phi = 0.25$ . The actual  $y$ -distributions for the energy ranges 30 - 50 GeV and 50 - 100 GeV are given in Fig. 30 for these two models as well as the G-S(B) model with  $\cos^2 \phi = 0.50$  (dashed curves). It is clear from the higher energy data that the  $(0, 1)_6$  model fits the data slightly better though the data are not good enough to distinguish models. The two models predict noticeably different  $y$ -distributions for neutron targets, especially above 50 GeV as shown in Fig. 31. To the extent that the FIIM bubble chamber group can distinguish proton from neutron events<sup>21</sup> its data will accordingly serve to differentiate between these two models.

Finally we comment on the Argonne-Carnegie Mellon hydrogen bubble chamber experiment, for which again a marked contrast exists between the  $(1, 0)_6$  and  $(0, 1)_6$  models. The energy dependence of the inclusive cross sections and their ratio are plotted in Figs. 32 and 33. The G-S(B) model (solid curves) predicts a much more rapid increase in the  $\bar{\nu}p$  cross section than does the exotic  $(0, 1)_6$  model; however, the  $\nu p$  results are nearly identical for the two models since no valence right-handed current transitions contribute to this latter reaction.

In Figs. 33 and 34 we illustrate predictions for  $R_{\text{ch}}$  and  $B$  for both proton and neutron targets in the two models. It is evident that in the  $(0, 1)_6$  model there is a considerably greater contrast between the curves for proton and for neutron targets than is the case in the G-S(B)  $(1, 0)_6$  model. Beyond 100 GeV, the exotic  $(0, 1)_6$  model predicts a  $y$ -distribution which rises as  $y$  increases for the new quark transitions  $(d_\phi \rightarrow x, s_\phi \rightarrow y)_R$  overwhelm the old quark transition  $(u \rightarrow d)_\phi_L$ . Recall that the right-handed current transition is three times more effective than the left-handed current transition in antineutrino reactions and that there are two  $d$  valence quarks but only one  $u$  valence quark in the neutron. These predictions clearly indicate the importance of obtaining bubble chamber results for antineutrinos incident on deuterium.

The actual  $y$ -distributions for antineutrinos on protons are shown in Fig. 35 with the ACM cuts and flux-averaging. The solid curves refer to the G-S(B) model and the broken curves to the  $(0, 1)_6$  model with the (A) set of parameters and  $\cos^2 \phi = 0.25$ . The  $(0, 1)_6$  model predictions are in somewhat better agreement with the preliminary results presented at the Aachen Neutrino Conference by the ACM group.<sup>4</sup> The rise in the  $\sigma^{\bar{\nu}p}/\sigma^{\nu p}$  ratio measured by this group is also more consistent with the exotic model predictions than the G-S(B) model predictions.<sup>34</sup>

## V. CONCLUDING REMARKS

In this work we have considered right-handed current models of the  $(1, 0)_5$ ,  $(1, 0)_6$ , and  $(0, 1)_6$  types and have compared their predictions directly with the HPWF counter and FIIM bubble chamber data by applying the appropriate cuts and flux averaging. We recall that for definiteness we chose to consider the particular version of the  $(1, 0)_6$  model known as the Gürsey-Sikivie (B) model; however, other types of  $(1, 0)_6$  theories would give very similar results. This analysis was undertaken in an effort to understand better the apparent discrepancy between the counter and bubble chamber results; the former reveal a high  $y$ -anomaly and favor the presence of right-handed current transitions while the latter suggest no strong evidence for such a  $y$ -anomaly or the right-handed currents inferred therefrom. In the framework of the above models, we have determined which values of the quark masses,  $m_j$ , the threshold masses  $W_j$  for each new flavor production, and the mixing angle  $\phi$  yield the optimal fits to the HPWF data. Then, using these choices of parameters, we have compared the model predictions, folded with appropriate cuts, with the FIIM bubble chamber data. From this study we can draw several general conclusions.

First, all three types of models with right-handed currents give reasonable simultaneous fits to the HPWF and FIIM data (within  $\sim 1$  standard deviation) for the following choices of parameters:

$$m_c = 1.5 \text{ GeV}, \quad W_c = 2.25 \text{ GeV} \quad (5.1a)$$

$$m_b = 4.0 \text{ GeV}, \quad W_b = 5.0 \text{ GeV} \quad (5.1b)$$

and in the case of the six-quark models

$$m_{b'} = 6.0 \text{ GeV}, \quad W_{b'} = 7.0 \text{ GeV} \quad (5.1c)$$

The mixing angle was best taken to be

$$\cos^2 \phi = 0.25 \quad (0.50) \quad (5.1d)$$

for the six-quark (five-quark) models. We consider selection of the  $b'$  parameters considerably less certain than that for the  $c$  and  $b$  sets; this results in an ambiguity between the choice of five- vs. six-quark models. In particular, the  $W$ -distributions do not favor one over the other. The above choice of quark masses satisfying condition (4.12a) is preferred, however, over the choice (4.12b) corresponding to the situation where the constraint (3.11) does not apply. The choice (4.12b) results in too gradual an approach to rescaling. One should note, however, that with this set of parameters, which gives the best overall fit to the  $y$ -distributions, the data for  $x < .15$  appear to be somewhat flatter than the predictions of the  $(1, 0)_6$  or  $(0, 1)_6$  models, especially for  $E > 50 \text{ GeV}$ . The minimal Weinberg-Salam model fails to fit the HPWF data in particular.

In order to obtain reasonable fits with the five-quark model, one must choose the mixing angle as indicated in (5.1d) so as to suppress somewhat the right-handed current effect. This choice of angle can be interpreted in two ways. If the mixing occurs between u and c quarks, the neutral current will be charm-changing in lowest order. If the mixing involves the b quark instead, there must be a (massive) sixth quark, so that the model is not a five-quark model at all.

The  $(1, 0)_6$  and  $(0, 1)_6$  models give nearly identical antineutrino results for isoscalar targets; however they lead to greatly different predictions for proton, as contrasted with neutron, targets, since the basic right-handed current transitions are  $u \rightarrow b, b'$  vs.  $d \rightarrow x, y$ . With proton targets, the  $(0, 1)_6$  model predicts that only a small departure from the  $(1 - y)^2$  behavior should be observed in the y-distributions with the horn spectra available to the bubble chamber groups at Fermilab, and that the rise in  $\sigma^{\bar{\nu}p}/\sigma^{\nu p}$  with energy should be very gradual. Both of these predictions are in better agreement with the ACM data than are those of the G-S(B) model.<sup>34</sup> The decisive test of this  $(0, 1)_6$  model will require information on neutron targets.

ACKNOWLEDGMENTS

We are grateful to S. J. Barish, A. Benvenuti, D. Buchholtz, D. Cline, M. Derrick, O. Fackler, T. Y. Ling, A. K. Mann, F. Nezrick, P. Schreiner, W. Scott, and R. Stefanski for discussing their experimental data and flux with us. We would also like to thank B. W. Lee, C. Quigg, and S. B. Treiman for helpful conversations.

## REFERENCES

- <sup>1</sup>The HPWF data have been published in the following papers: B. Aubert et al., Phys. Rev. Lett. 33, 984 (1974); A. Benvenuti et al., ibid. 34, 419, 597 (1975); ibid. 35, 1199, 1203, 1249 (1975); ibid. 36, 1478 (1976); ibid. 37, 189, 1039, 1095(C) (1976). Also of interest are the reviews: C. Rubbia, in Proceedings of the 1975 International Symposium on Lepton and Photon Interactions at High Energies, Stanford, ed. W. T. Kirk (Stanford; SLAC, 1976); T. Y. Ling and P. Wanderer, in Proceedings of the International Conference on the Production of Particles with New Quantum Numbers, Madison, Wisconsin (April, 1976); A. Benvenuti, in Proceedings of the Aachen Neutrino Conference, Aachen, Germany (June, 1976); A. K. Mann, in Proceedings of the XVIIIth International Conference on High Energy Physics, Tbilisi, USSR (July 1976); D. Cline, in Proceedings of the Annual Meeting of the American Physical Society, Division of Particles and Fields, on Particles and Fields 1976, Brookhaven National Laboratory (October, 1976).
- <sup>2</sup>B. C. Barish et al., Phys. Rev. Lett. 38, 314 (1977). For reviews of the CF data, see B. C. Barish, in Proceedings of the 1975 Symposium on Lepton and Photon Interactions at High Energies, Stanford, op. cit.; F. Sciulli, in Particles and Fields 1975, eds. H. Lubatti and P. Mockett (Seattle, University of Washington Press, 1976); L. Stutte, in Proceedings of the Madison Conference, op. cit.; B. C. Barish, in Proceedings of the Aachen Neutrino Conference, op. cit. The relevant data from these

papers are the values for  $\alpha$ , the fraction of positive helicity coupling.

The "non-scaling" fit gives  $\alpha = 0.17^{+0.13}_{-0.11}$  at  $E = 50$  GeV and  $\alpha = 0.32^{+0.18}_{-0.15}$

at  $E \approx 150$  GeV. These values of  $\alpha$  yield directly the values of  $R_{ch}$ , i. e.

$R = 0.52^{+0.15}_{-0.11}$  at  $E = 50$  GeV and  $R = 0.69^{+0.31}_{-0.19}$  at  $E \approx 150$  GeV.

<sup>3</sup>J. P. Berge et al., Phys. Rev. Lett. 36, 639 (1976).

<sup>4</sup>M. Derrick et al., Phys. Rev. Lett. 36, 936 (1976). Also see the review by M. Derrick, in Proceedings of the Aachen Neutrino Conference, op. cit.

<sup>5</sup>J. Von Krogh et al., Phys. Rev. Lett. 36, 710 (1976). See also the review by J. Von Krogh, in Proceedings of the Madison Conference, op. cit.

<sup>6</sup>J. P. Berge et al., Phys. Rev. Lett. 38, 266 (1977). See also the reviews by F. A. Nezrick, in Proceedings of the Aachen Neutrino Conference, op. cit.; B. P. Roe, in Proceedings of the Tbilisi Conference, op. cit.

<sup>7</sup>C. Baltay, in Proceedings of the APS Conference at Brookhaven, op. cit.

<sup>8</sup>S. Weinberg, Phys. Rev. Lett. 19, 1264 (1967); ibid. 27, 1688 (1971); A. Salam, in Elementary Particle Theory, ed. N. Svartholm (Stockholm: Almquist and Wiksell, 1969), p. 367.

<sup>9</sup>A. Zee, F. Wilczek, and S. B. Treiman, Phys. Rev. D10, 2884 (1974).

This paper contains a rigorous calculation of the effect of asymptotic freedom scaling deviations on  $d\sigma/dy$ . For an estimate

of the combined effect of AFSD and charm production which, however,

assumes factorization of the  $x$  and  $q^2$  dependence of the parton distributions

and does not actually invert the moment integrals to obtain the structure functions, see R. M. Barnett, H. Georgi, and H. D. Politzer, Phys. Rev. Lett. 37, 3131 (1976) and references contained therein. In the latter paper it is shown that even when the combined effects of asymptotic freedom and charm production are consistently overestimated by various approximations, they are still not sufficient to account for the high  $y$ -anomaly. For a contrary view, see G. Altarelli, R. Petronzio, and G. Parisi, Phys. Lett. 63B, 183 (1976). These questions have also been considered by G. Fox (private communication).

<sup>10</sup>See, e.g., A. De Rujula, H. Georgi, S. L. Glashow, and H. R. Quinn, Rev. Mod. Phys. 46, 391 (1974), who suggested that  $SU(2) \times U(1)$  gauge models containing right-handed currents provided a natural mechanism for enhancing the antineutrino  $y$ -distributions at high  $y$ . For subsequent work, see R. M. Barnett, Phys. Rev. Lett. 36, 1163 (1976) and Phys. Rev. D14, 70 (1976); S. Pakvasa, L. Pilachowski, W. A. Simmons, and S. F. Tuan, Nucl. Phys. B109, 469 (1976); V. Barger, T. Weiler, and R. J. N. Phillips, Phys. Rev. D14, 1276 (1976); J. Kaplan and F. Martin, Nucl. Phys. B115, 333 (1976); C. H. Albright and R. E. Shrock, Fermilab Report 76/50-THY submitted to the XVIIIth International Conference on High Energy Physics, Tbilisi, USSR (July, 1976). In the present work, we have included all the cuts, flux averaged where necessary, and presented the model predictions for all relevant experiments.

<sup>11</sup>S. L. Glashow, J. Iliopoulos, and L. Maiani, Phys. Rev. D2, 1285 (1970).

- <sup>12</sup>De Rujula, Georgi, Glashow, and Quinn, ref. 10.
- <sup>13</sup>The five-quark model of type  $(1, 0)_5$  without mixing was first considered by Y. Achiman, K. Koller, and T. Walsh, Phys. Lett. 58B, 261 (1975).
- <sup>14</sup>Six-quark models of this type have been proposed by P. Fayet, Nucl. Phys. B78, 14 (1974); R. M. Barnett, Phys. Rev. Lett. 34, 41 (1975) and Phys. Rev. D11, 3246 (1975); F. Gürsey and P. Sikivie, Phys. Rev. Lett. 36, 775 (1976); P. Ramond, Nucl. Phys. B110, 214 (1976). The latter two references construct these models in the context of  $E_7$ .
- <sup>15</sup>See Barnett, ref. 14.
- <sup>16</sup>S. L. Glashow and S. Weinberg, Phys. Rev. D (to be published).
- <sup>17</sup>Concerning the  $(0, 1)_6$  model, it has been shown by B. W. Lee that with a minimal Higgs scheme consisting of one doublet and one triplet there is a constraint between  $m_W$ ,  $m_Z$ , and  $\theta_W$ :  $\frac{1}{4} \leq \kappa \leq 1$ , where  $\kappa \equiv (m_W^2/m_Z^2) \sec^2 \theta_W$ . See B. W. Lee, Fermilab Pub-76/101-THY, and B. W. Lee, in Proceedings of the XVI International Conference on High Energy Physics, 1972 (ed. J. D. Jackson and A. Roberts, National Accelerator Laboratory, Batavia, Illinois 1972), vol. IV, p. 266. See footnote 19.
- <sup>18</sup>C. H. Albright, C. Quigg, R. E. Shrock, and J. Smith, Phys. Rev. D14, 1780 (1976) and references therein; V. Barger and D. V. Nanopoulos, Phys. Lett. 63B, 168 (1976); D. P. Sidhu, Phys. Rev. D14, 2235 (1976); R. M. Barnett, Phys. Rev. D14, 2990 (1976) and SLAC preprint; T. Hagiwara and E. Takasugi, SLAC preprint.

- <sup>19</sup> We have compared the predictions of the  $(0, 1)_6$  model with inclusive and elastic neutral current data, as was done for other models in C. H. Albright et al., Ref. 18; see C. H. Albright, C. Quigg, and R. E. Shrock, to be published. We have found, interestingly, that the value of  $\kappa$  which best fits the elastic data,  $\kappa \approx 0.6$ , is in the middle of the range allowed by Lee's inequality (Ref. 17).
- <sup>20</sup> P. E. Baird et al., Nature 264, 528 (1976).
- <sup>21</sup> Vector models have been proposed by A. De Rujula, H. Georgi, and S. L. Glashow, Phys. Rev. Lett. 35, 702 (1975) and Phys. Rev. D12, 3589 (1975); S. Pakvasa, W. Simmons, and S. F. Tuan, ibid. 35, 702 (1975); F. Wilczek, A. Zee, R. Kingsley, and S. B. Treiman, Phys. Rev. D12, 2768 (1975); H. Fritzsch, M. Gell-Mann, and P. Minkowski, Phys. Lett. 59B, 256 (1975). For a comparison of the vector model with ~~elastic and inclusive neutral current data~~, see C. H. Albright, et al., and the other papers in Ref. 18.
- <sup>22</sup> Results for neutron targets are best obtained with deuterium, although one can attempt to separate neutron-induced events from proton-induced events by comparing the number of charged prongs in the light neon-hydrogen mixture. This is only accurate to the extent that one can ignore final state interactions.
- <sup>23</sup> D. Gross and F. Wilczek, Phys. Rev. Lett. 26, 1343 (1973); Phys. Rev. D8, 3633 (1973) and ibid. D9, 980 (1974); H. D. Politzer, Phys. Rev. Lett. 26, 1346 (1973); H. Georgi and H. D. Politzer, Phys. Rev. D9,

416 (1974); H. D. Politzer, ibid. D9, 2174 (1974); A. Zee, F. Wilczek, and S. B. Treiman, ref. 9; W. K. Tung, Phys. Rev. Lett. 35, 490 (1975); and Phys. Rev. D12, 3613 (1975).

- <sup>24</sup> H. Georgi and H. D. Politzer, Phys. Rev. Lett. 36, 1281 (1976); Phys. Rev. D14, 1829 (1976); A. De Rujula, H. Georgi, and H. D. Politzer, Annals of Physics (to be published); Harvard preprint HUTP 76/A179; J. Q. Nachtmann, Nucl. Phys. B63, 237 (1973); ibid. B78, 455 (1974); V. Baluni and E. Eichten, Phys. Rev. Lett. 37, 1181 (1976); R. Barbieri, J. Ellis, M. K. Gaillard, and G. G. Ross, Nucl. Phys. B117, 50 (1976); R. Ellis, R. Petronzio, and G. Parisi, Phys. Lett. 64B, 97 (1976); D. J. Gross, S. B. Treiman, and F. A. Wilczek, Princeton preprint.

- <sup>25</sup> To keep such a nucleon mass correction factor would be inconsistent with using Eq. (3.2) for the differential cross section, with  $(1 - y - Mxy/2E)F_2$  approximated as  $(1 - y)F_2$ . Moreover, we prefer the simpler form of  $\xi$  given in Eq. (3.7) because of subtleties which arise in using the full expression for  $\xi$ ; see Gross, Treiman, and Wilczek, ref. 23.

- <sup>26</sup> S. D. Drell and T.-M. Yan, Phys. Rev. Lett. 24, 181 (1970); G. West, ibid. 24, 1206 (1970).

- <sup>27</sup> C. G. Callan and D. J. Gross, Phys. Rev. Lett. 22, 156 (1969).

- <sup>28</sup> R. D. Field, Caltech report, unpublished. A newer version of this parton parametrization which breaks the SU(3) symmetry for the sea contributions is contained in R. P. Feynman and R. D. Field, Caltech report (to be published).

- <sup>29</sup>S. Pakvasa and S. F. Tuan, Phys. Rev. D10, 2124 (1974); see also J. Okada, S. Pakvasa, and S. F. Tuan, Nucl. Phys. B112, 400 (1976).
- <sup>30</sup>The masses for the charmed D meson and  $C_0$  baryon are given in the following papers which report their discovery: G. Goldhaber et al., Phys. Rev. Lett. 37, 255 (1976); I. Peruzzi et al., ibid. 37, 569 (1976); B. Knapp et al., ibid. 37, 882 (1976).
- <sup>31</sup>R. J. Stefanski and H. B. White, Fermilab report No. FN-292, unpublished.
- <sup>32</sup>J. J. Sakurai, preprint UCLA/73/TEP/79, 1973, unpublished.
- <sup>33</sup>Only data points based on the Sakurai method for  $W_{\max} \leq 2.2$  GeV are shown for legibility.
- <sup>34</sup>Private communication from S. Barish.

TABLE I. Left-handed and right-handed doublet structures for the  $SU(2) \otimes U(1)$  models considered in the text.

Model	Left-handed doublets	Right-handed doublets
Weinberg-Salam	$\begin{pmatrix} u \\ d_\theta \end{pmatrix}_L, \begin{pmatrix} c \\ s_\theta \end{pmatrix}_L$	...
$(1, 0)_5$	$\begin{pmatrix} u \\ d_\theta \end{pmatrix}_L, \begin{pmatrix} c \\ s_\theta \end{pmatrix}_L$	$\begin{pmatrix} u_\phi \\ b \end{pmatrix}_R$
$(1, 0)_6$ G-S(B)	$\begin{pmatrix} u \\ d_\theta \end{pmatrix}_L, \begin{pmatrix} c \\ s_\theta \end{pmatrix}_L$	$\begin{pmatrix} u \\ b_\phi \end{pmatrix}_R, \begin{pmatrix} c \\ s \end{pmatrix}_R$
$(0, 1)_6$	$\begin{pmatrix} u \\ d_\theta \end{pmatrix}_L, \begin{pmatrix} c \\ s_\theta \end{pmatrix}_L$	$\begin{pmatrix} d_\phi \\ x \end{pmatrix}_R, \begin{pmatrix} s_\phi \\ y \end{pmatrix}_R$

## FIGURE CAPTIONS

- Fig. 1: Kinematic regions in (a) the  $Q^2 - \nu$  plane and (b) the  $x - y$  plane with several invariant masses indicated for  $E = 30$  GeV; (c) depicts the allowed range of  $\xi$  for given  $E$ ; (d), (e), and (f) indicate the kinematic regions in the  $y - \xi$ ,  $x - \xi$  and  $W - \xi$  planes, respectively, again for  $E = 30$  GeV. Labels  $\alpha$ ,  $\beta$ ,  $\gamma$  refer to the set of parameters indicated in (a) and (b) and  $m = 1.5(2.0)$ ,  $4.0(4.9)$ , and  $6.0(6.9)$  GeV, respectively, for the solid (dashed) curves.
- Fig. 2: Isoscalar target  $y$ -distributions for (a)  $x \leq 0.1$  and (b) all  $x$  at  $E = 30$  GeV for the G-S(B) model with  $\cos^2 \phi = 0.5$ . The solid and dashed curves apply for the  $(m_j, W_j)$  parameters of cases (A) and (B) respectively. We normalize the distributions by dividing by  $\sigma_f$ , the part of  $\sigma^{\nu N}$  arising from light quark transitions ( $d \rightarrow u$ ,  $s \rightarrow u$ ,  $\bar{u} \rightarrow \bar{d}$ , and  $\bar{u} \rightarrow \bar{s}$ ).
- Fig. 3:  $y$ -distributions for (a)  $x \leq 0.1$  and (b) all  $x$  at  $E = 100$  GeV for the same model and choice of parameters, and with the same normalization, as in Fig. 2. The W-S model curves apply with  $W_c = 2.25$  GeV and  $m_c = 1.5$  GeV.
- Fig. 4:  $y$ -distributions for  $x = 0, 0.1, 0.3$  and  $0.5$  at (a) 30 GeV and (b) 100 GeV for the G-S(B) model and case (A) parameters with  $\cos^2 \phi = 0.5$ . The solid curves refer to the antineutrino reaction, the dashed curves to the neutrino reaction. The normalization is the same as in Fig. 2.

- Fig. 5:  $\sigma/E$  curves applicable to Figs. 2, 3, and 4.
- Fig. 6: Effect on average  $y$  of varying  $W_{b'}$  =  $m_{b'} + 1$  GeV in the G-S(B) model with  $\cos^2 \phi = 0.5$  and the (A) choice of  $c$  and  $b$  parameters.
- Fig. 7: Energy dependence of  $B^{\bar{\nu}N}$  corresponding to Fig. 6.
- Fig. 8:  $\sigma^{\bar{\nu}N} / \sigma^{\nu N}$  curves applicable to Figs. 6 and 7.
- Fig. 9: The  $x - y$  plane with the HPWF cuts indicated for  $E = 50$  GeV.
- Fig. 10: Variation of average  $y$  with and without the HPWF cuts. The (B) set of parameters is used in the G-S(B) model with  $\cos^2 \phi = 1$ .
- Fig. 11: Energy dependence of B-parameter with and without HPWF or FIIM cuts corresponding to Fig. 10.
- Fig. 12: Variation of average  $y$  for neutrinos in the G-S(B) model with  $\cos^2 \phi = 0.25$ , the (A) set of parameters, and the HPWF cuts. The HPWF data points are plotted; the errors are statistical only.
- Fig. 13: The neutrino  $y$ -distributions applicable to the HPWF data for  $x \leq 0.6$  in the energy ranges (a) 30 - 50 GeV and (B) 50 - 100 GeV corresponding to the model of Fig. 12. The units are arbitrary but are proportional to  $(1/\sigma_\ell) d\sigma^{\nu N} / dy$ . The curves are area-normalized to the data.

- Fig. 14: Variation of average  $y$  for antineutrinos in the G-S(B) model with  $\cos^2 \phi = 0.25$  (0.50) for the solid (dashed) curves, the (A) set of parameters and the HPWF cuts. The HPWF data points are shown.
- Fig. 15: Energy dependence of  $B^{\bar{\nu}N}$  applicable to Fig. 14 with the HPWF points indicated by open circles and the CF points by solid points.
- Fig. 16: Antineutrino  $y$ -distributions for the G-S(B) model corresponding to Figs. 14 and 15 with the HPWF cuts applied and HPWF histograms indicated for  $x < 0.6$  and the energy ranges (a) 30 - 50 GeV and (b) 50 - 100 GeV. The units and normalization are as in Fig. 18.
- Fig. 17: Antineutrino  $y$ -distributions for the five-quark model with HPWF cuts and histograms. The (solid or broken) and (dashed) curves correspond, respectively to the (A) and (B) sets of parameters defined in the text. The lowest two B values refer to  $\cos^2 \phi = 1.0$ , while the other two refer to  $\cos^2 \phi = 0.5$ . For units and normalization, see Fig. 13.
- Fig. 18: Antineutrino  $y$ -distributions for  $x < 0.15$  in the energy ranges (a) 30 - 50 and (b) 50 - 100 GeV for the G-S(B) model (solid curves) with the (A) parameters and  $\cos^2 \phi = 0.25$  and for the five-quark model (dashed curves) with the (A)

parameters and  $\cos^2 \phi = 0.5$ . The HPWF cuts are applied and the HPWF distributions shown. The normalization of the theoretical curves is as in Fig. 13.

Fig. 19: Antineutrino W-distributions in the G-S(B) model with HPWF cuts, the (A) set of parameters and  $\cos^2 \phi = 0.25$  for the energies indicated. The units are arbitrary but proportional to  $(1/\sigma_\ell) d\sigma^{\bar{\nu}N}/dW$ . The dashed curve represents the flux-averaged result for the range 50 - 100 GeV; it has been scaled up slightly to separate it from the solid curves for clarity.

Fig. 20: Antineutrino W-distributions in the five-quark model with HPWF cuts, the (A) set of parameters and  $\cos^2 \phi = 0.5$  for the energies indicated. The dashed curve represents the flux-averaged result for the range 50 - 100 GeV. See Fig. 19 for normalization.

Fig. 21: Comparison of the flux-averaged antineutrino W-distributions with the HPWF histogram for the G-S(B) model (solid curve) and five-quark model (dashed curve) of Figs. 19 and 20, respectively. The units are arbitrary but proportional to  $(1/\sigma_\ell) d\sigma^{\bar{\nu}N}/dW$ , and the curves are area-normalized to the data.

Fig. 22:  $\sigma^{\bar{\nu}N}/\sigma^{\nu N}$  curves for the G-S(B) model (solid curve) and five-quark model (dashed curve) of Figs. 19 and 20, respectively with the HPWF data points indicated for  $W_{\max} \leq 2.2$  GeV.

Fig. 23: Antineutrino  $y$ -distributions for (a)  $x < 0.15$  and (b) all  $x$  at energies 50, 145, and 195 GeV for the G-S(B) model with  $\cos^2 \phi = 0.25$ , the (A) set of parameters and the CF cuts. We normalize the curves in Fig. 23(b) by dividing by  $\sigma_\ell$  and in Fig. 23(a) by dividing by

$$\sigma_\ell (x < 0.15) \equiv \int_0^{0.15} dx (d\sigma_\ell / dx).$$

Fig. 24: Energy dependence of the B-parameters for the G-S(B) model (solid curve) and exotic  $(0, 1)_6$  model with the (A) set of parameters,  $\cos^2 \phi = 0.25$  and the FIIM cuts applied. The FIIM data points are indicated.

Fig. 25: Antineutrino  $y$ -distributions for all  $x$  in the energy ranges (a) 30 - 50 GeV and (b) 50 - 150 GeV for the G-S(B) model with  $\cos^2 \phi = 0.25$  (solid curve) and  $\cos^2 \phi = 0.5$  (dashed curve) and for the exotic  $(0, 1)_6$  model with  $\cos^2 \phi = 0.25$  (dotted curve) with the FIIM cuts applied. The FIIM data points are shown. All curves refer to the (A) set of parameters. The units are arbitrary, but proportional to  $(1/\sigma_\ell) d\sigma_\ell / dy$  and the curves are area-normalized to the data.

Fig. 26: Normalized antineutrino-neutron  $y$ -distributions for all  $x$  and the energy ranges (a) 30 - 50 GeV and (b) 50 - 150 GeV for the G-S(B) model (solid curve) and the exotic  $(0, 1)_6$  model (dotted curves) with  $\cos^2 \phi = 0.25$ , the (A) set of parameters and FIIM cuts and flux-averaging applied.

- Fig. 27: Antineutrino  $\sigma/E$  curves for the G-S(B) model (solid) and exotic  $(0, 1)_6$  model (dotted) with  $\cos^2 \phi = 0.25$  and the (A) set of parameters. The neutrino curve applies for both models.
- Fig. 28:  $\sigma^{\bar{\nu}}/\sigma^{\nu}$  curves for proton and neutron targets in the G-S(B) model (solid and dashed) and exotic model (dotted) corresponding to Fig. 27.
- Fig. 29: **Energy dependence of the B-parameter for the antineutrino-proton and antineutrino-neutron reactions with the ACM cuts applied.** The convention is that of Fig. 28.
- Fig. 30: Normalized antineutrino-proton  $y$ -distribution for the G-S(B) model (solid curves) and exotic  $(0, 1)_6$  model (dotted curves) of Fig. 28.

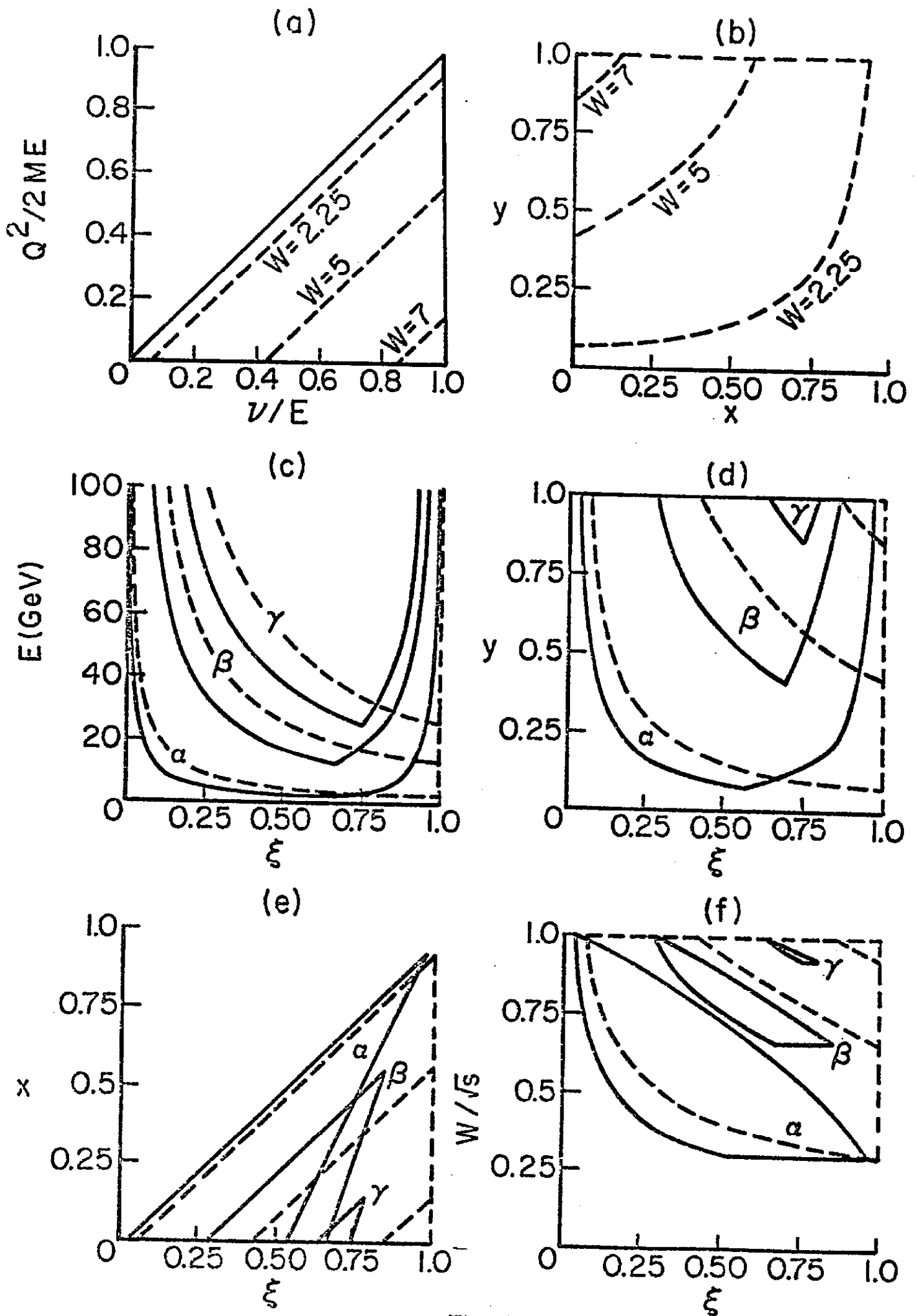


Fig. 4

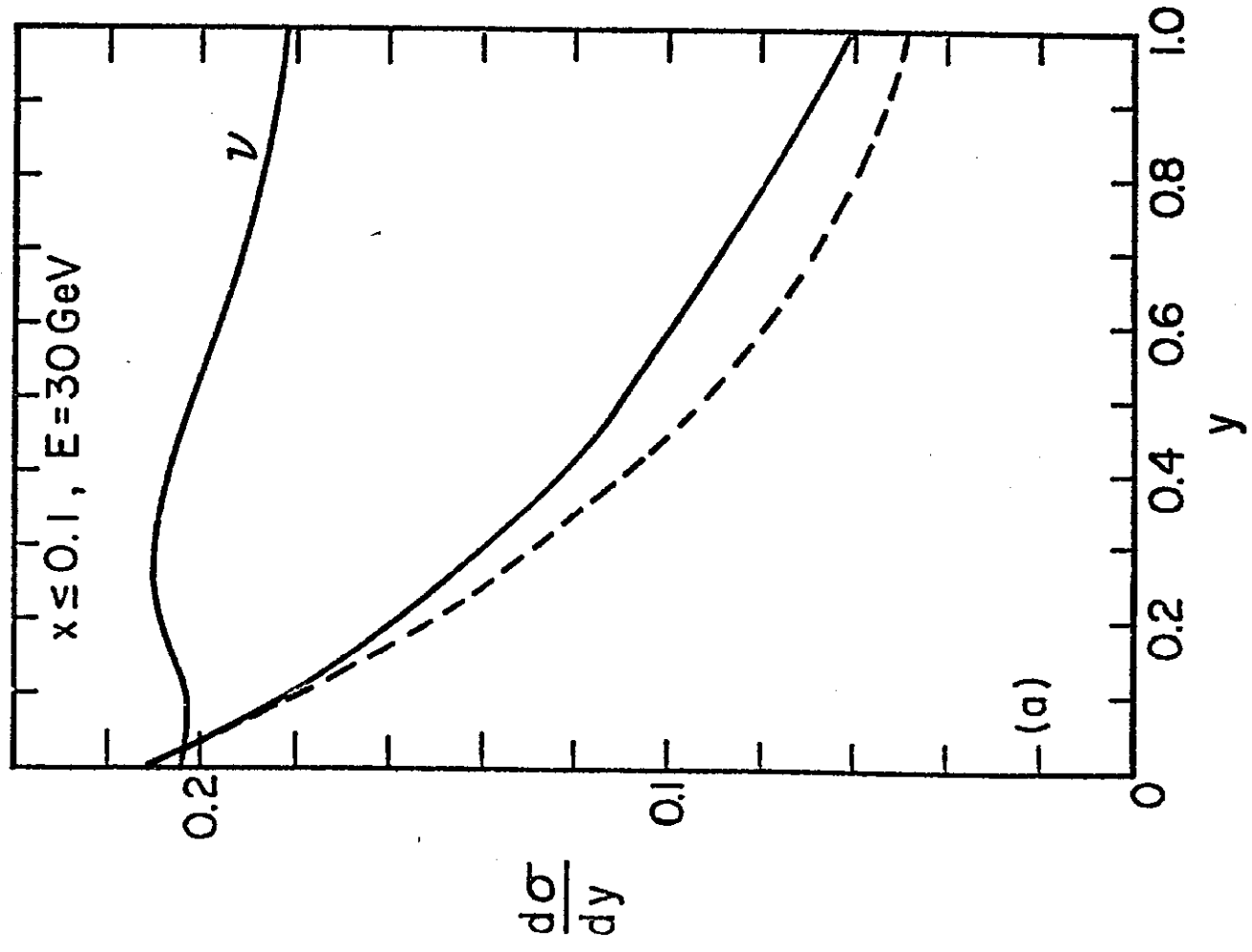
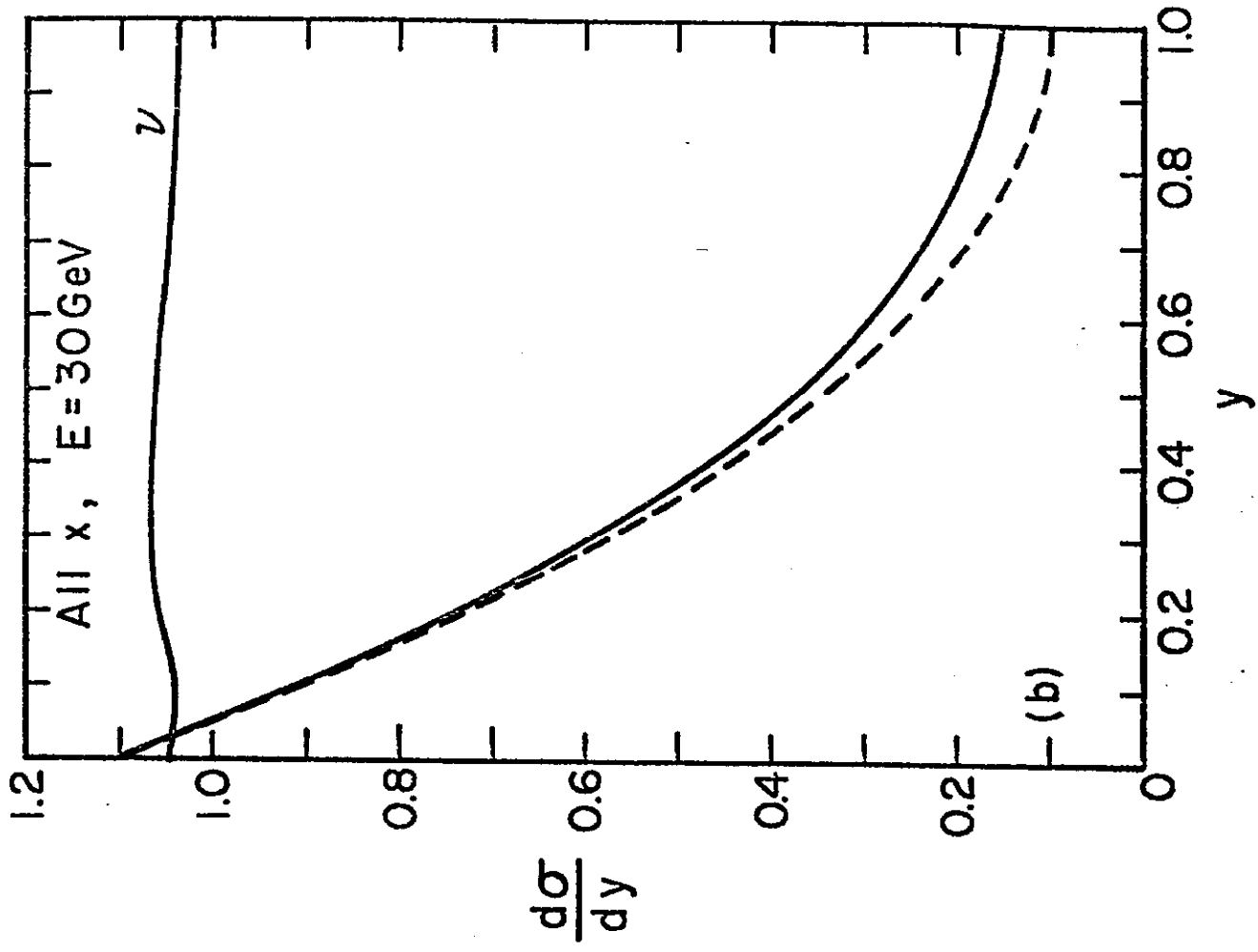


Fig. 2

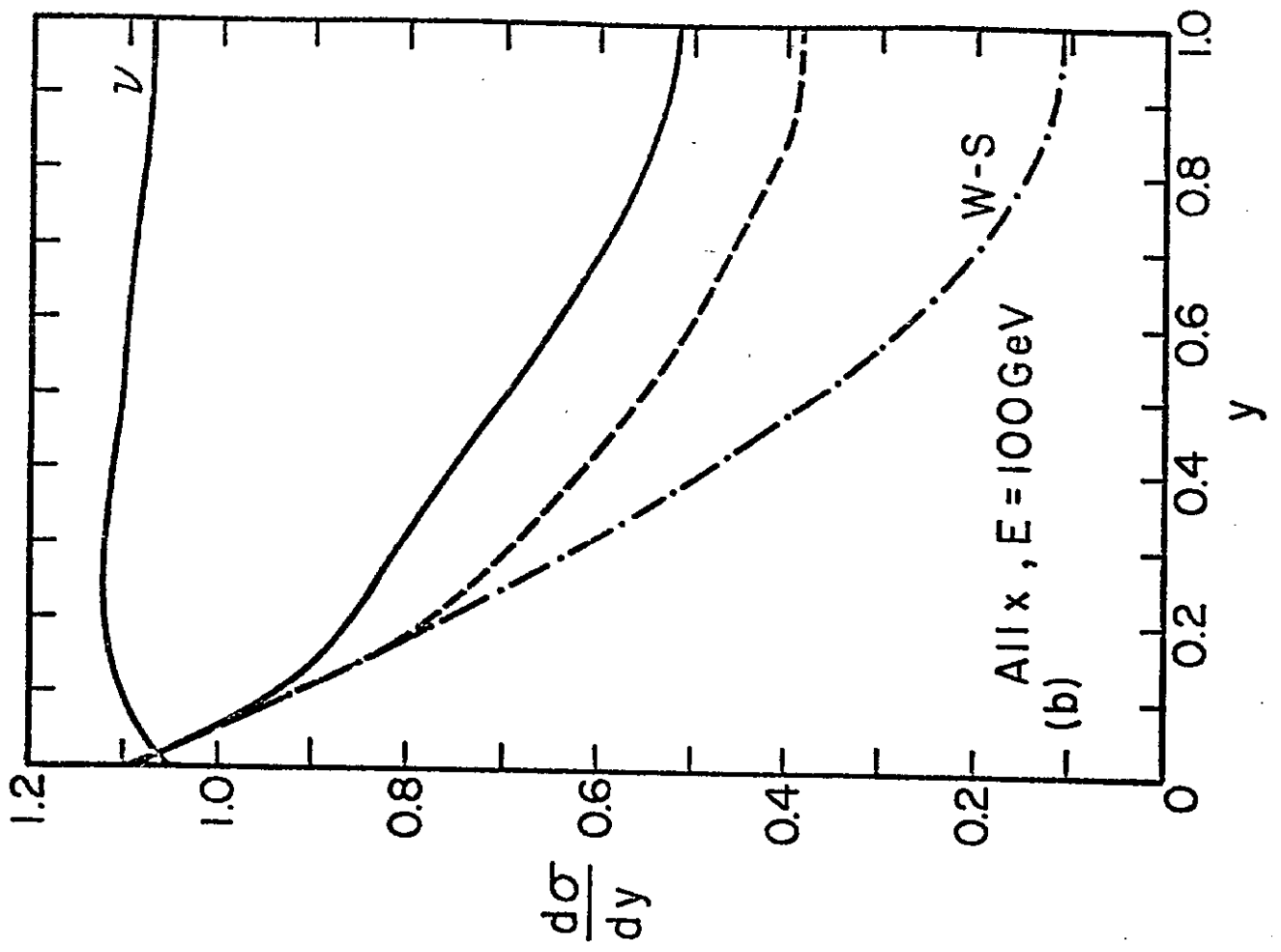
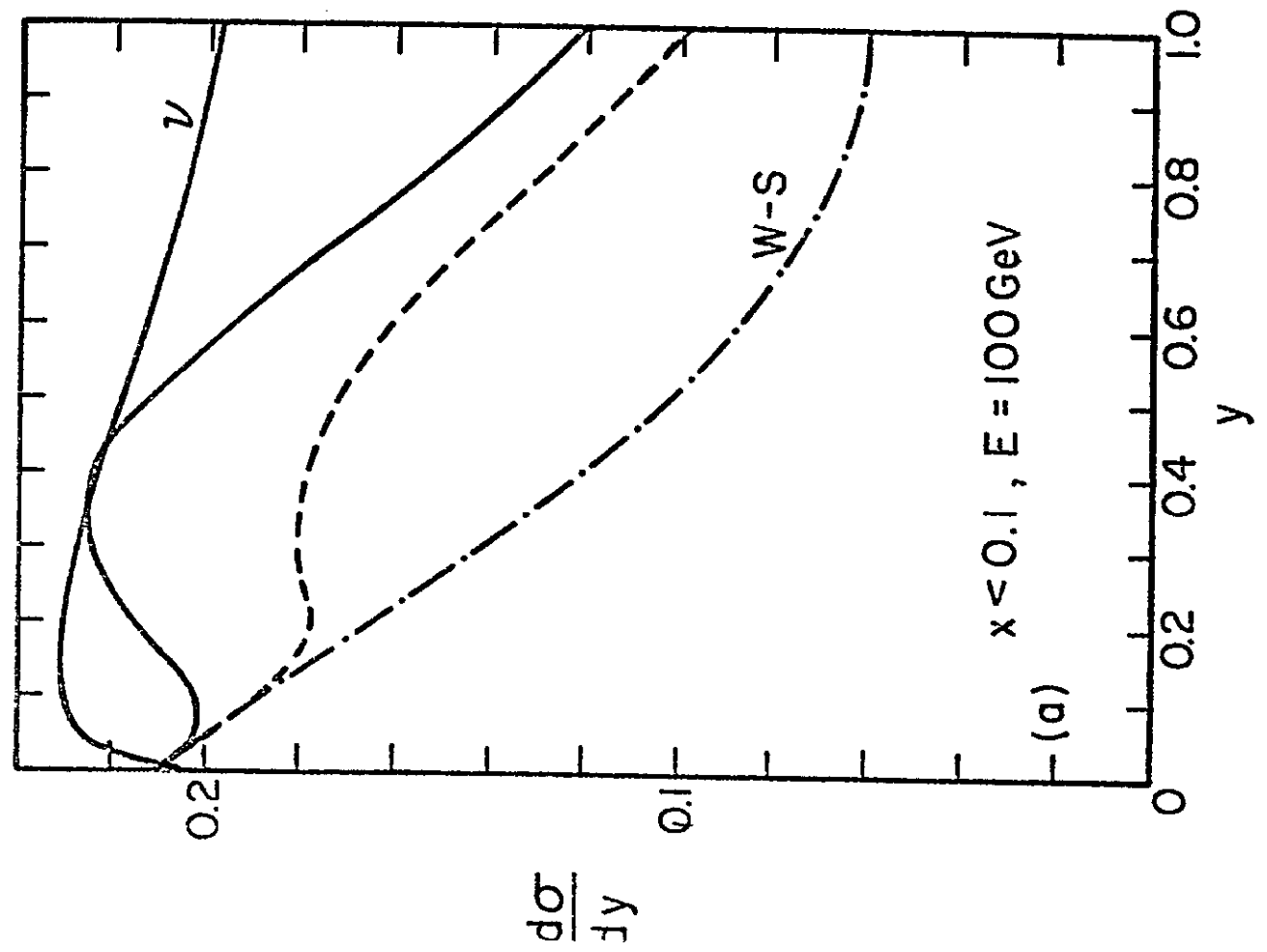


Fig. 3

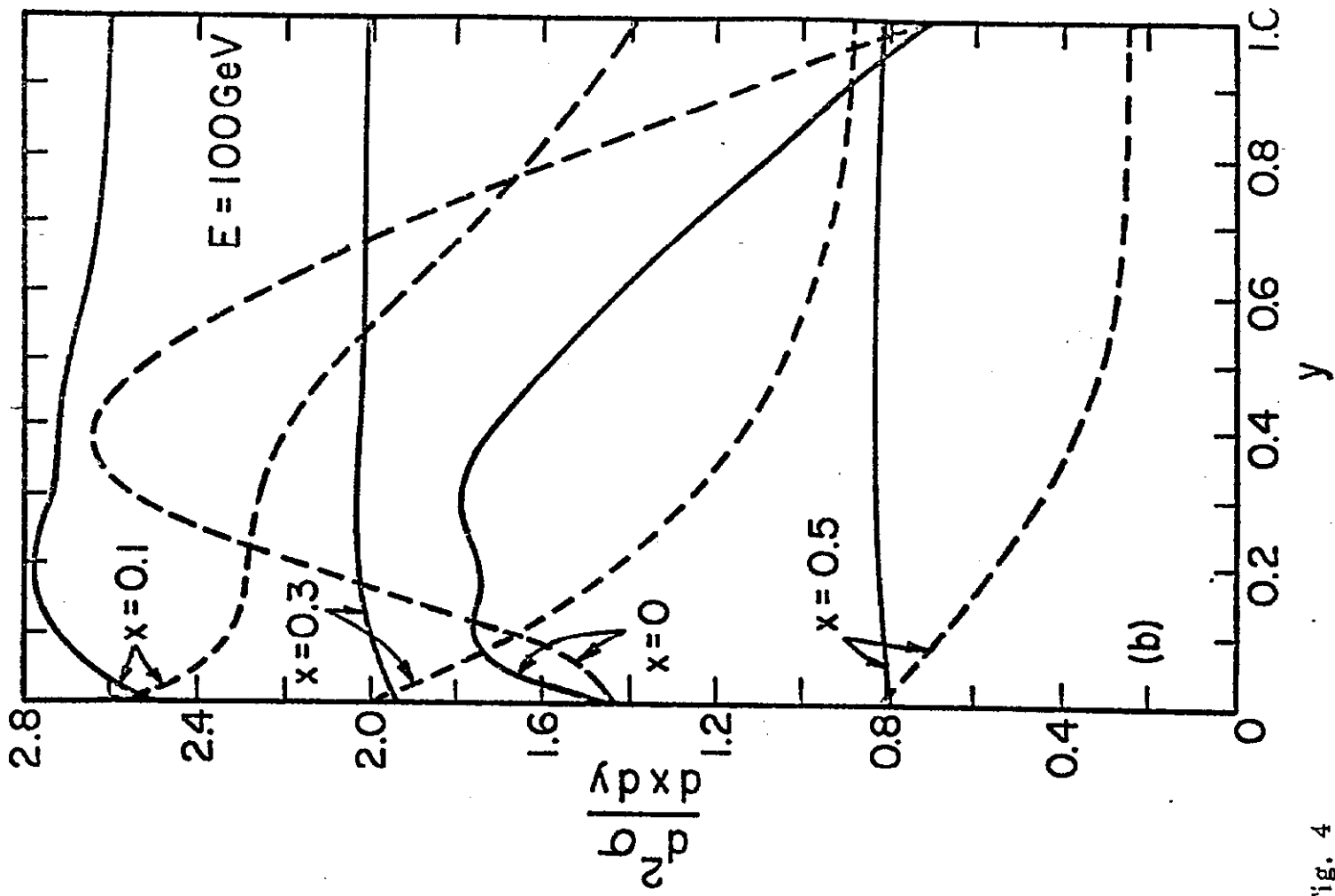
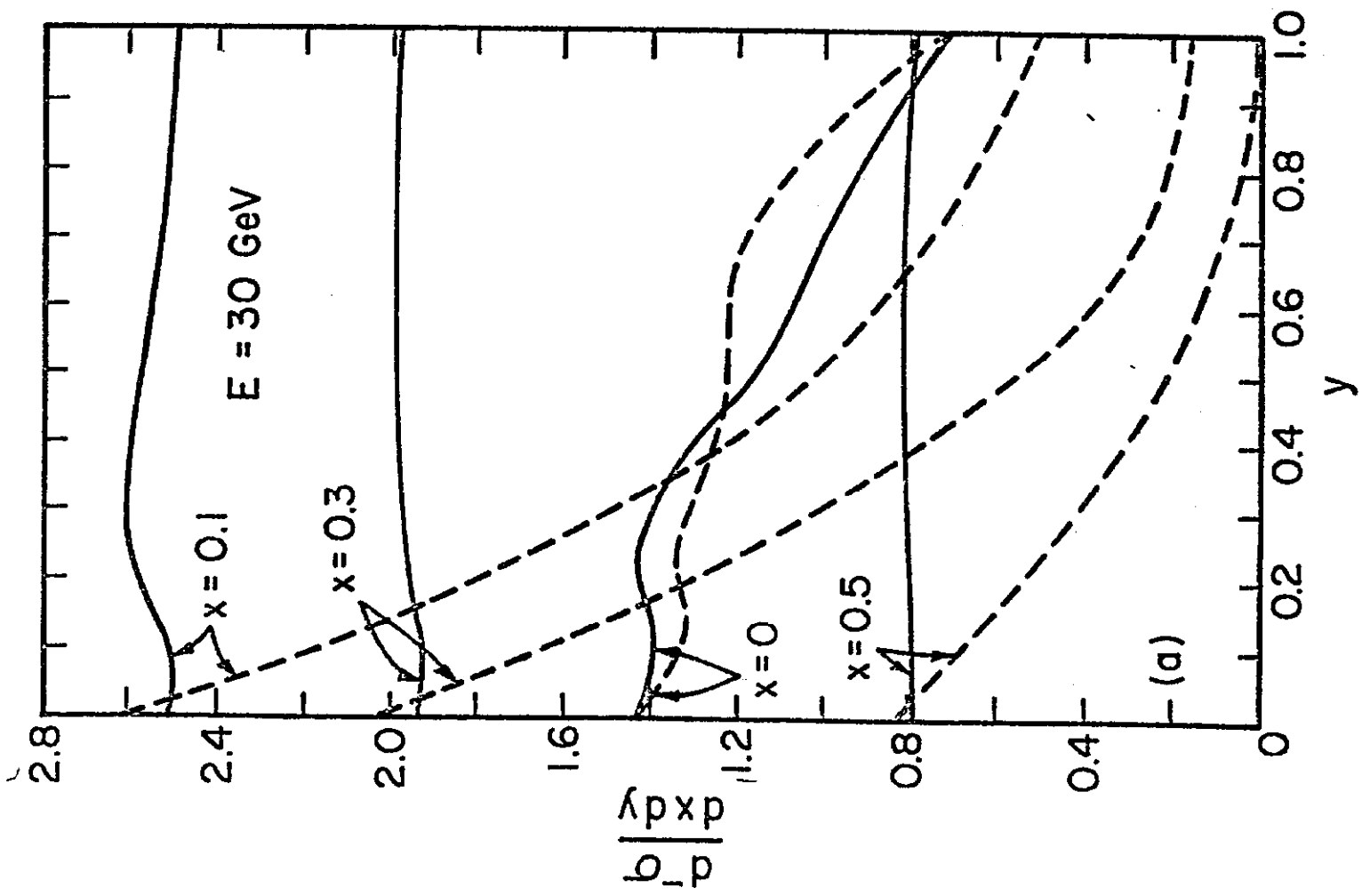


Fig. 4

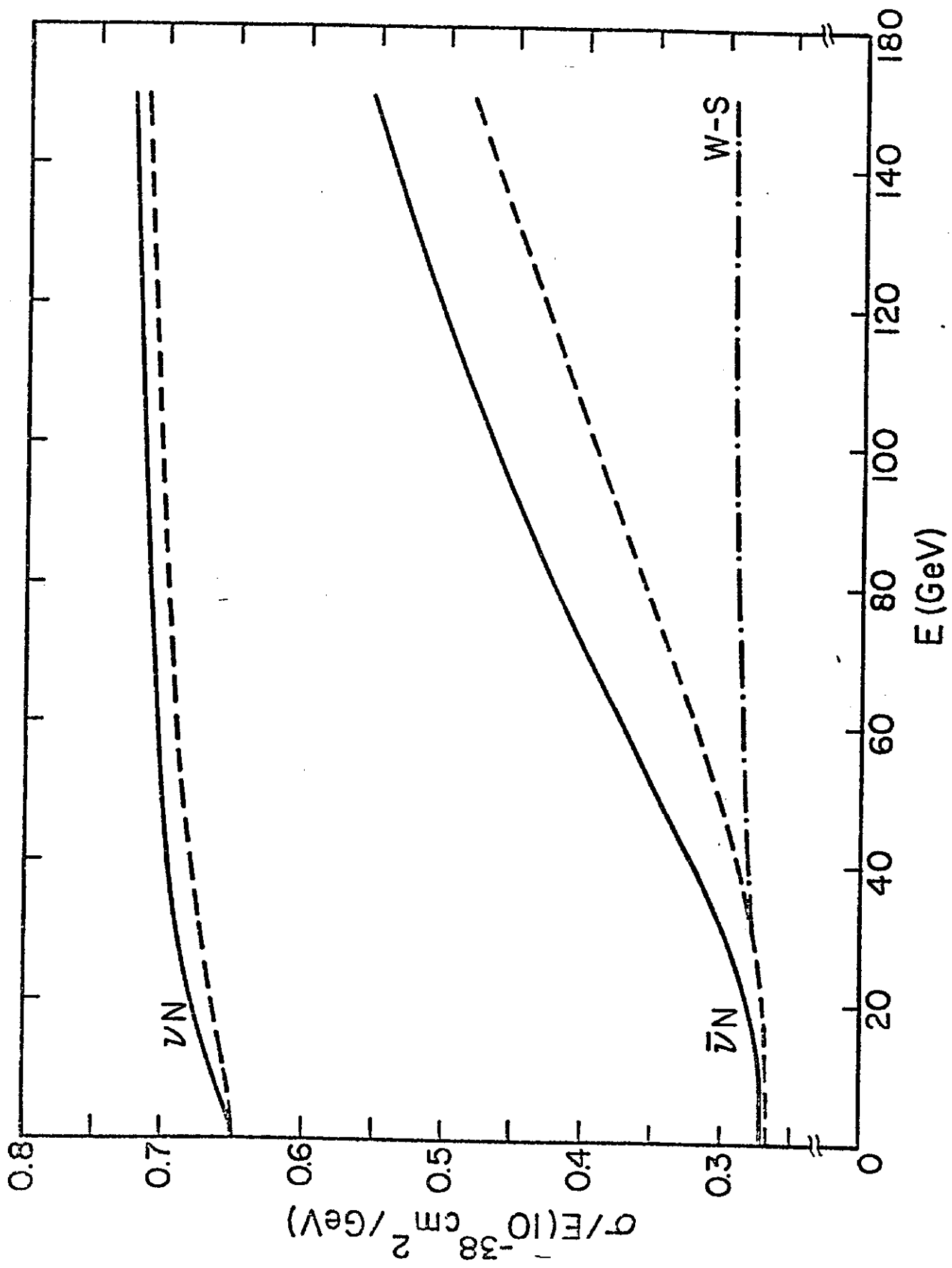


Fig. 5

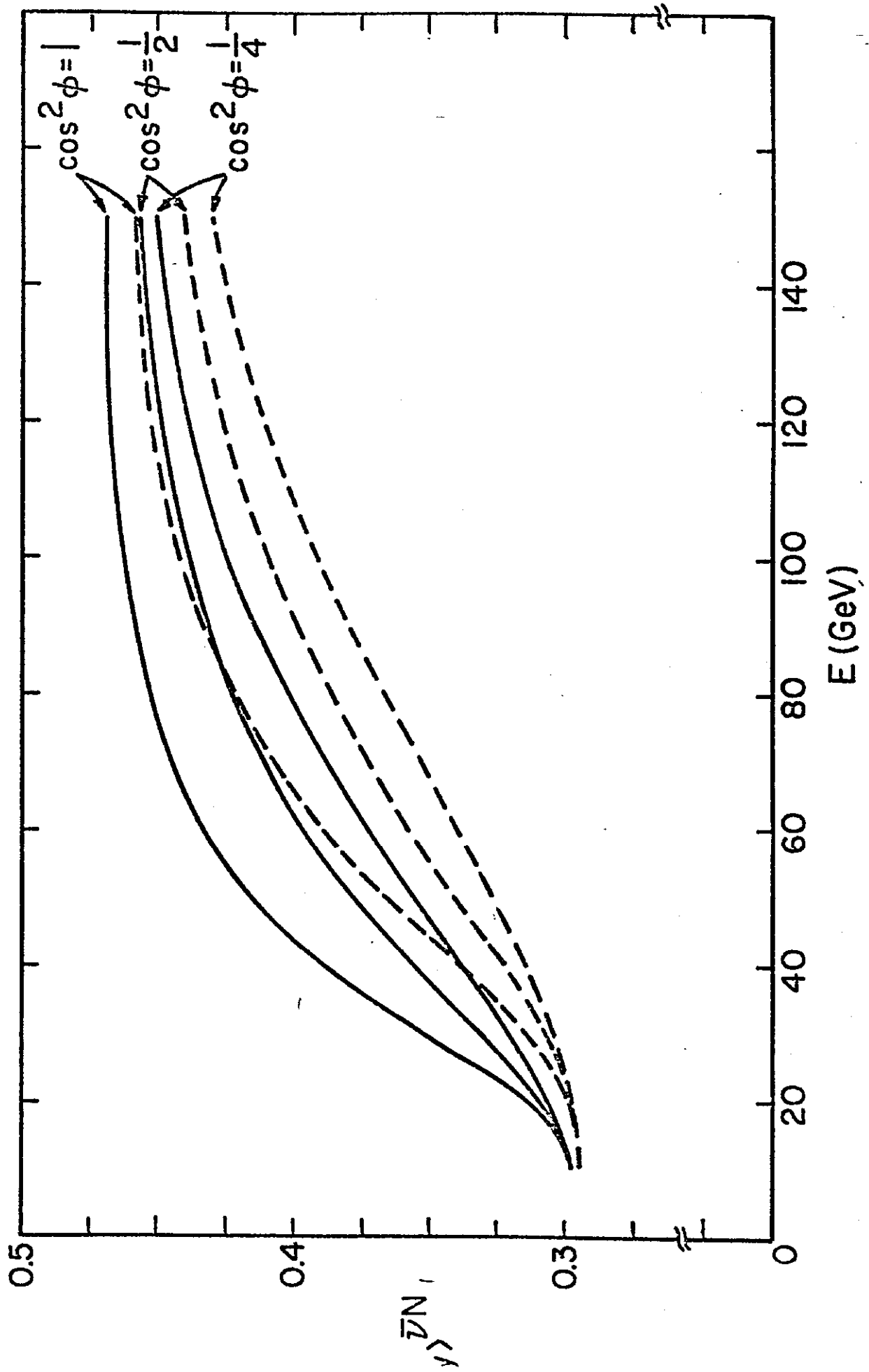


Fig. 6

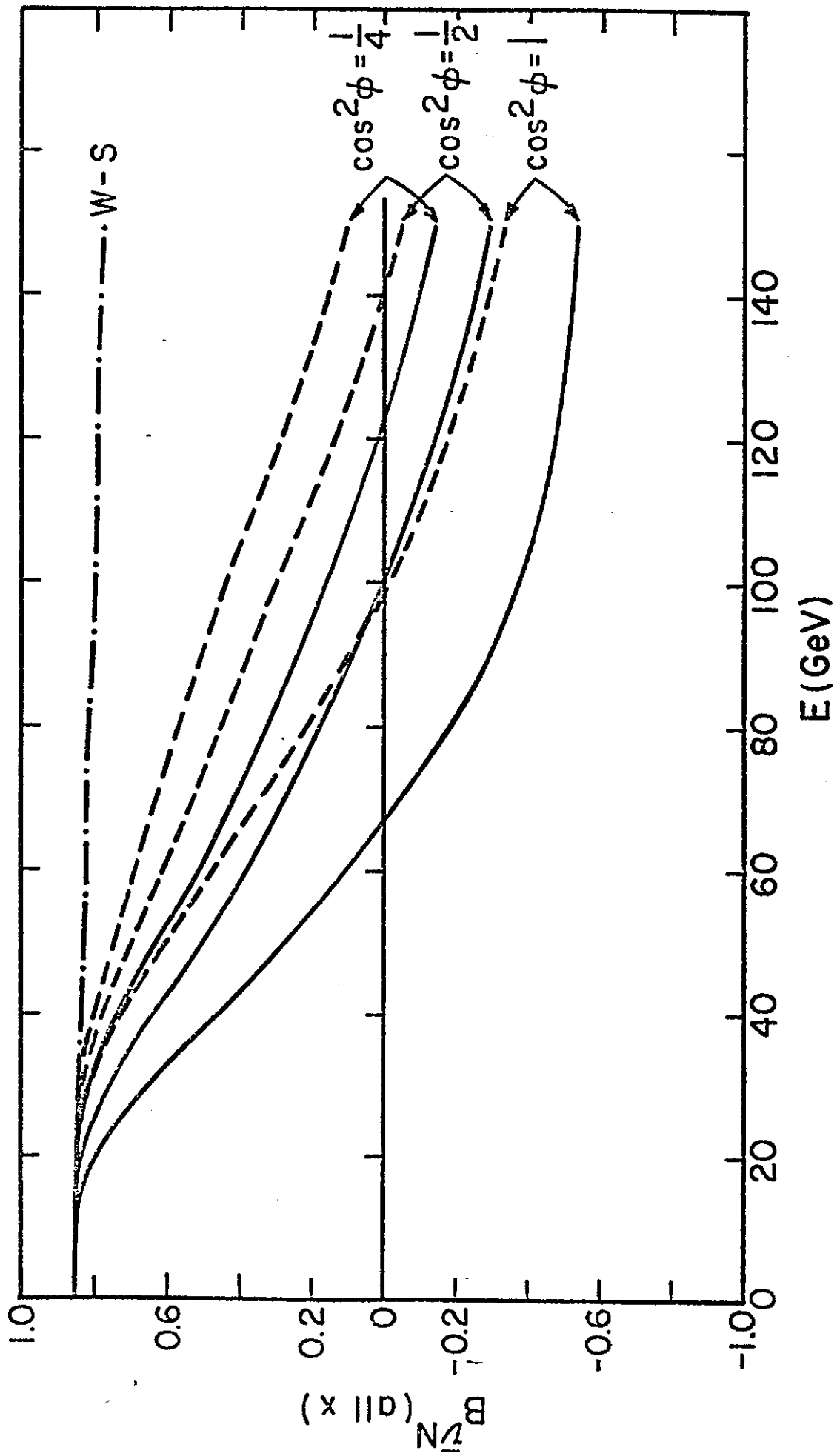


Fig. 7

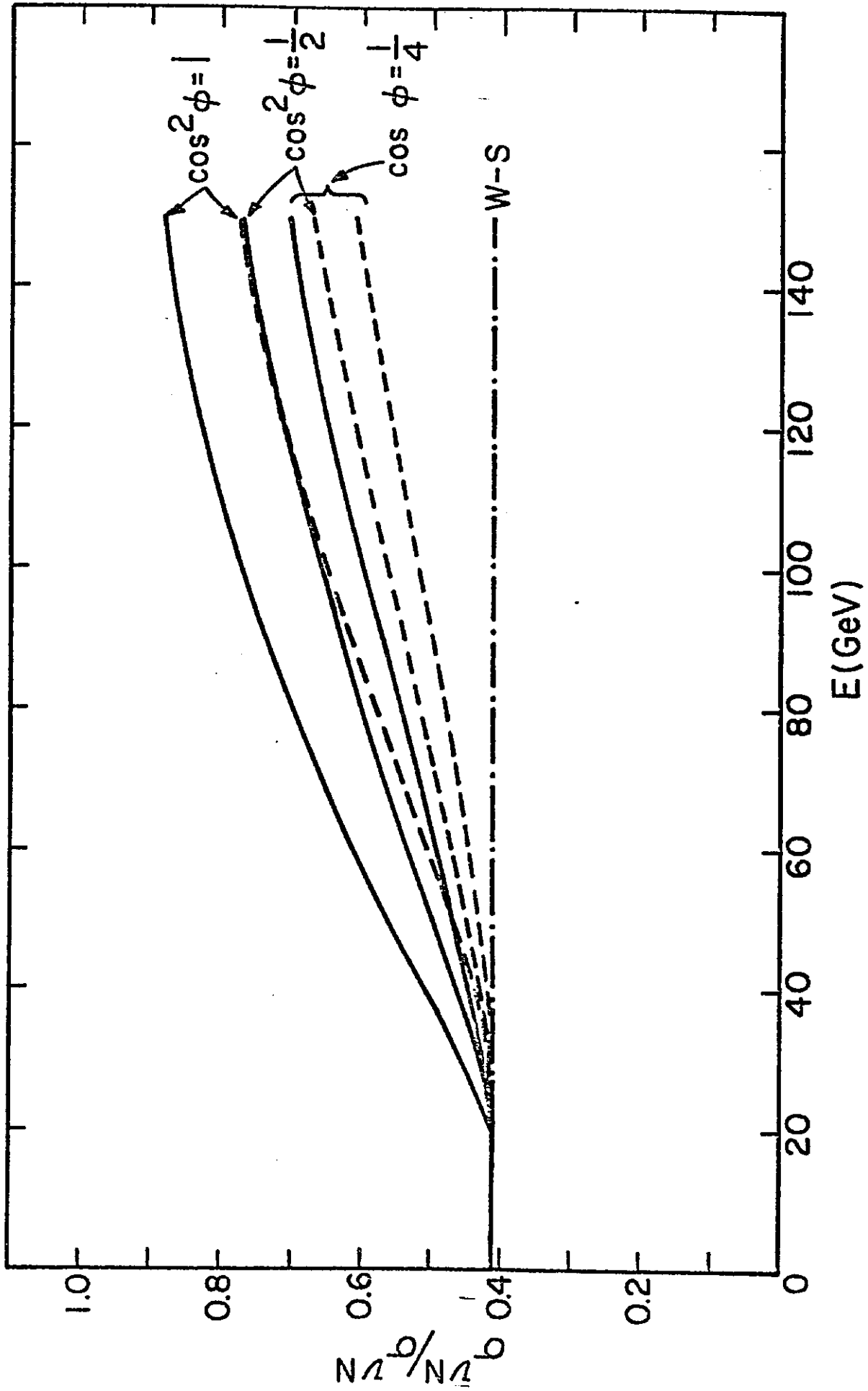


Fig. 8

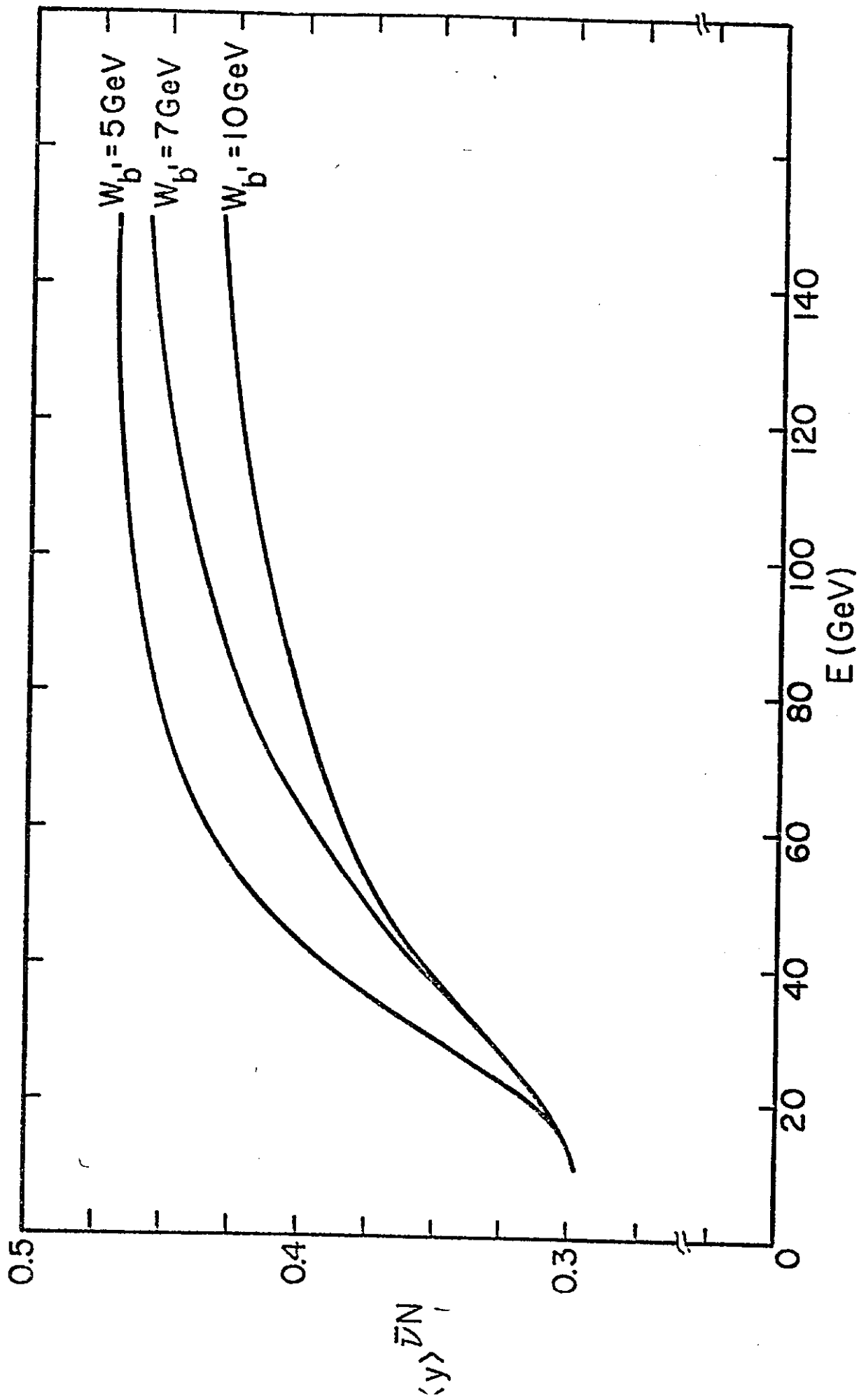


Fig. 9

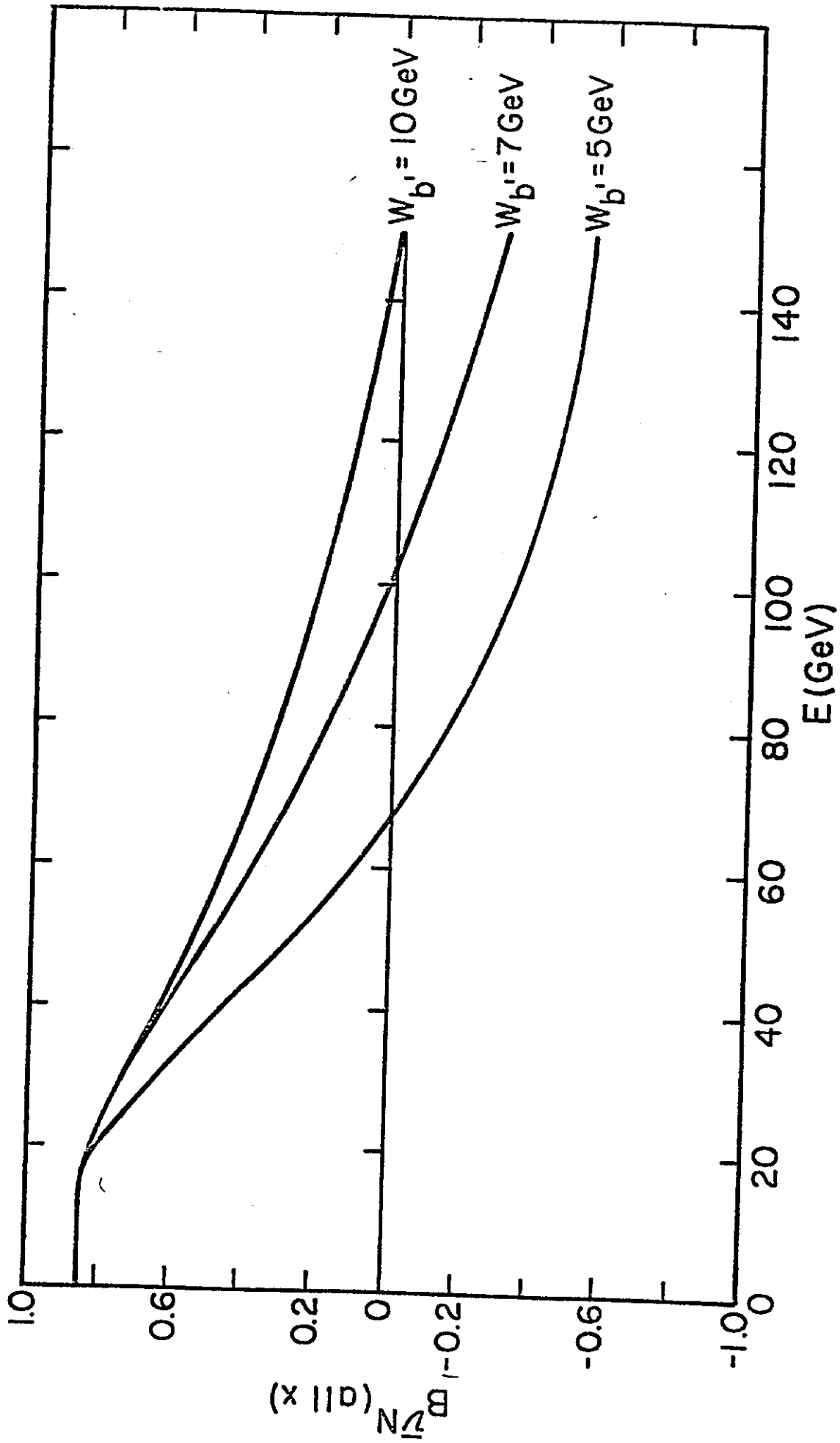


Fig. 10

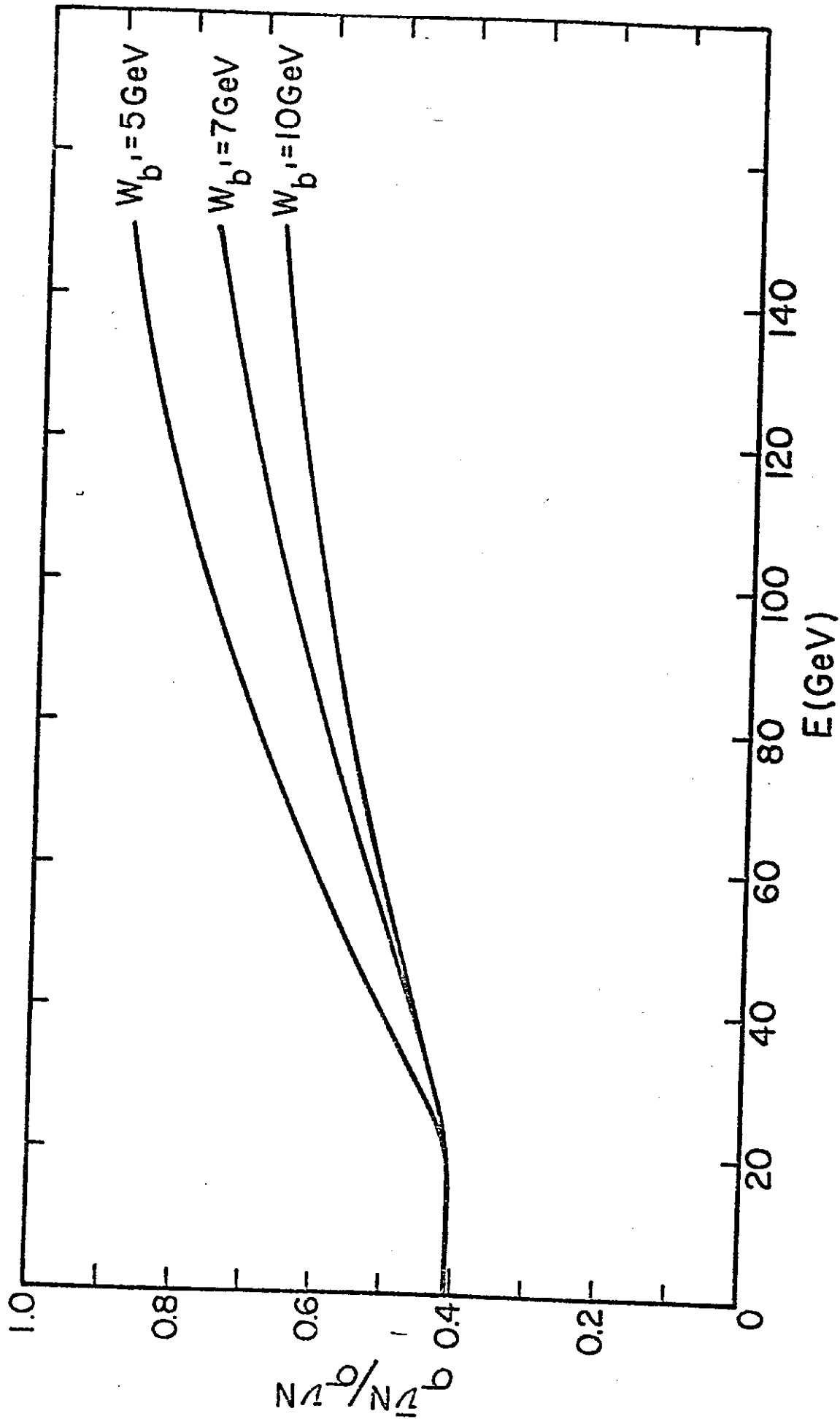


Fig. 11

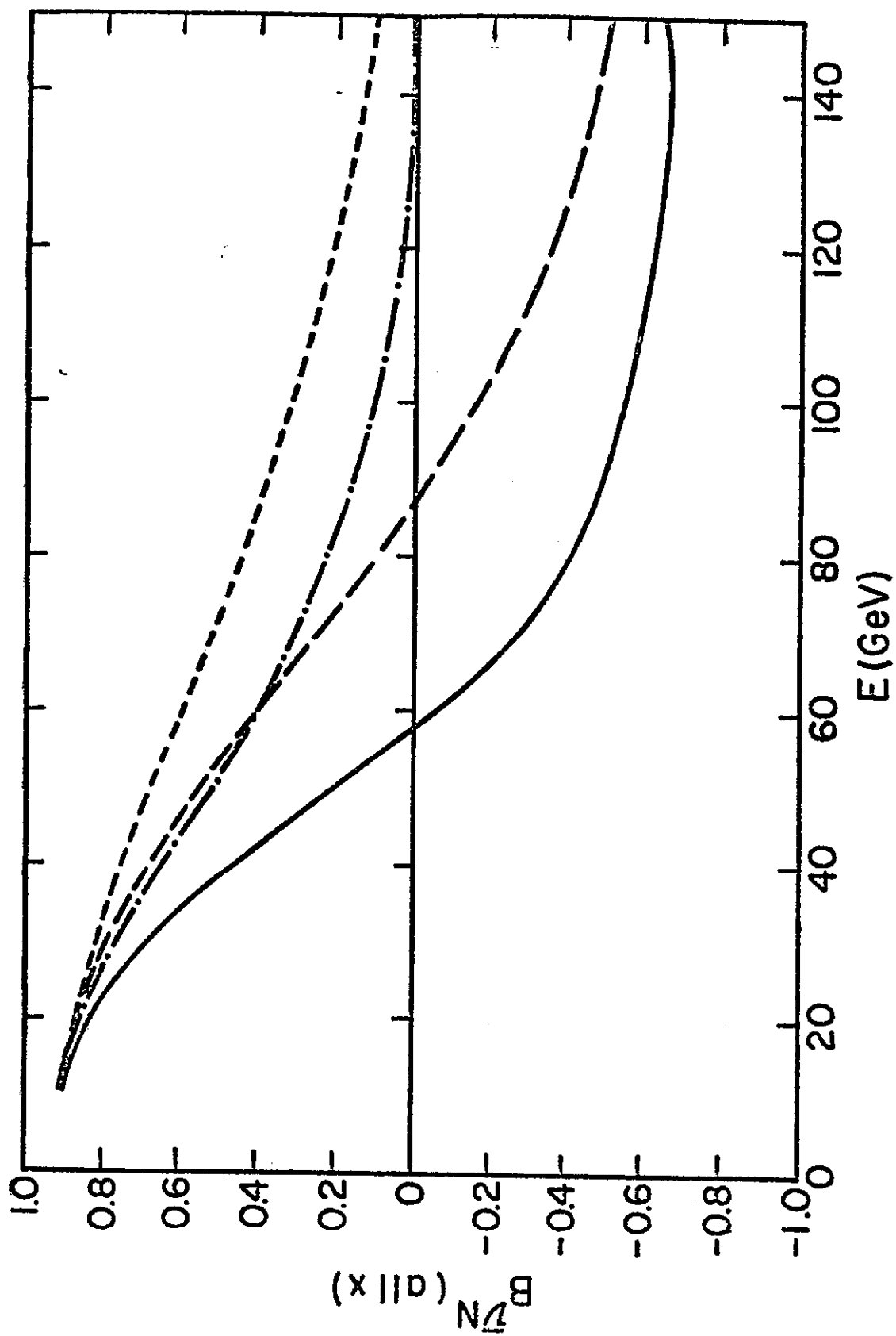


Fig. 12

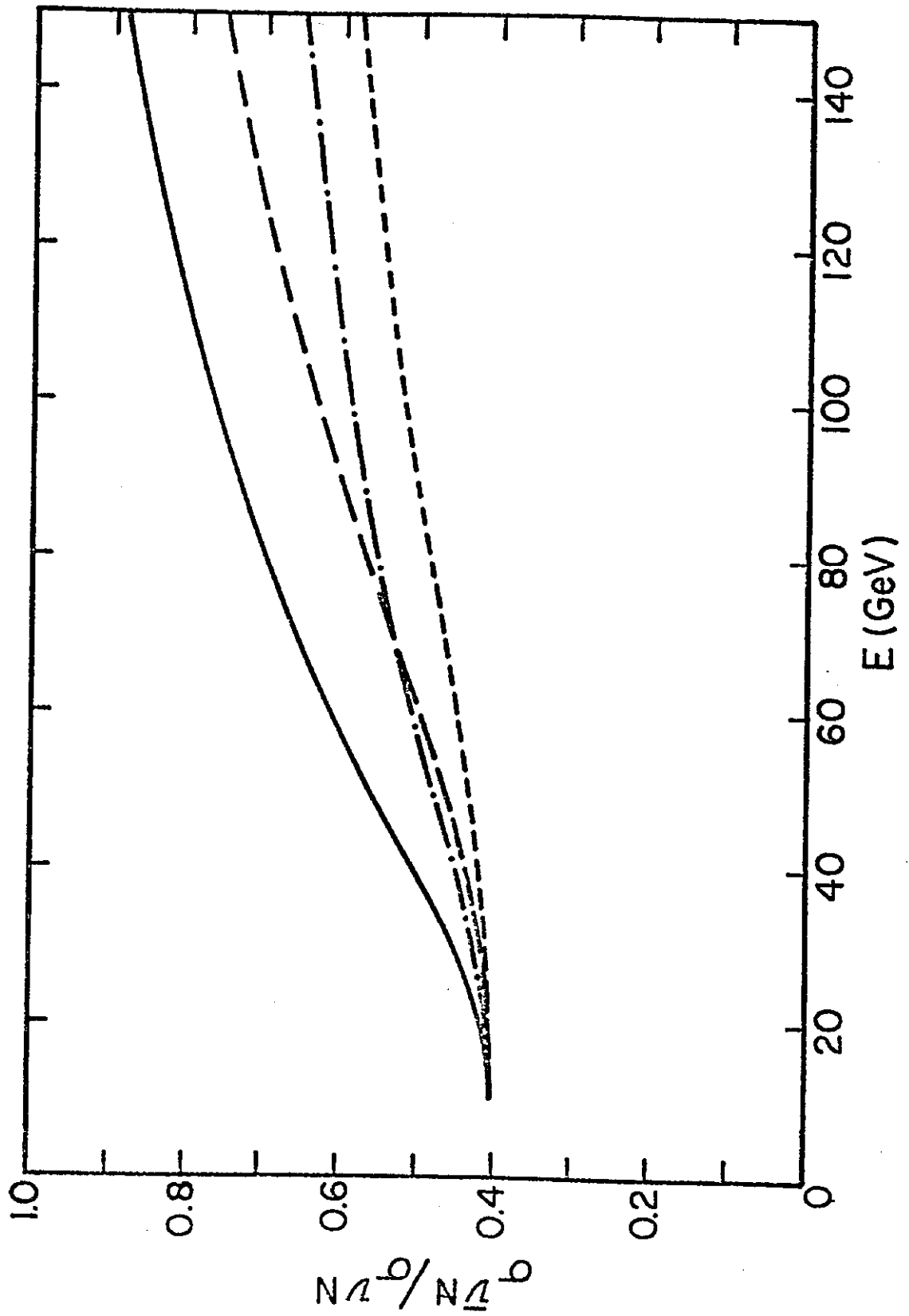


Fig. 13

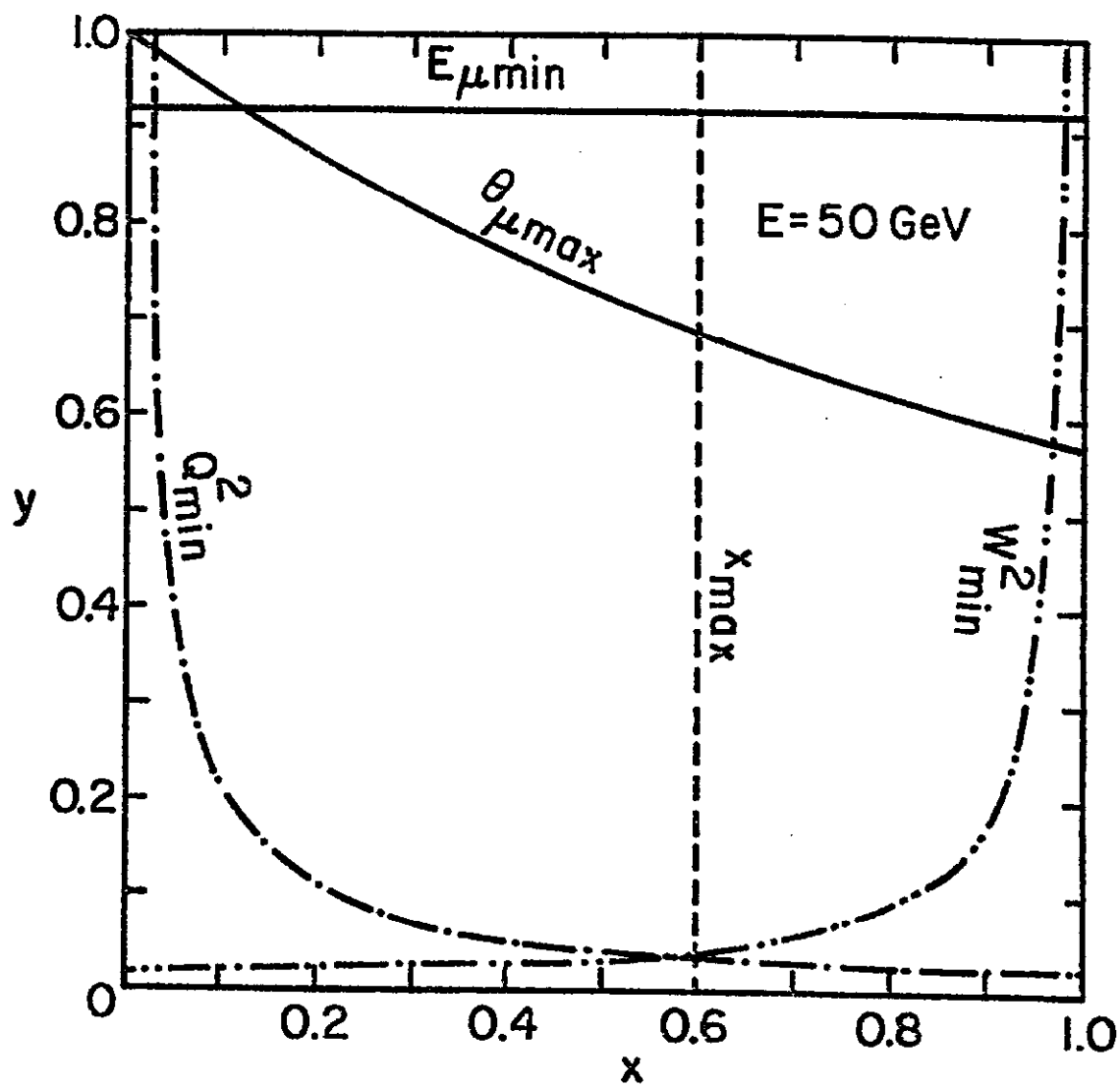


Fig. 14

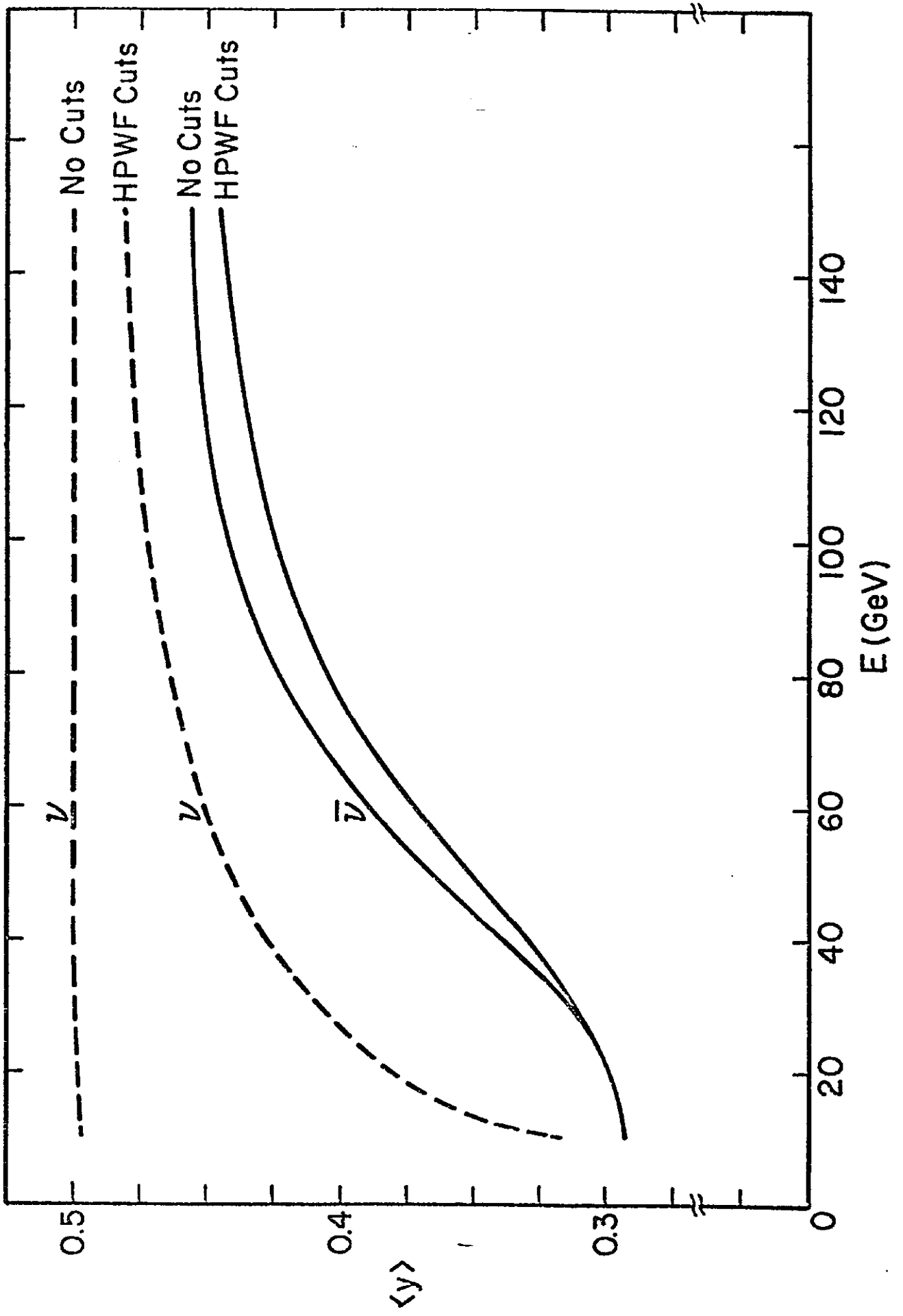


Fig. 15

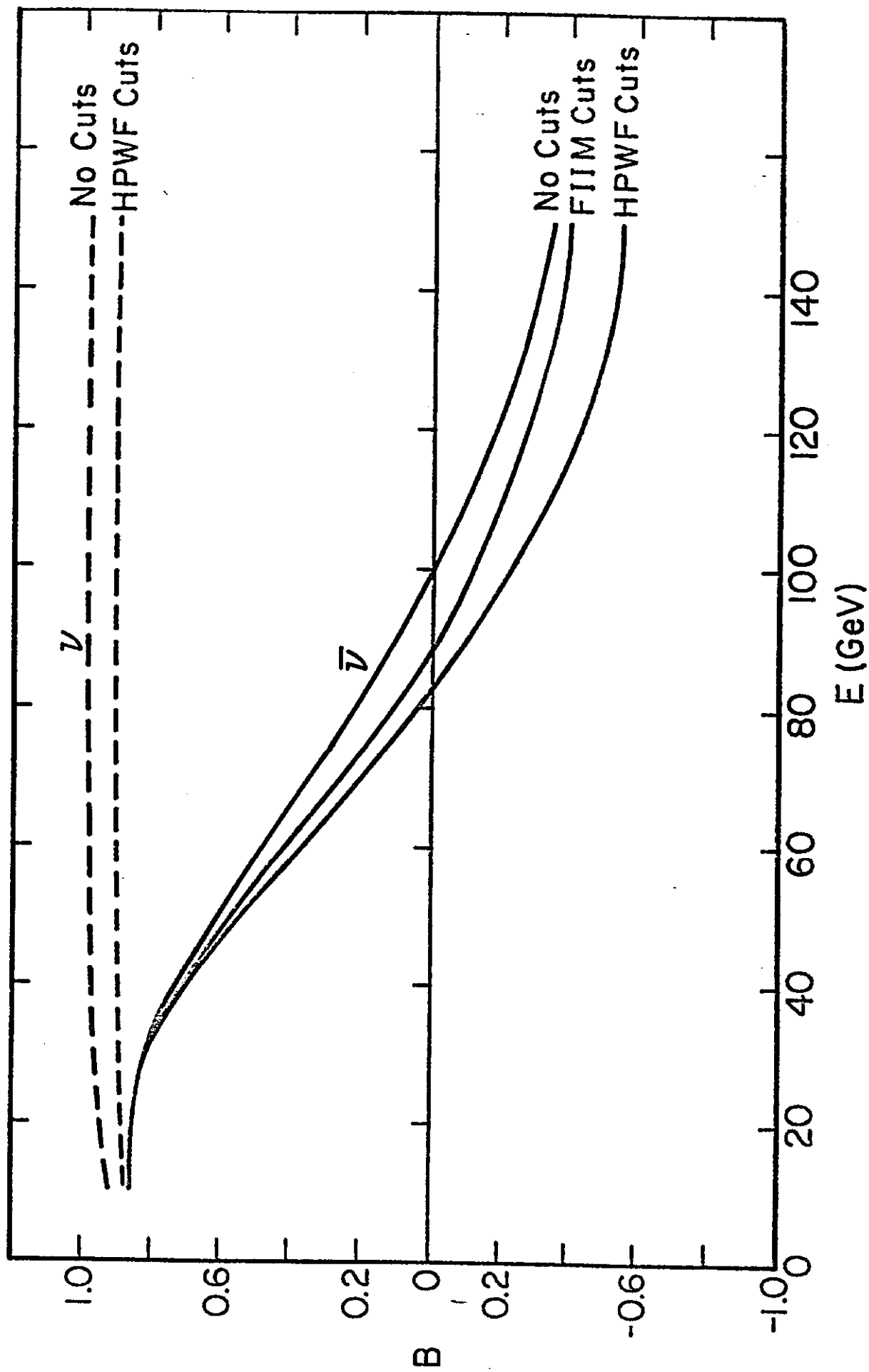


Fig. 16

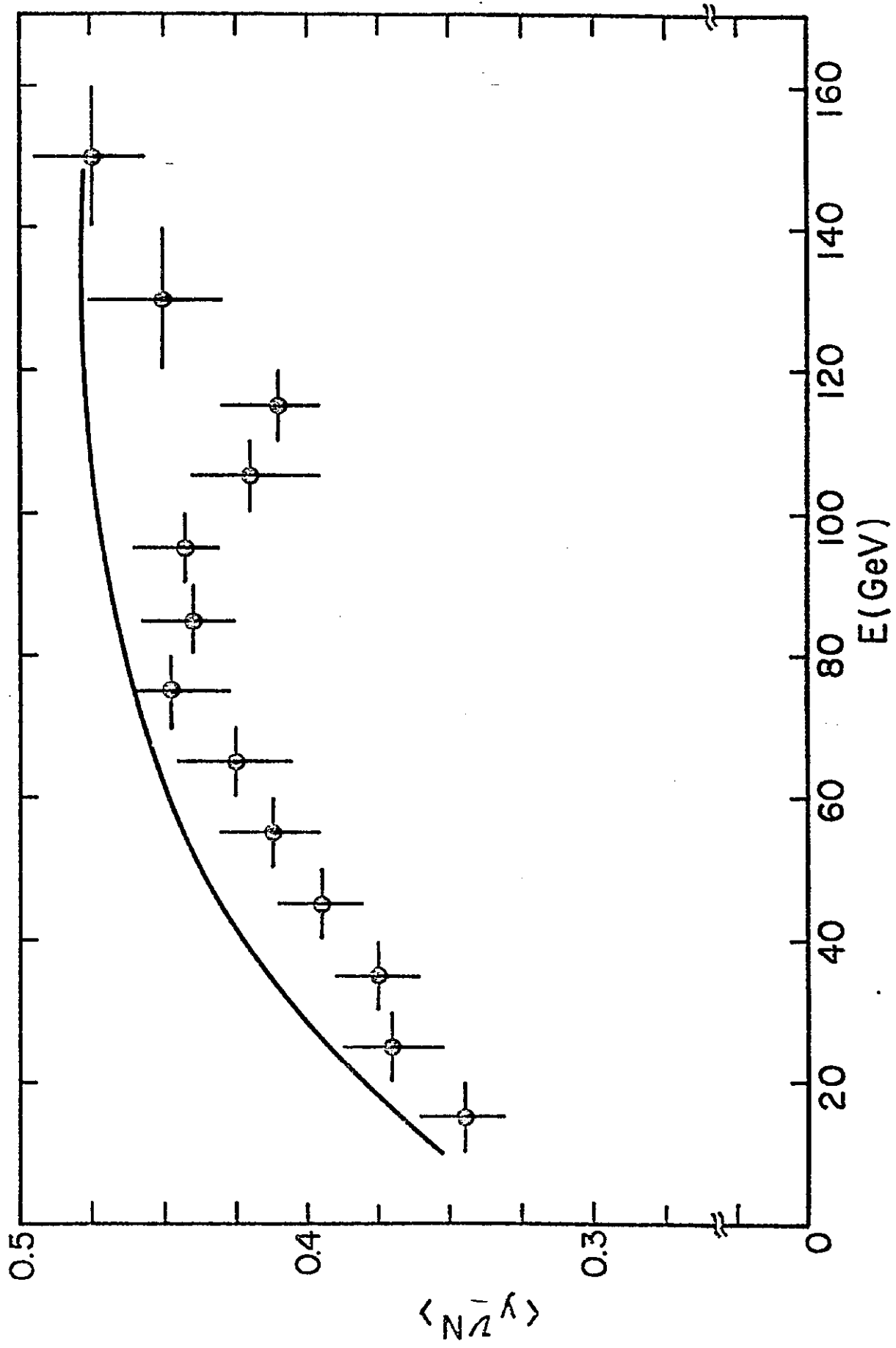


Fig. 17

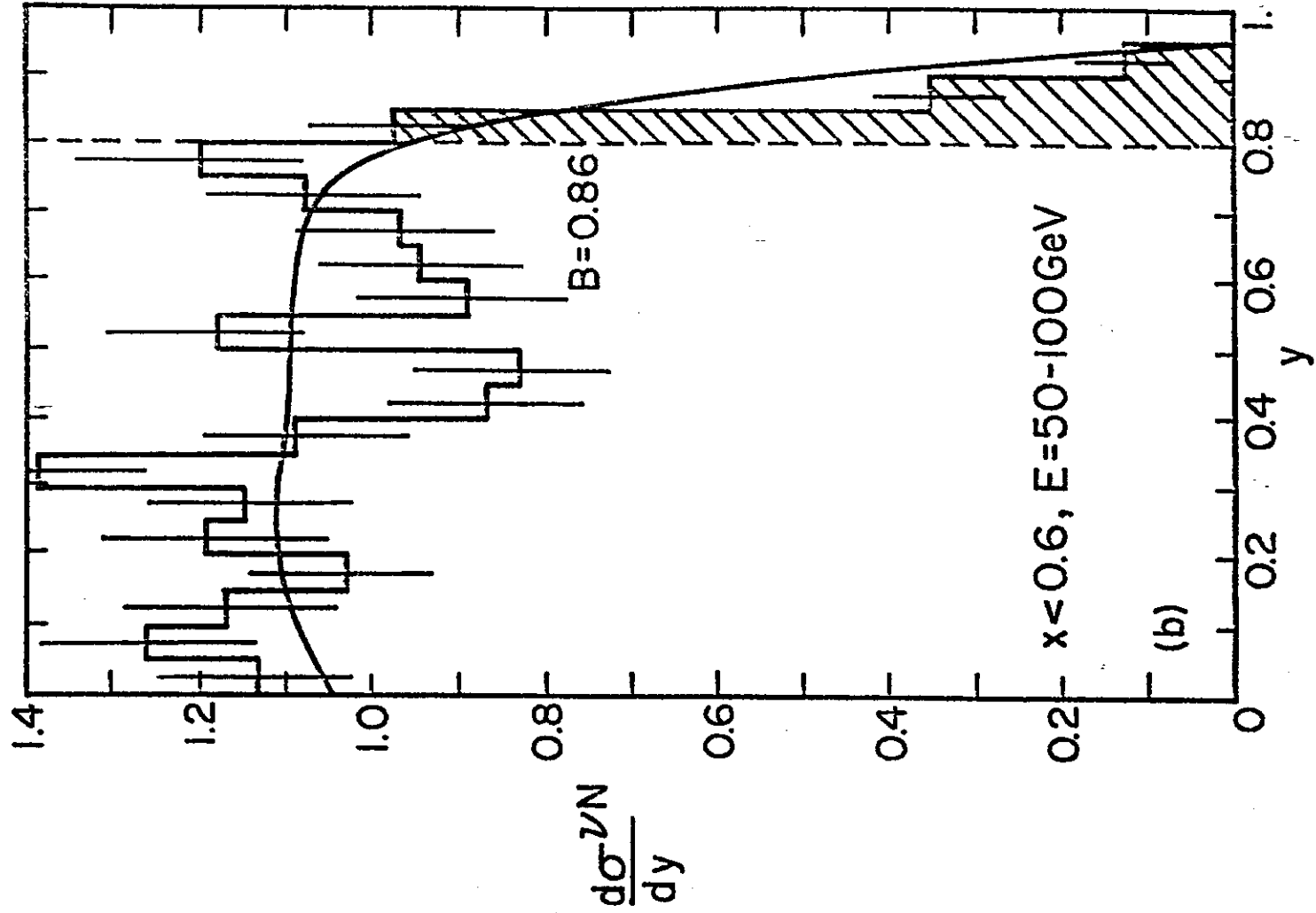
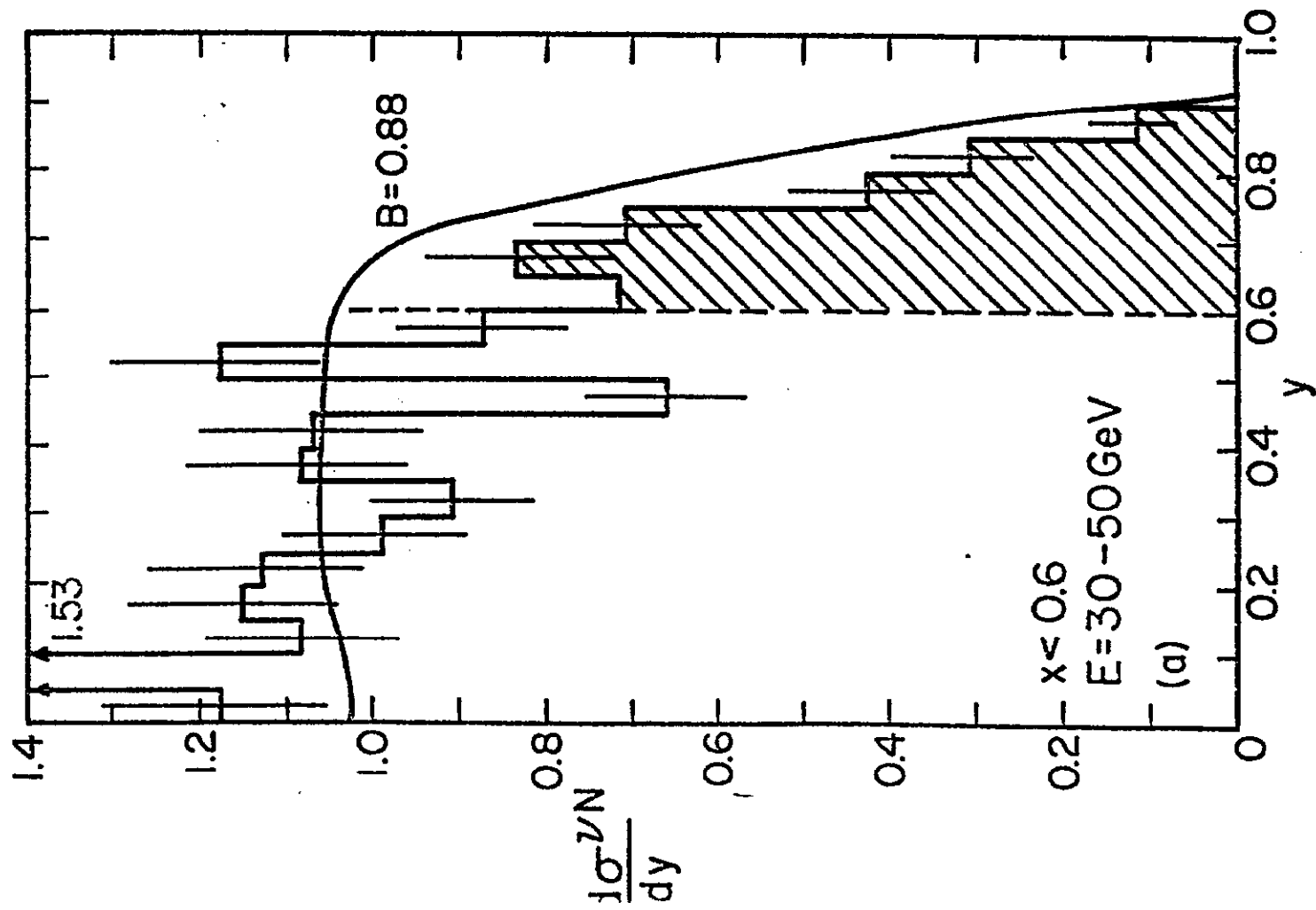


Fig. 18

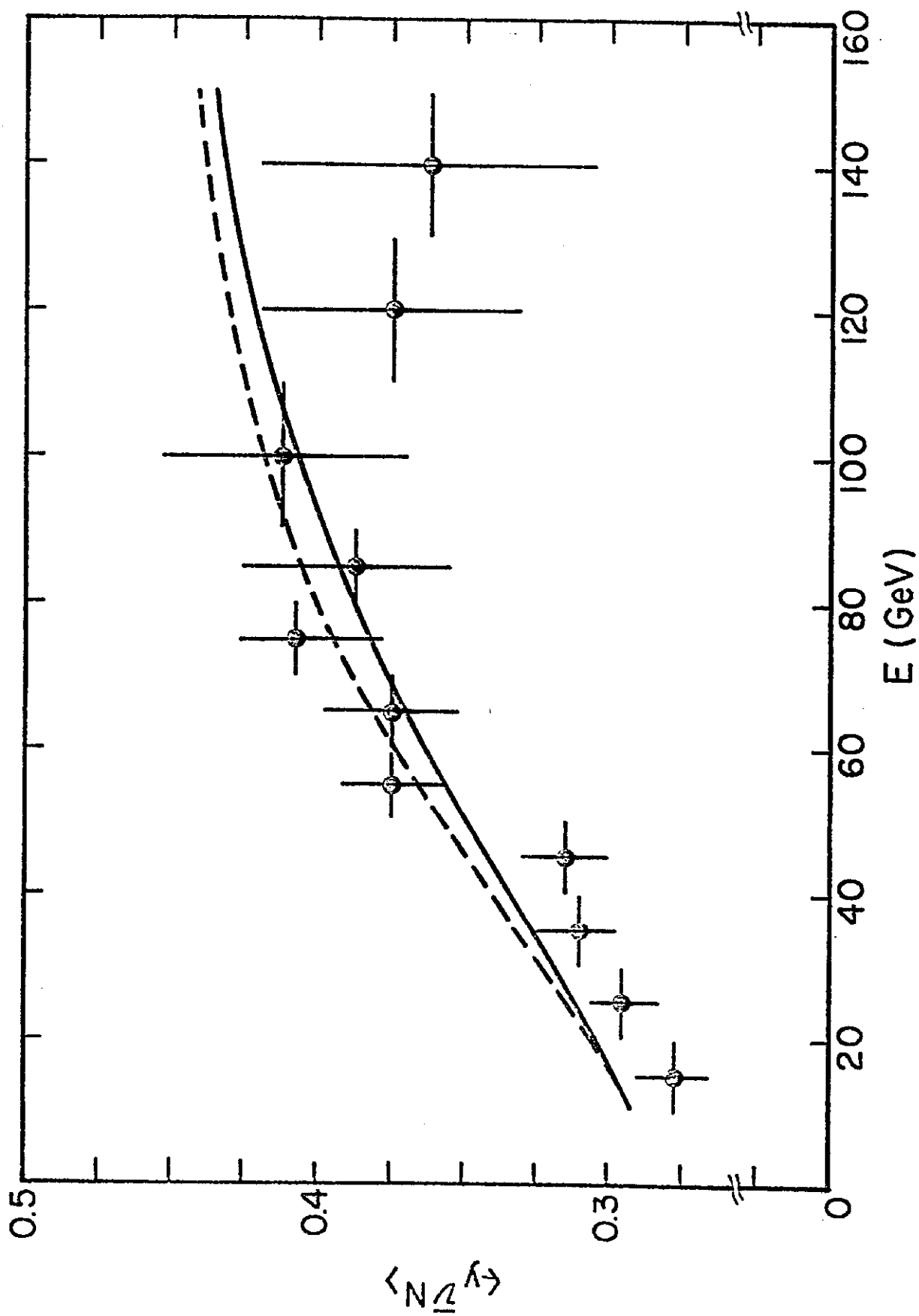


Fig. 19

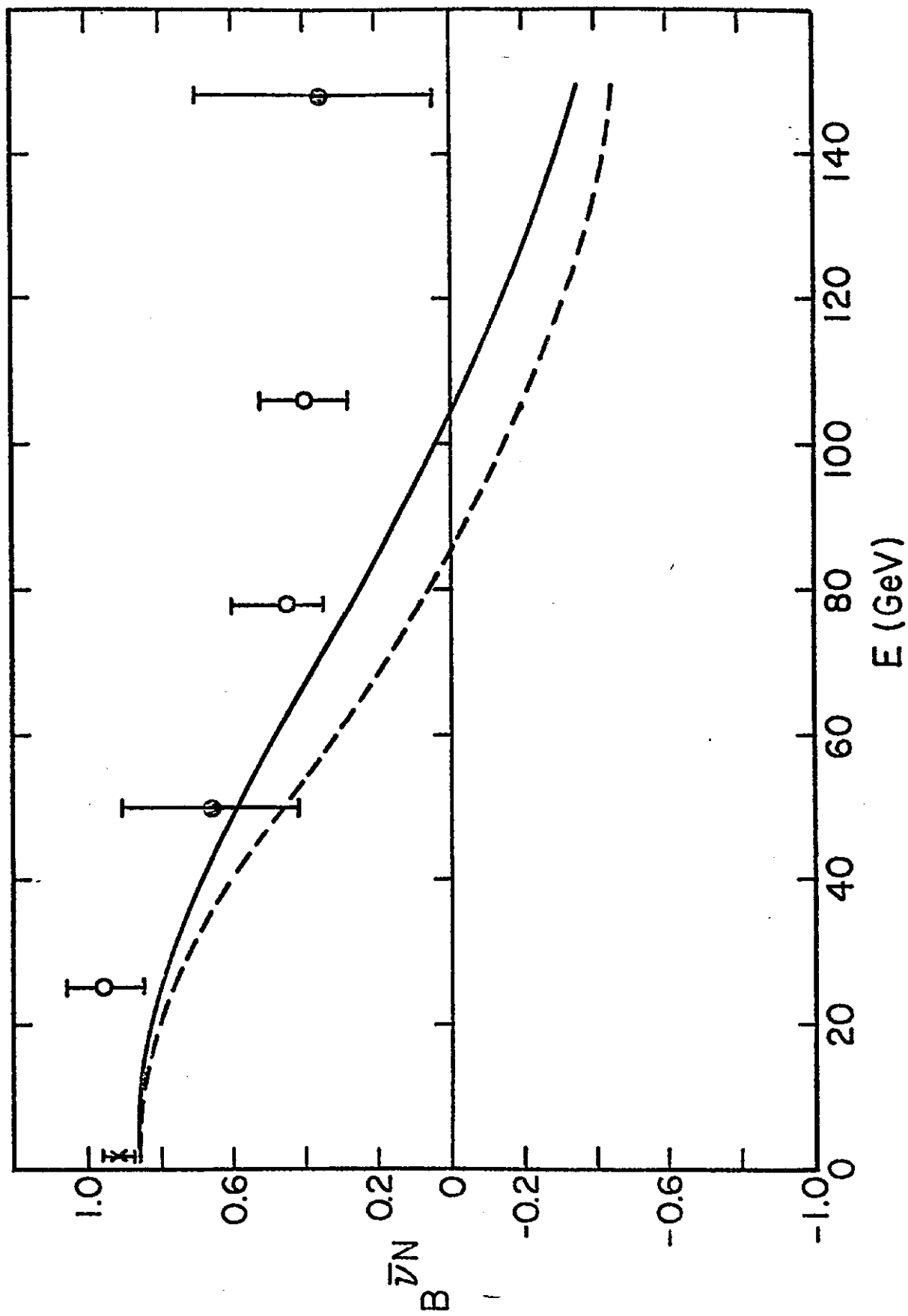


Fig. 20

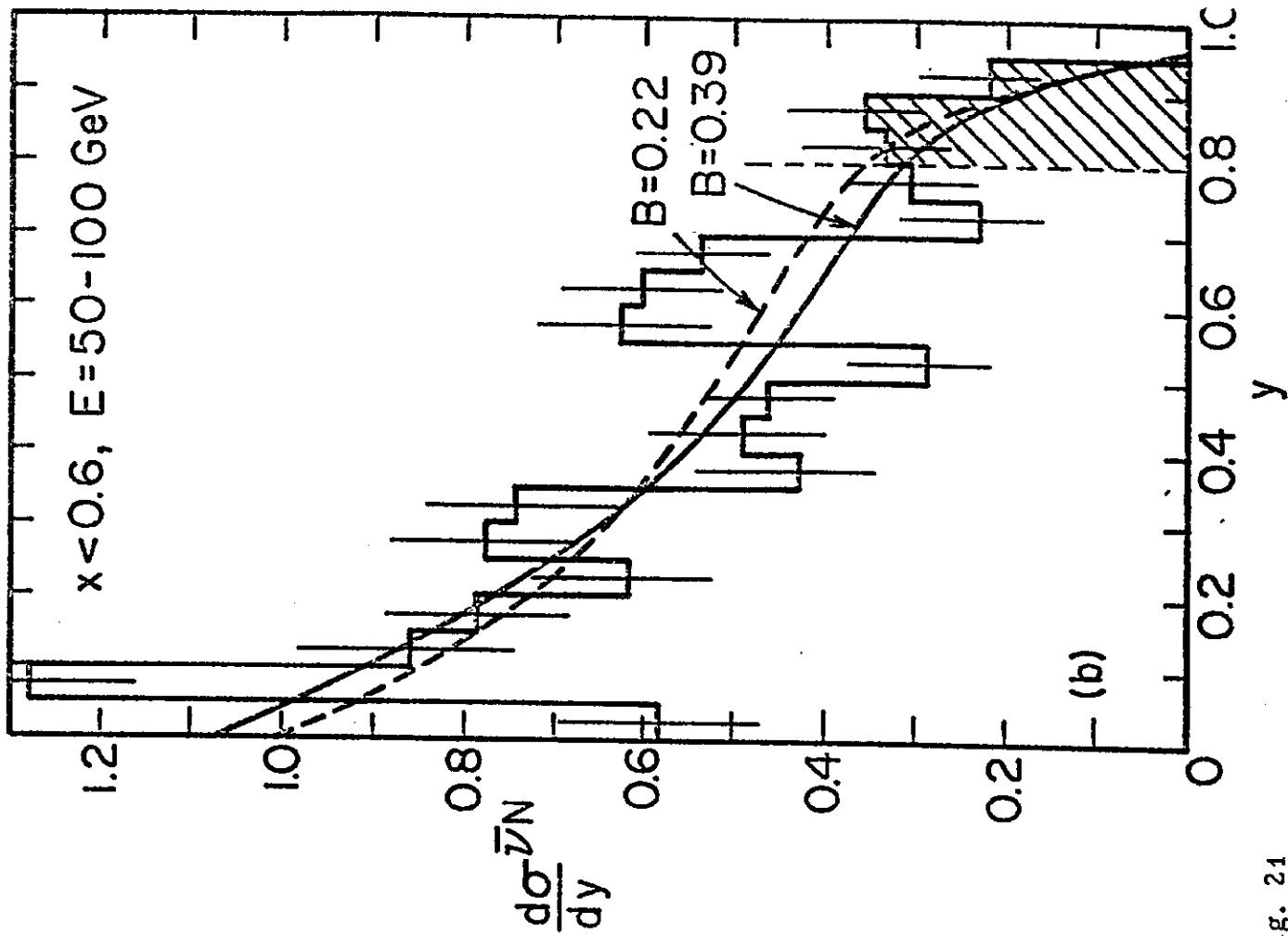
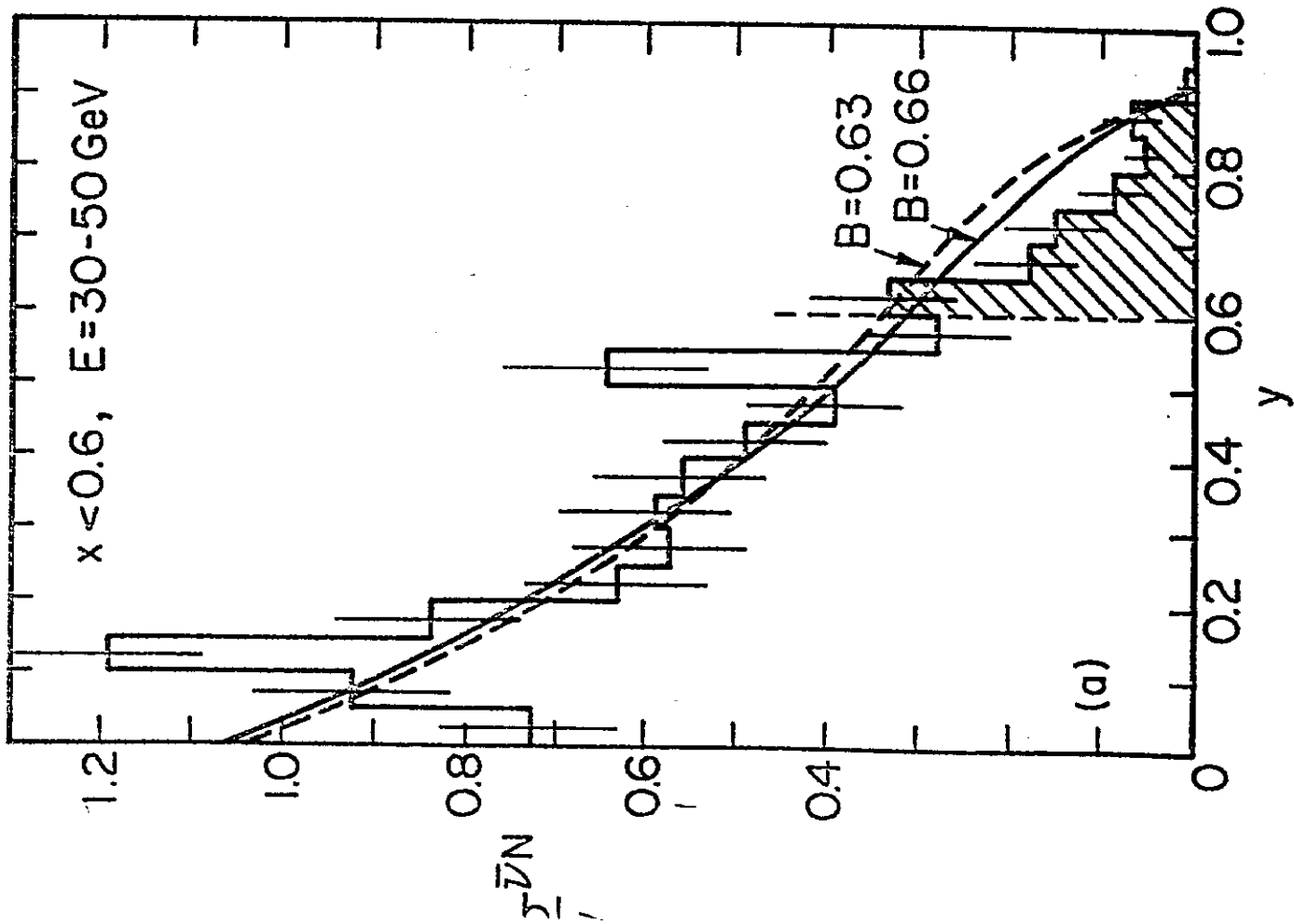


Fig. 21

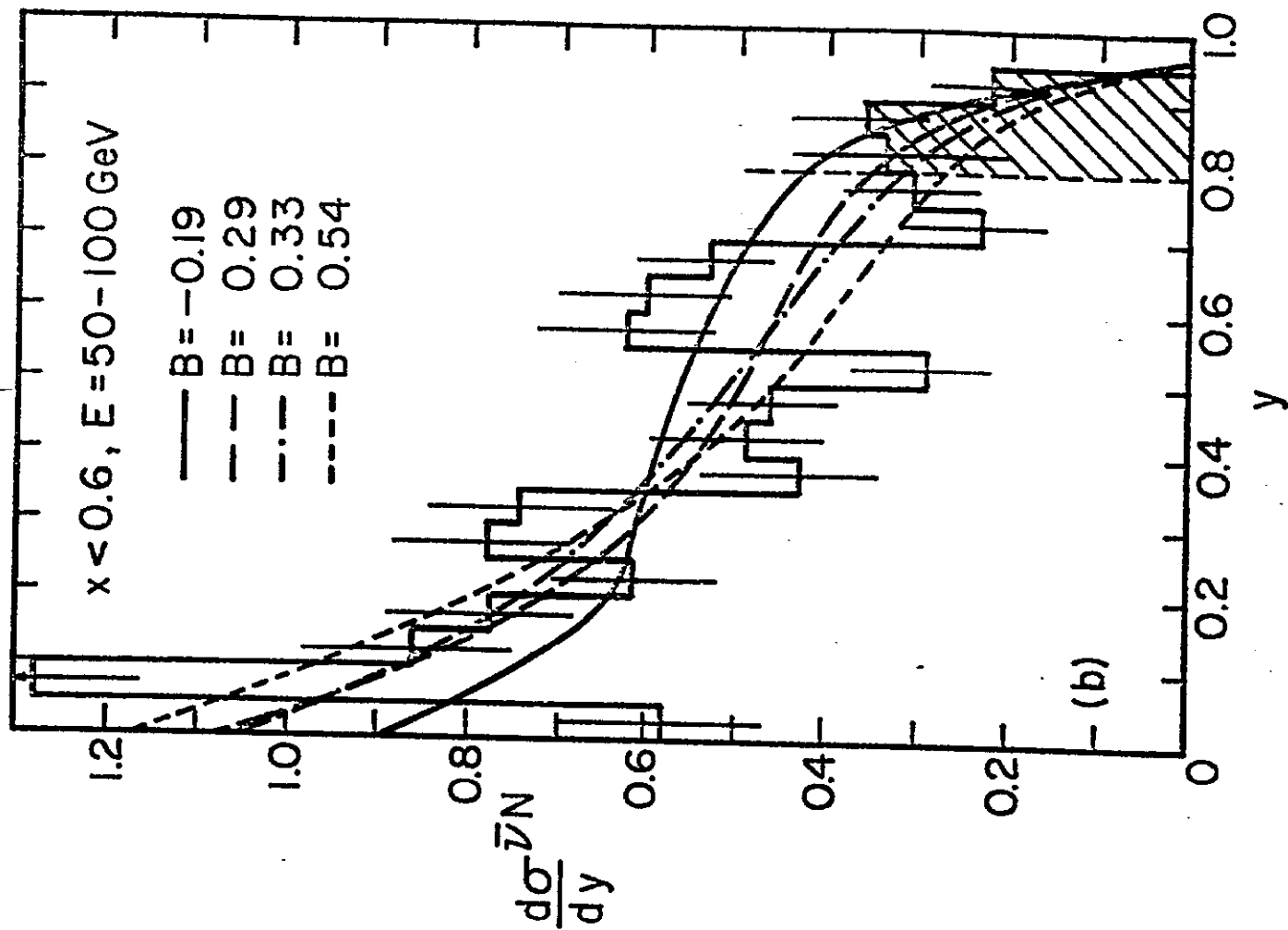
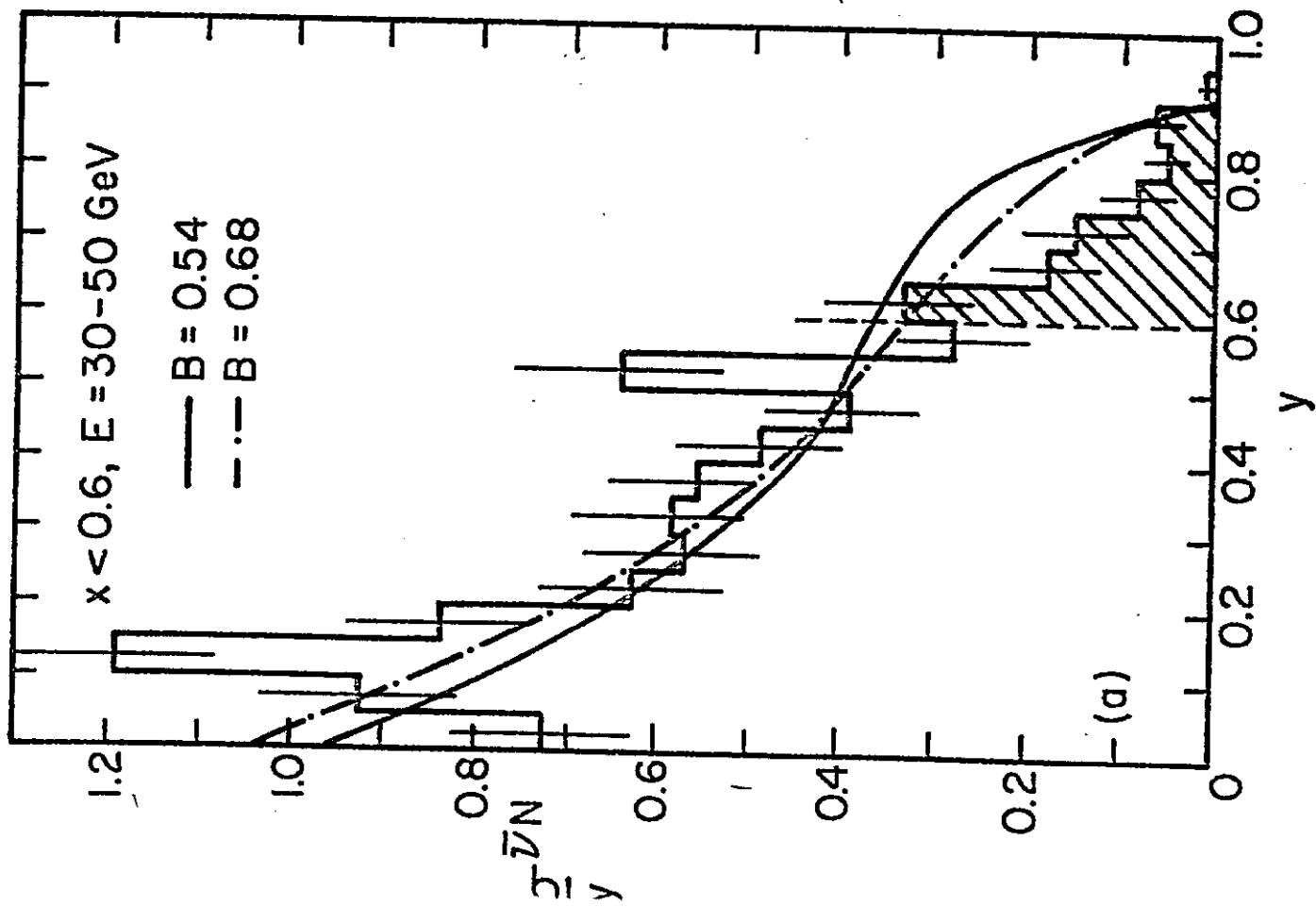


Fig. 22

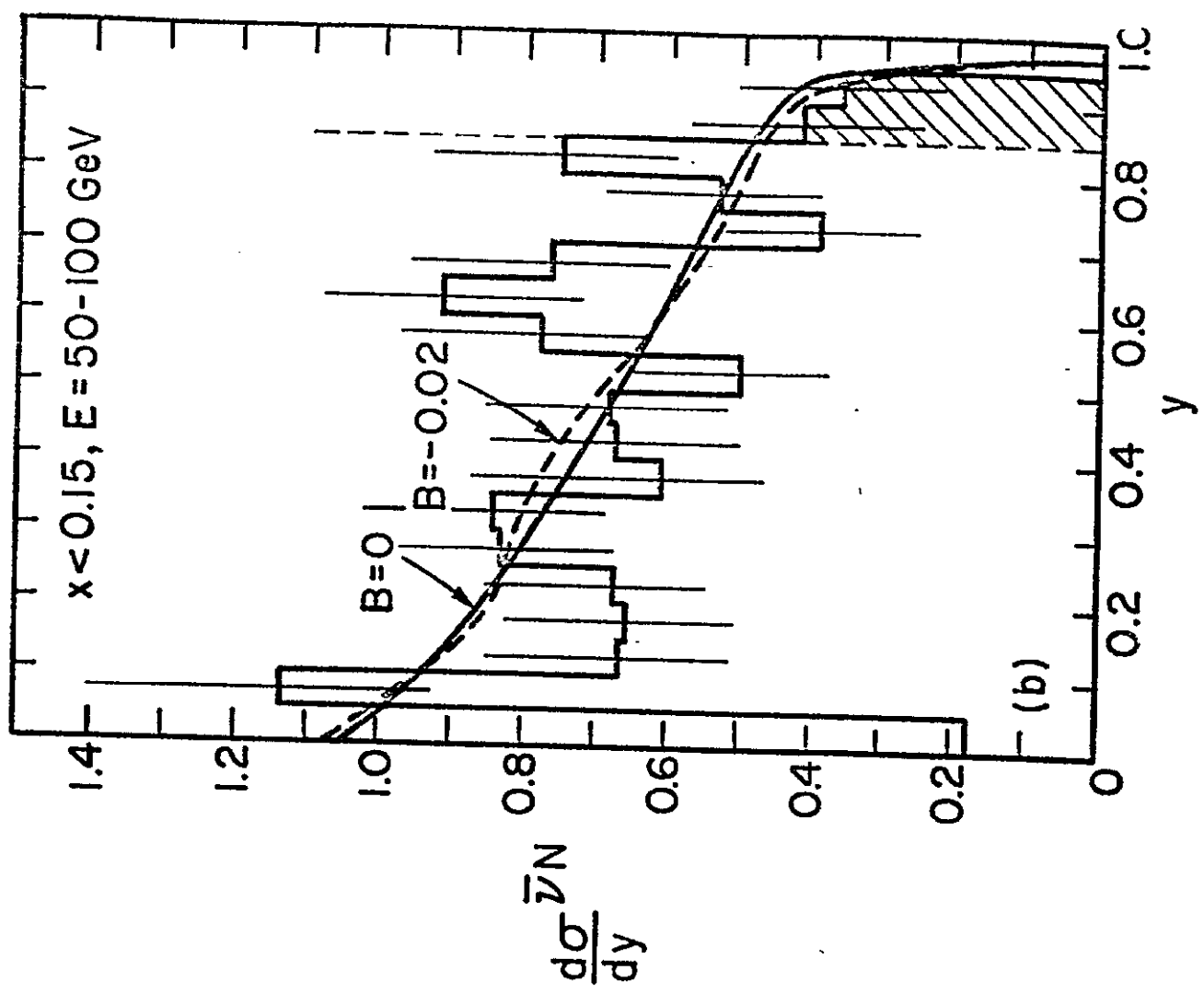
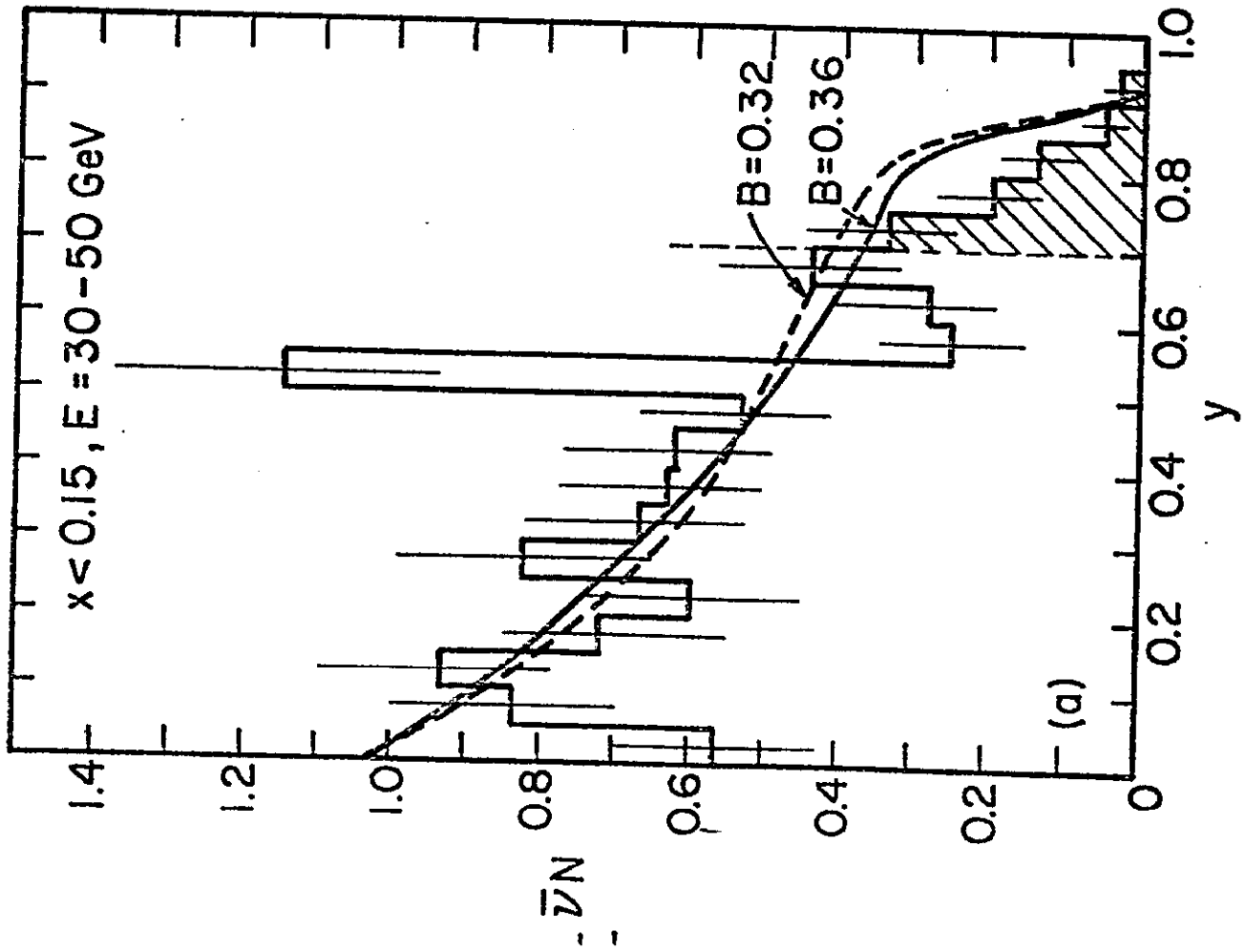


Fig. 23

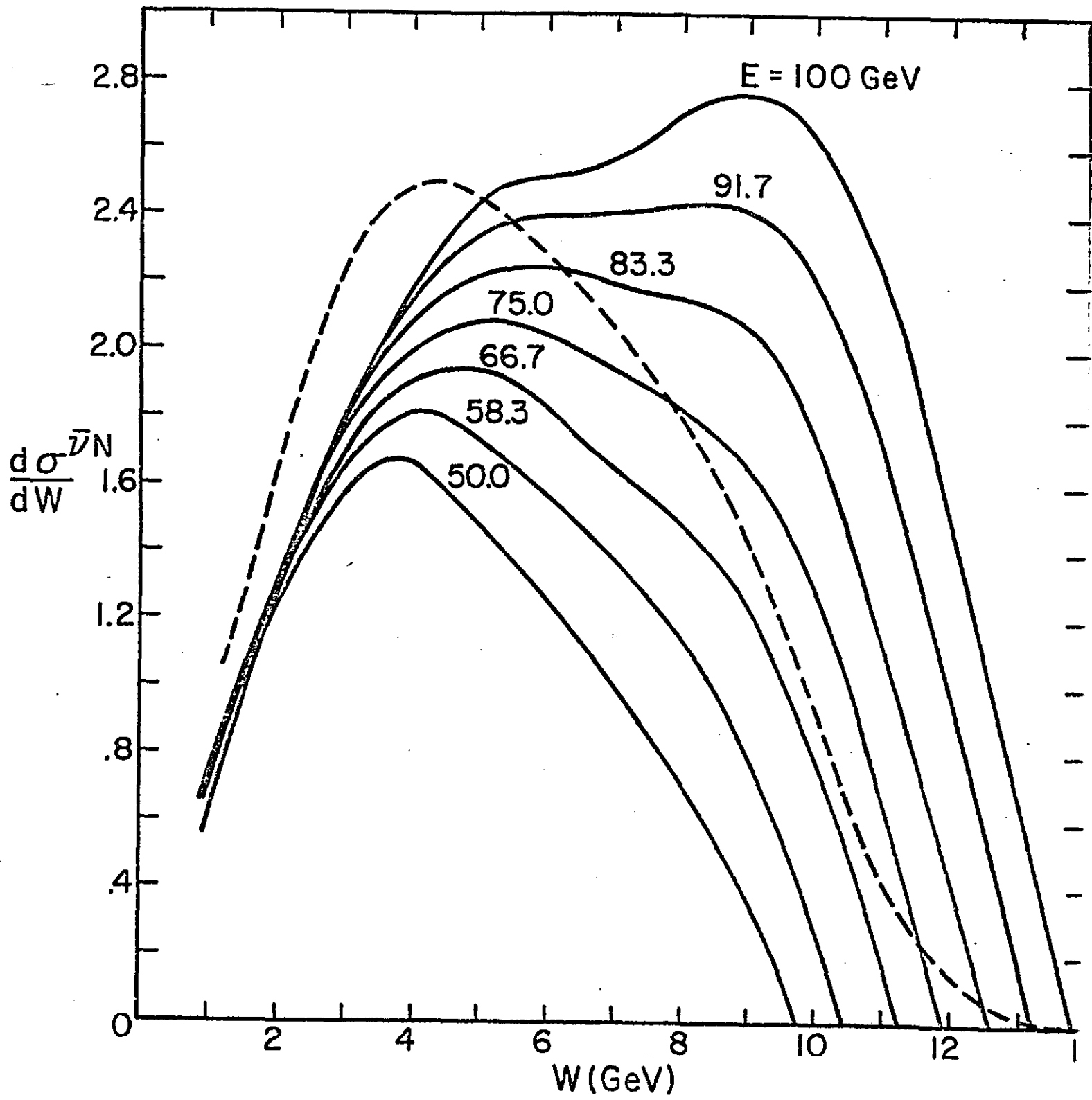


Fig. 24

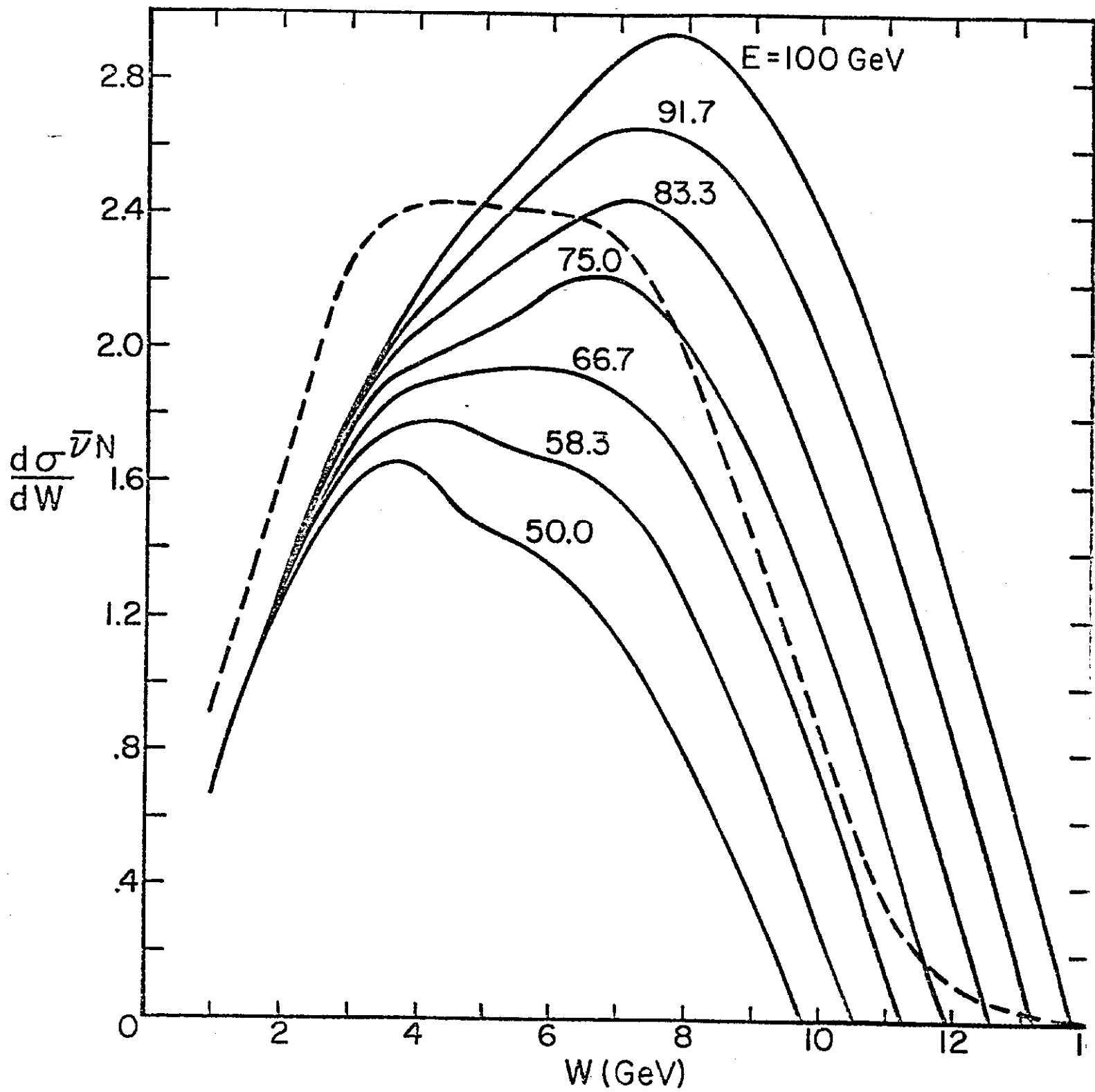


Fig. 25

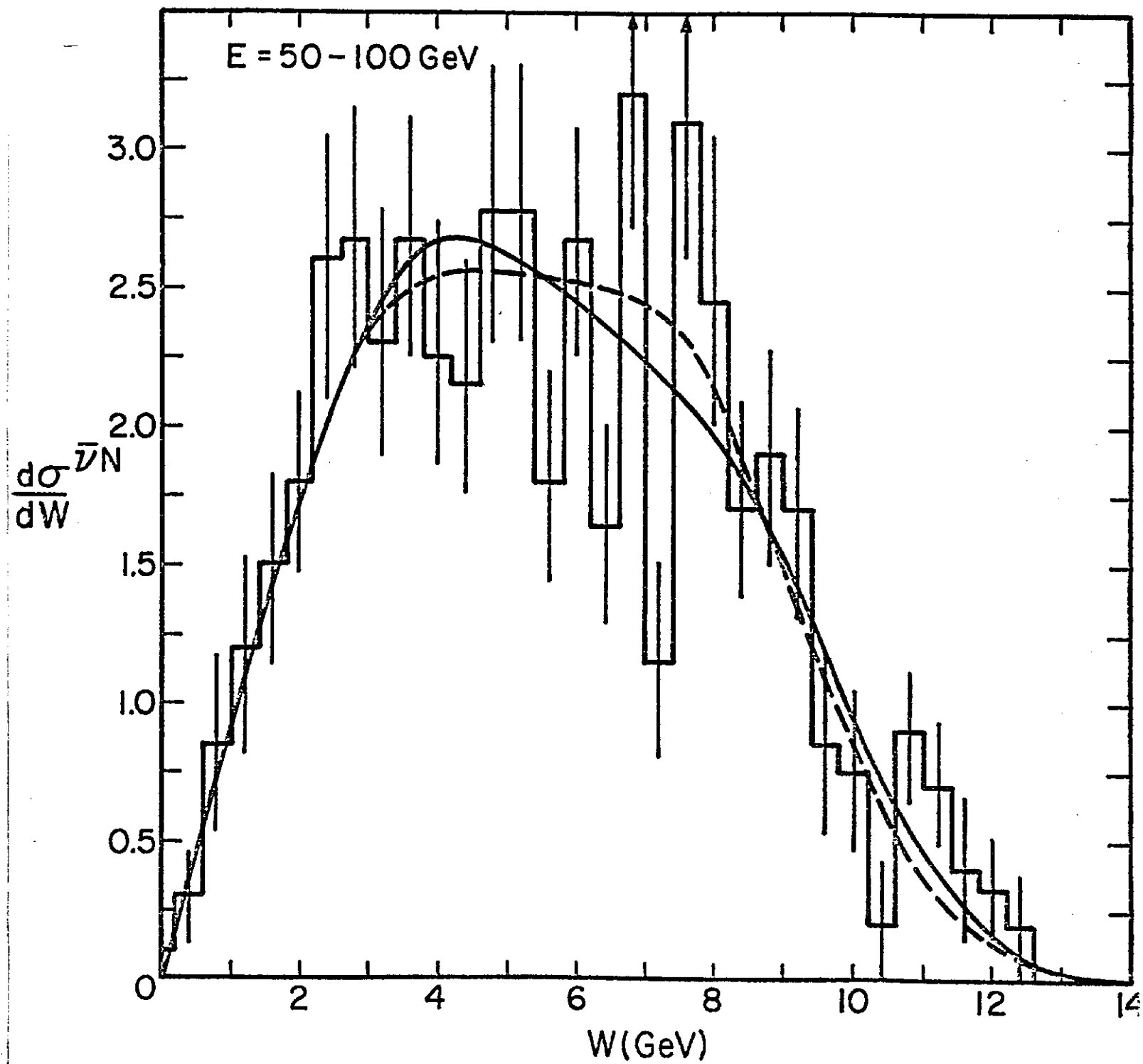


Fig. 26

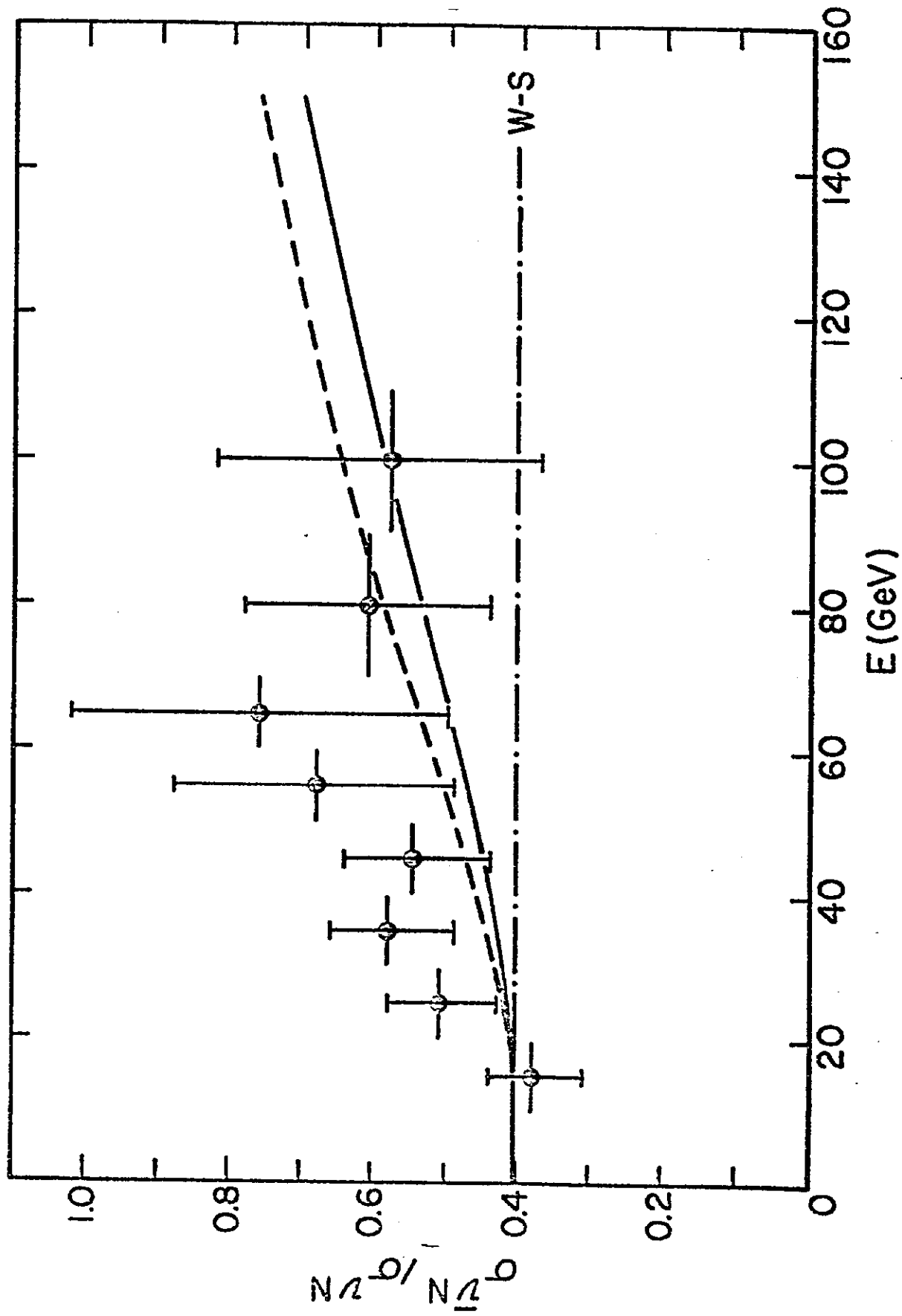


Fig. 27

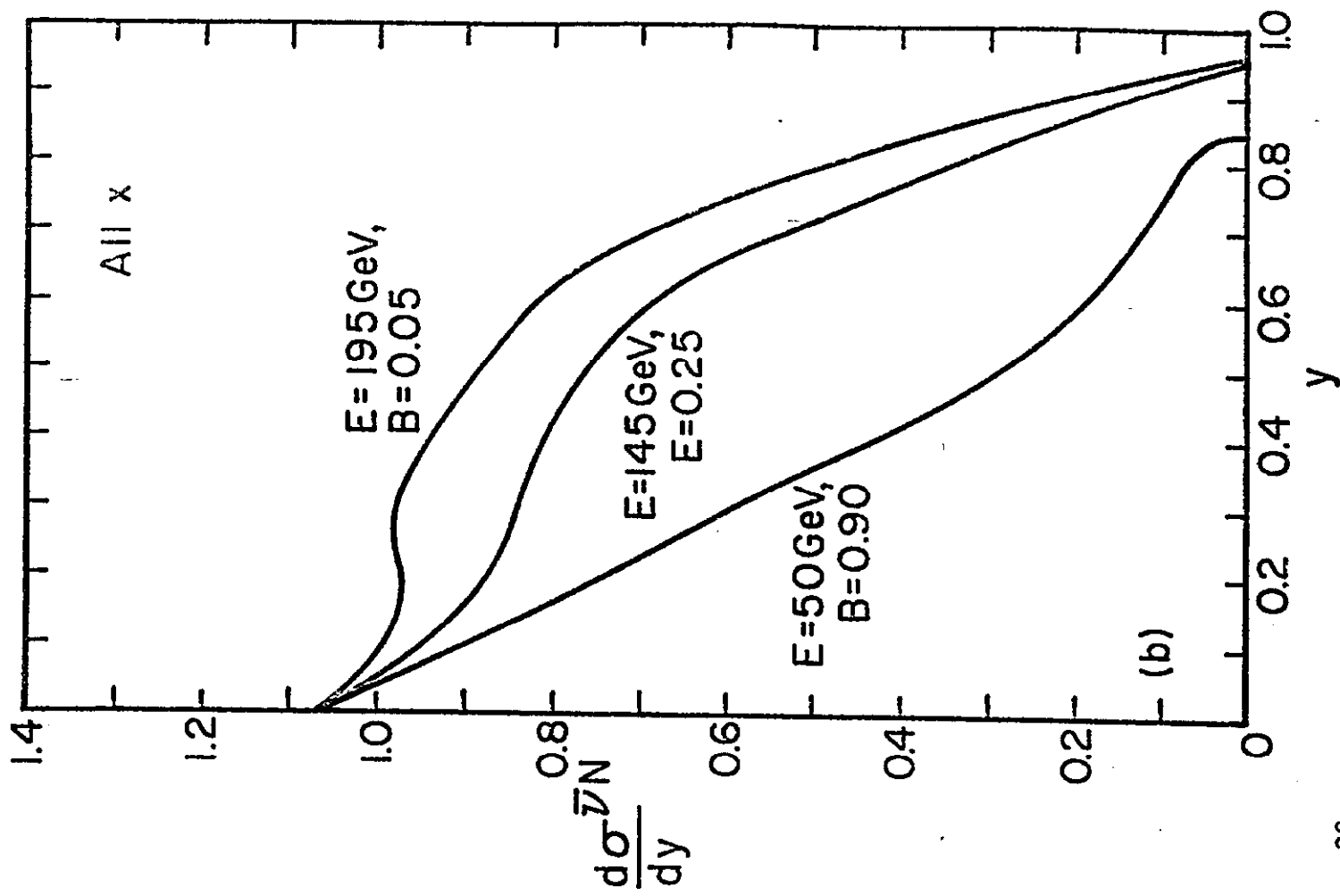
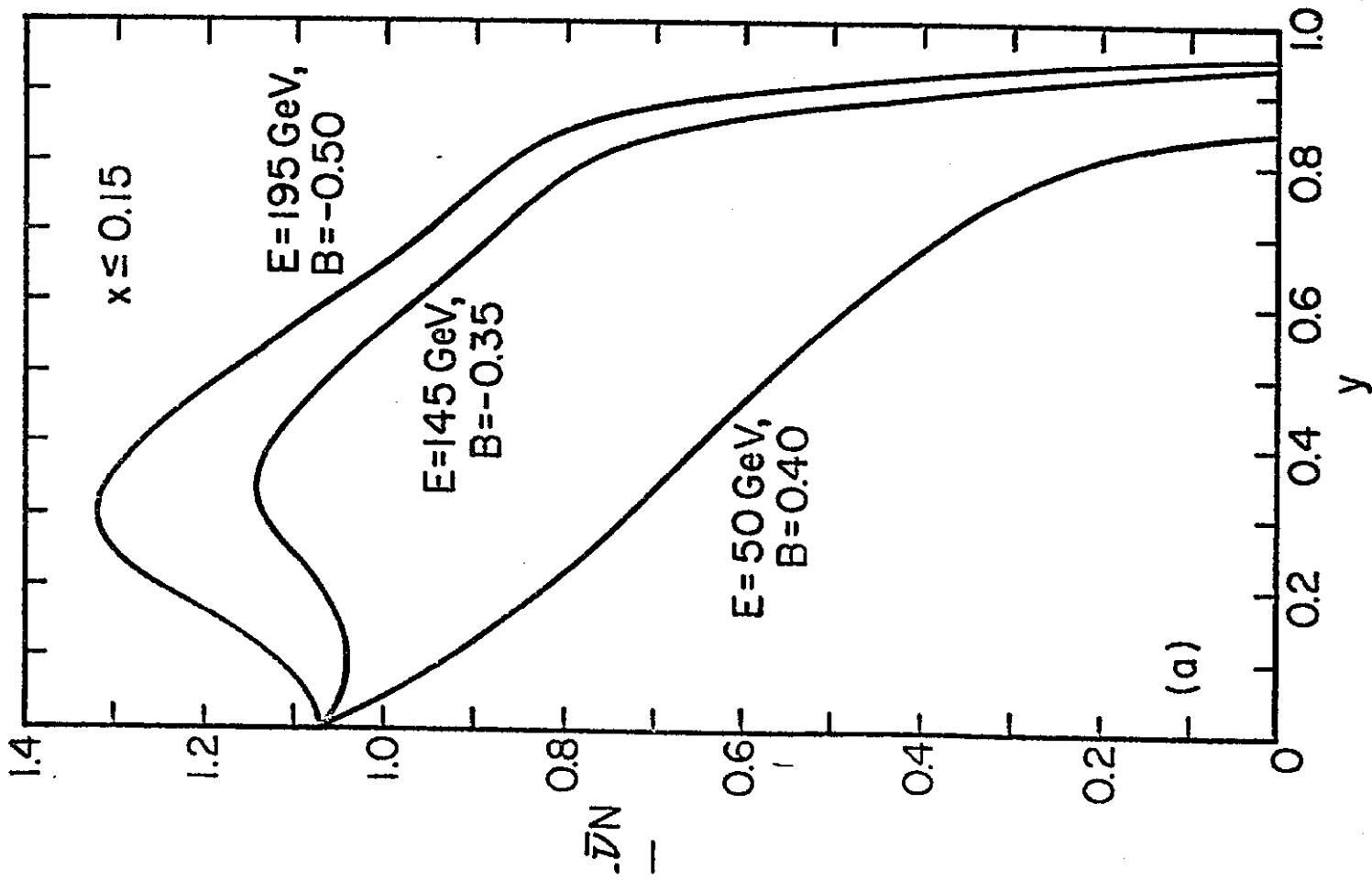


Fig. 28

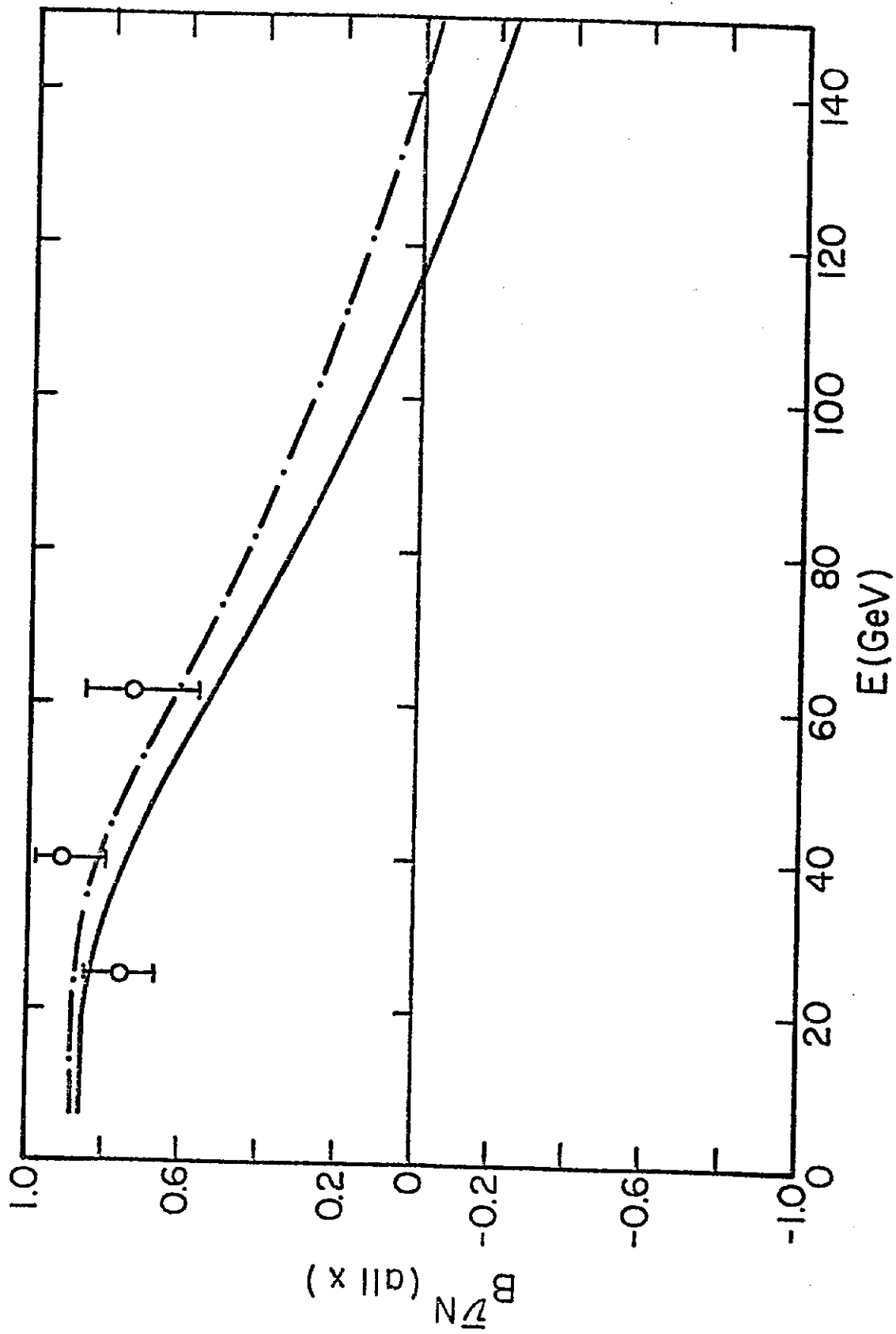


Fig. 29

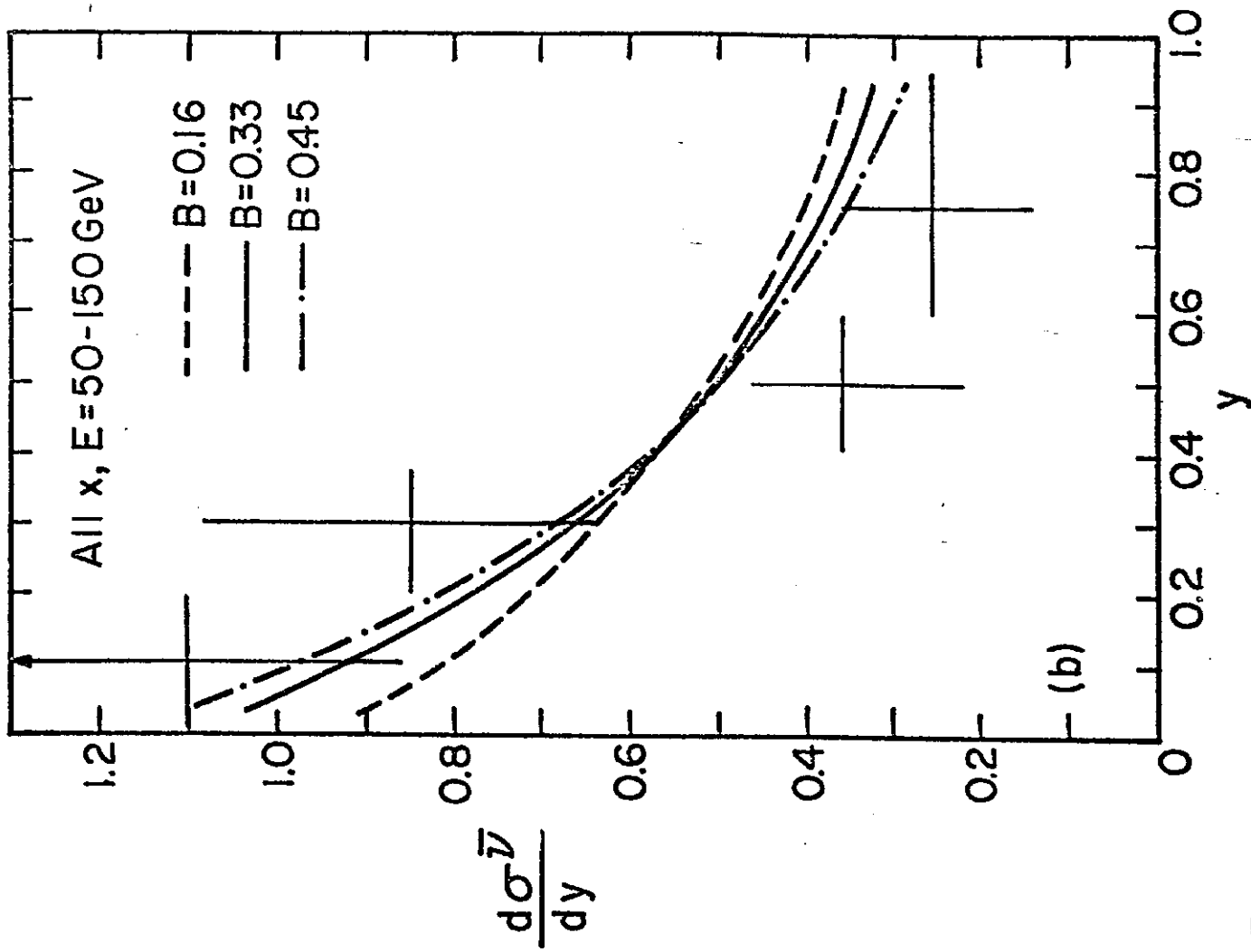
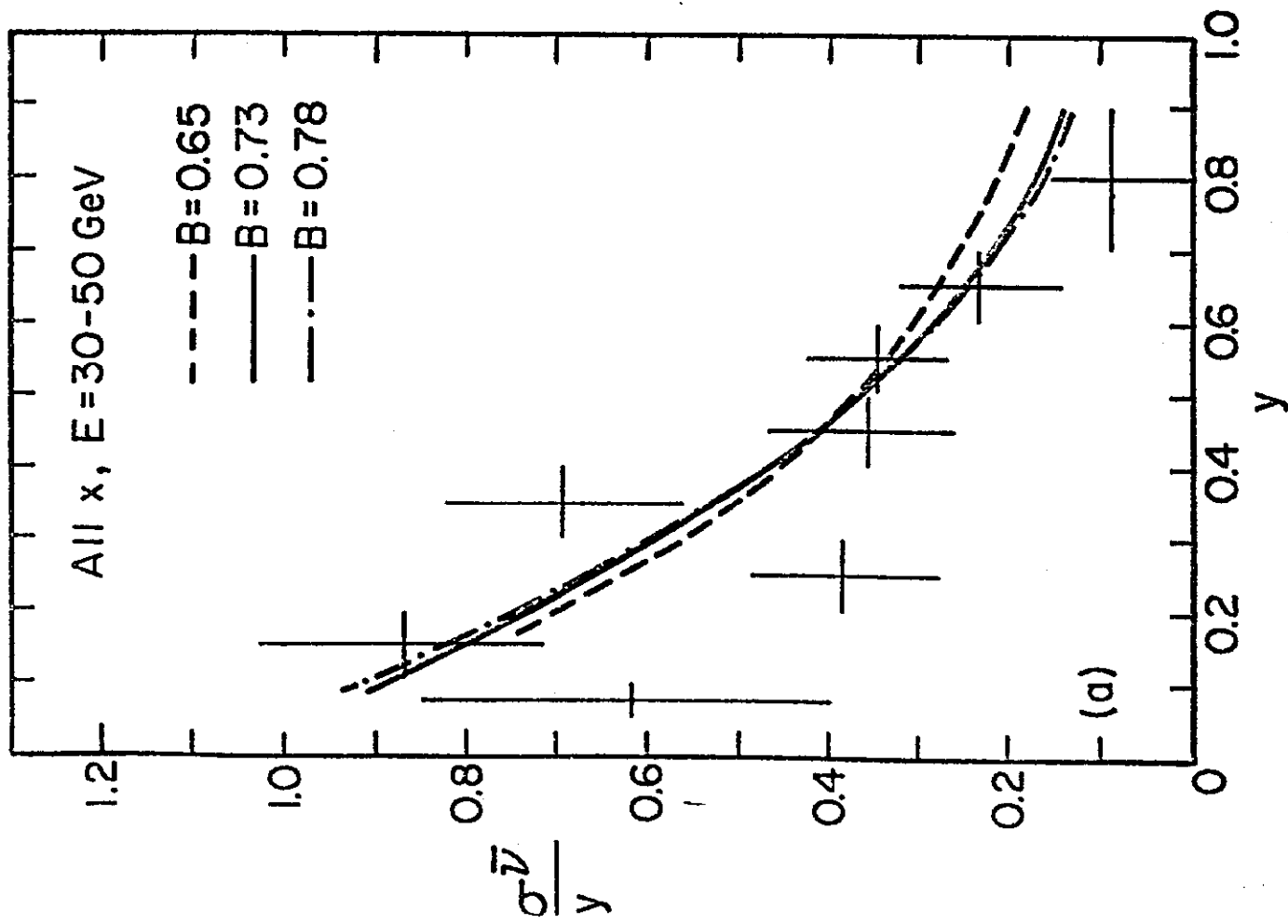


Fig. 30

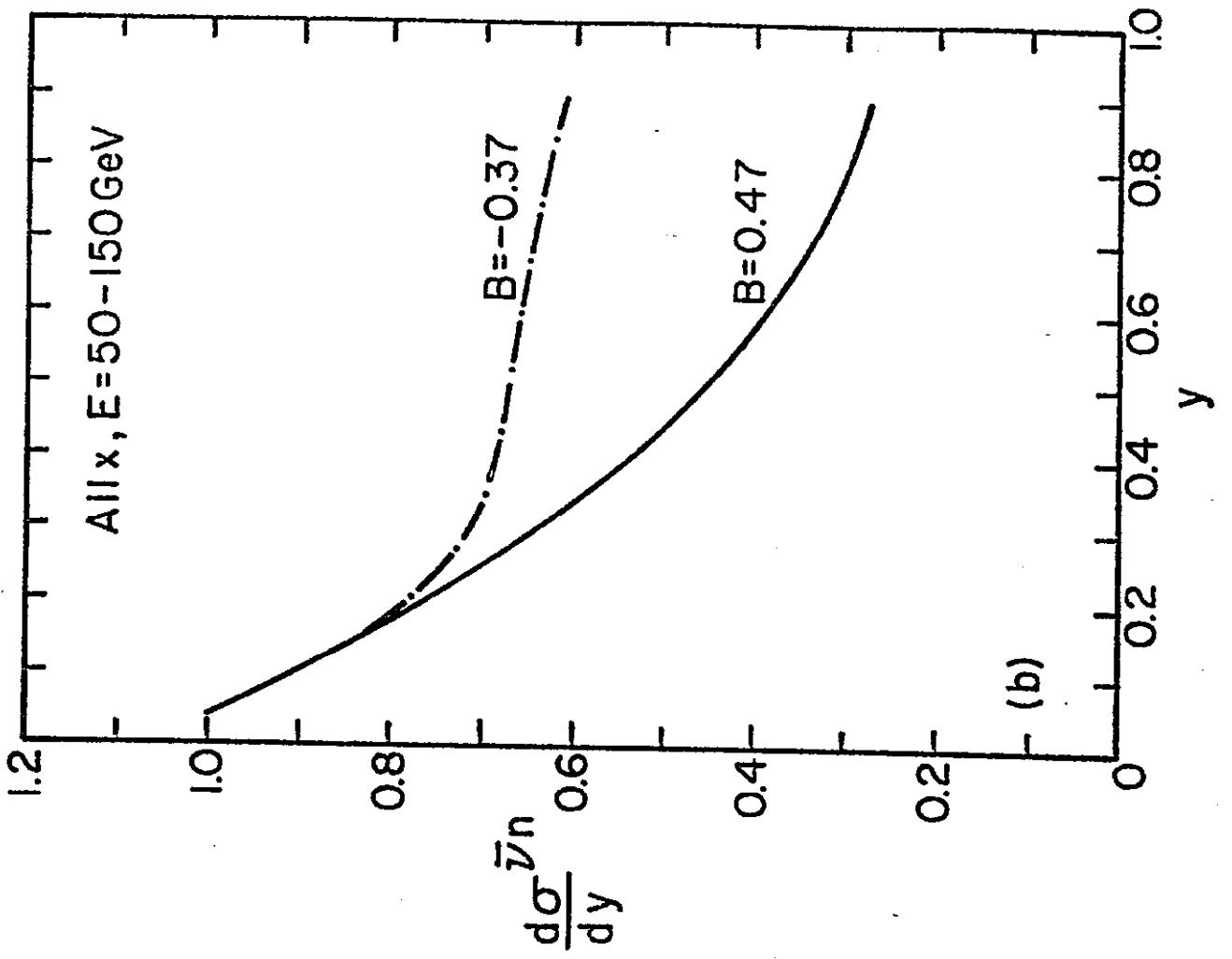
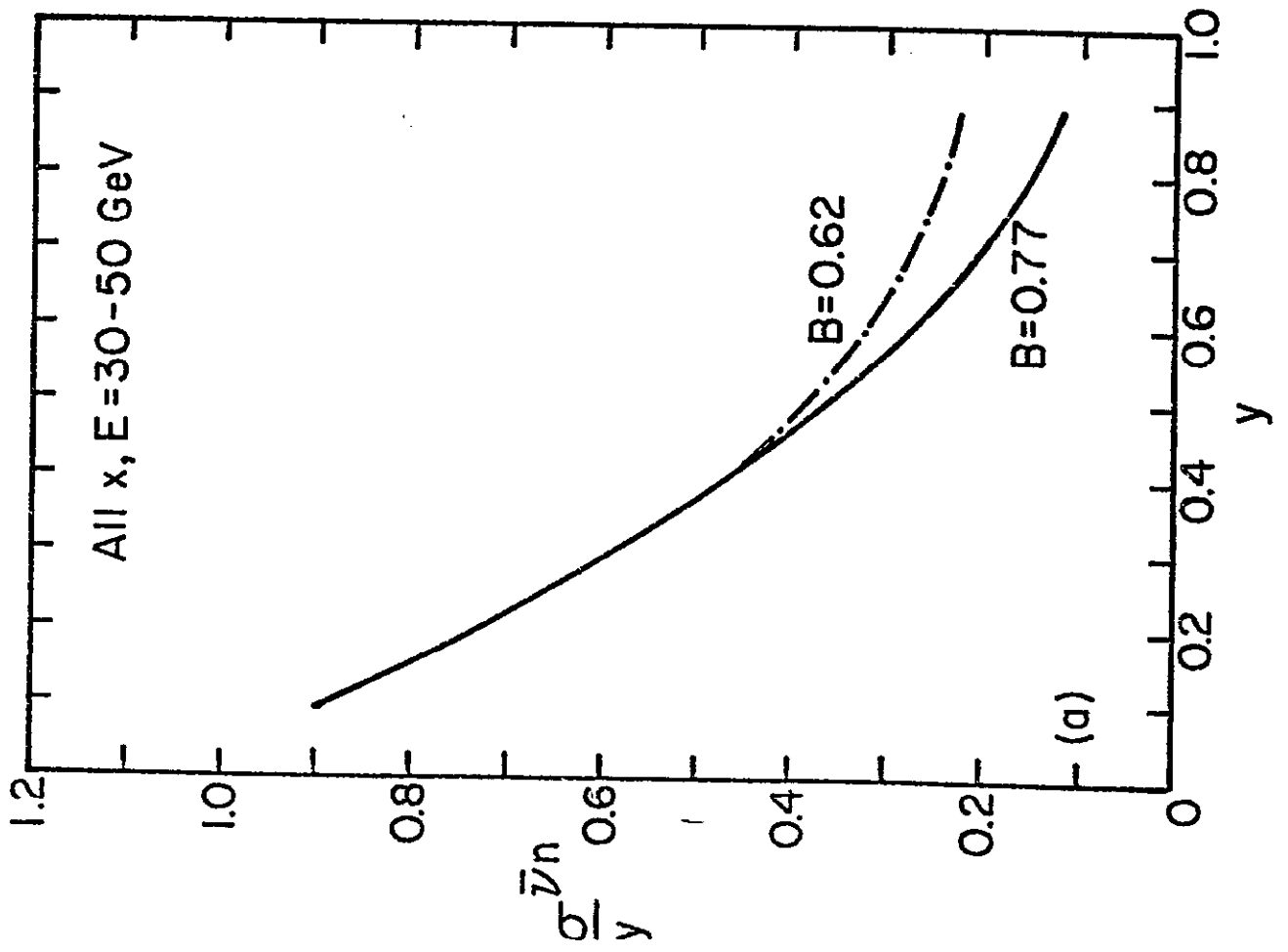


Fig. 31

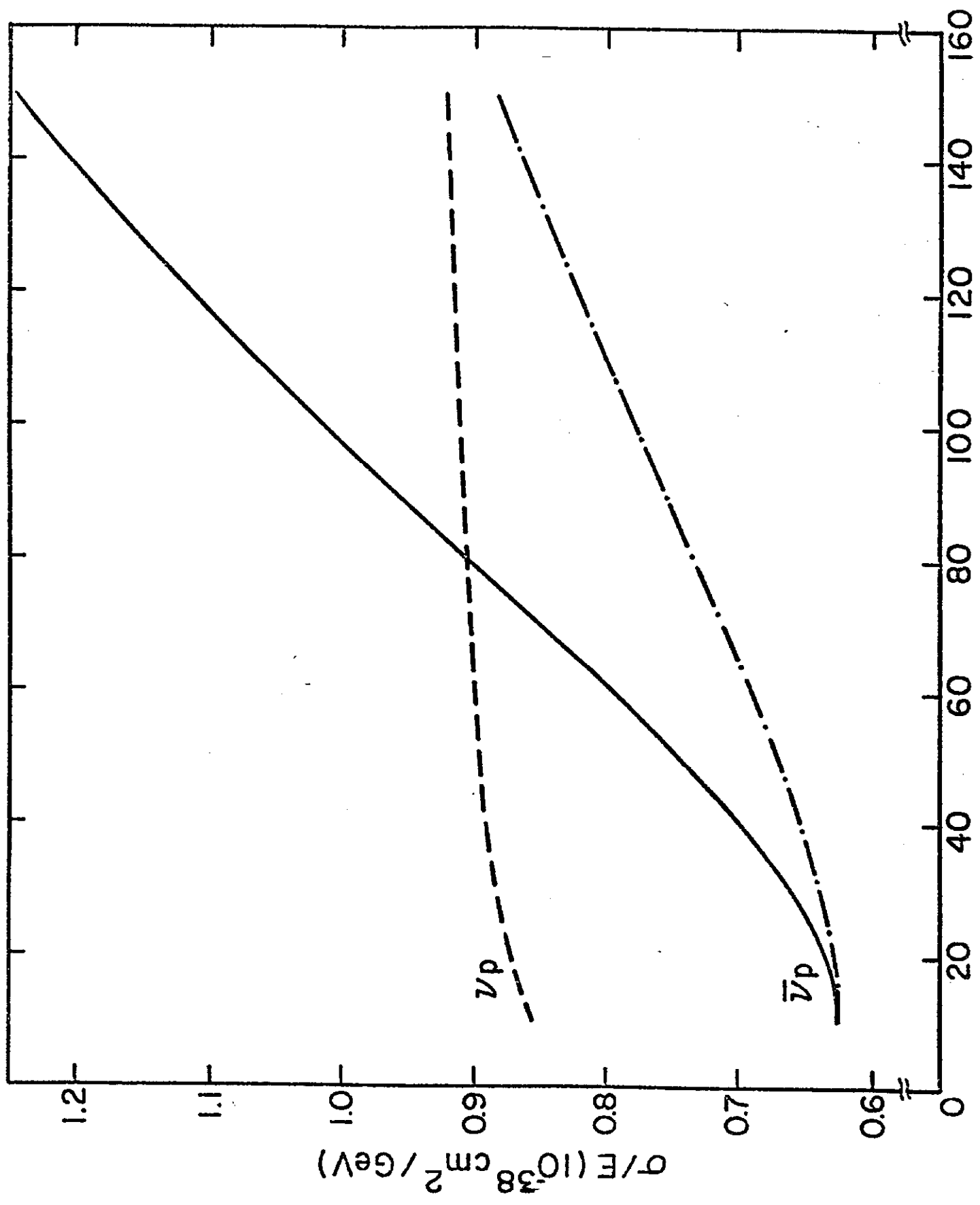


Fig. 32

F (GeV)

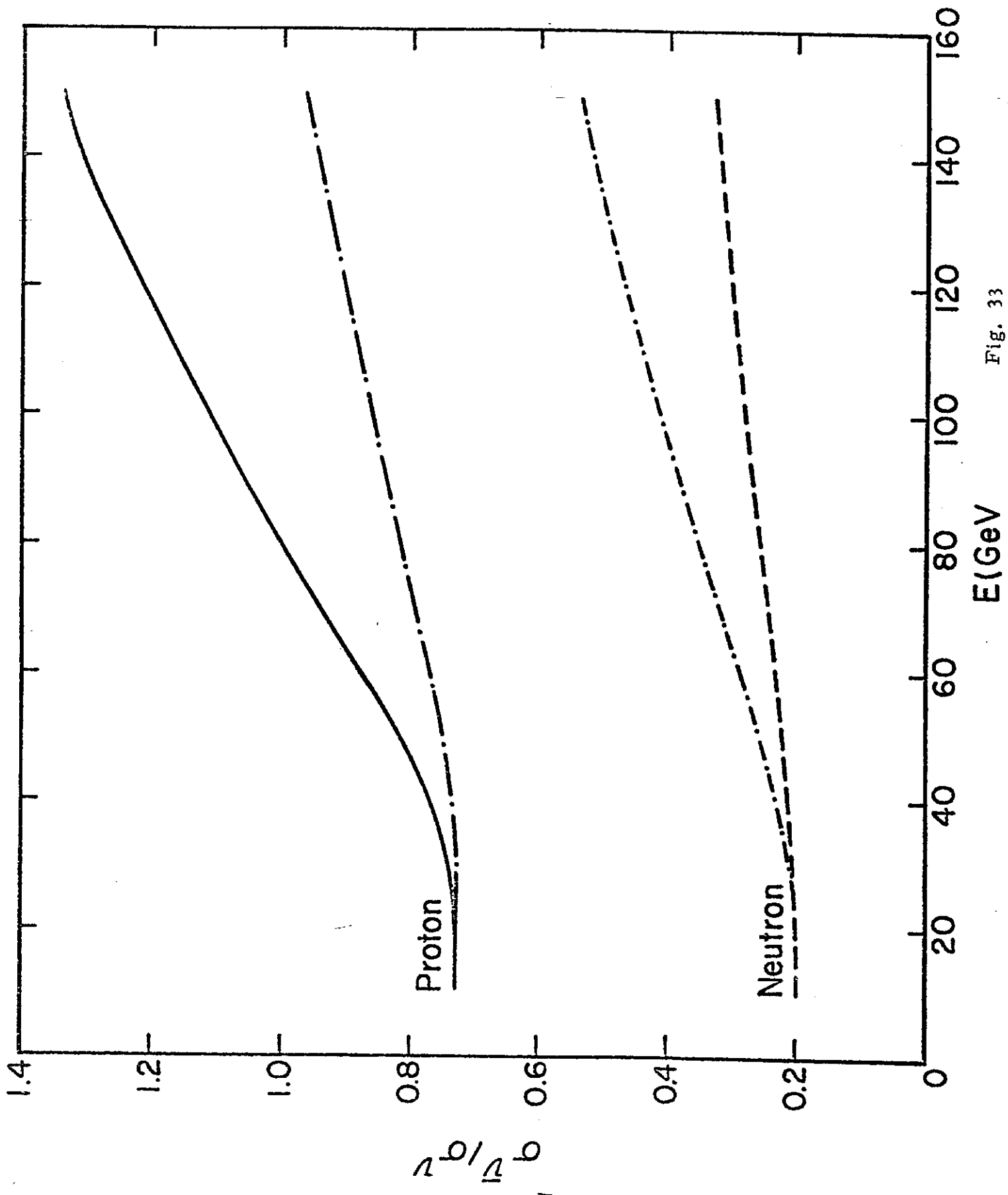


Fig. 33

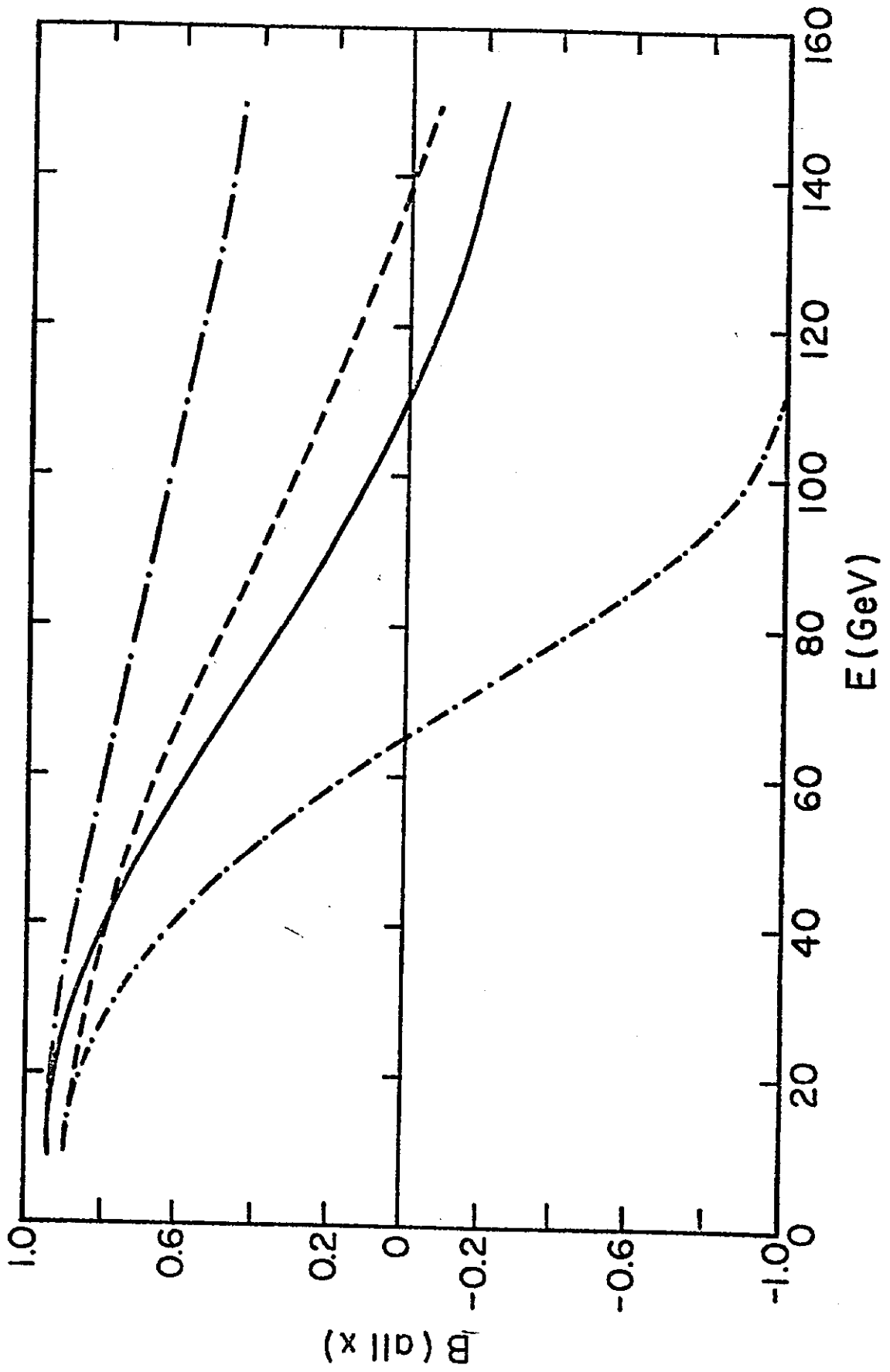


Fig. 34

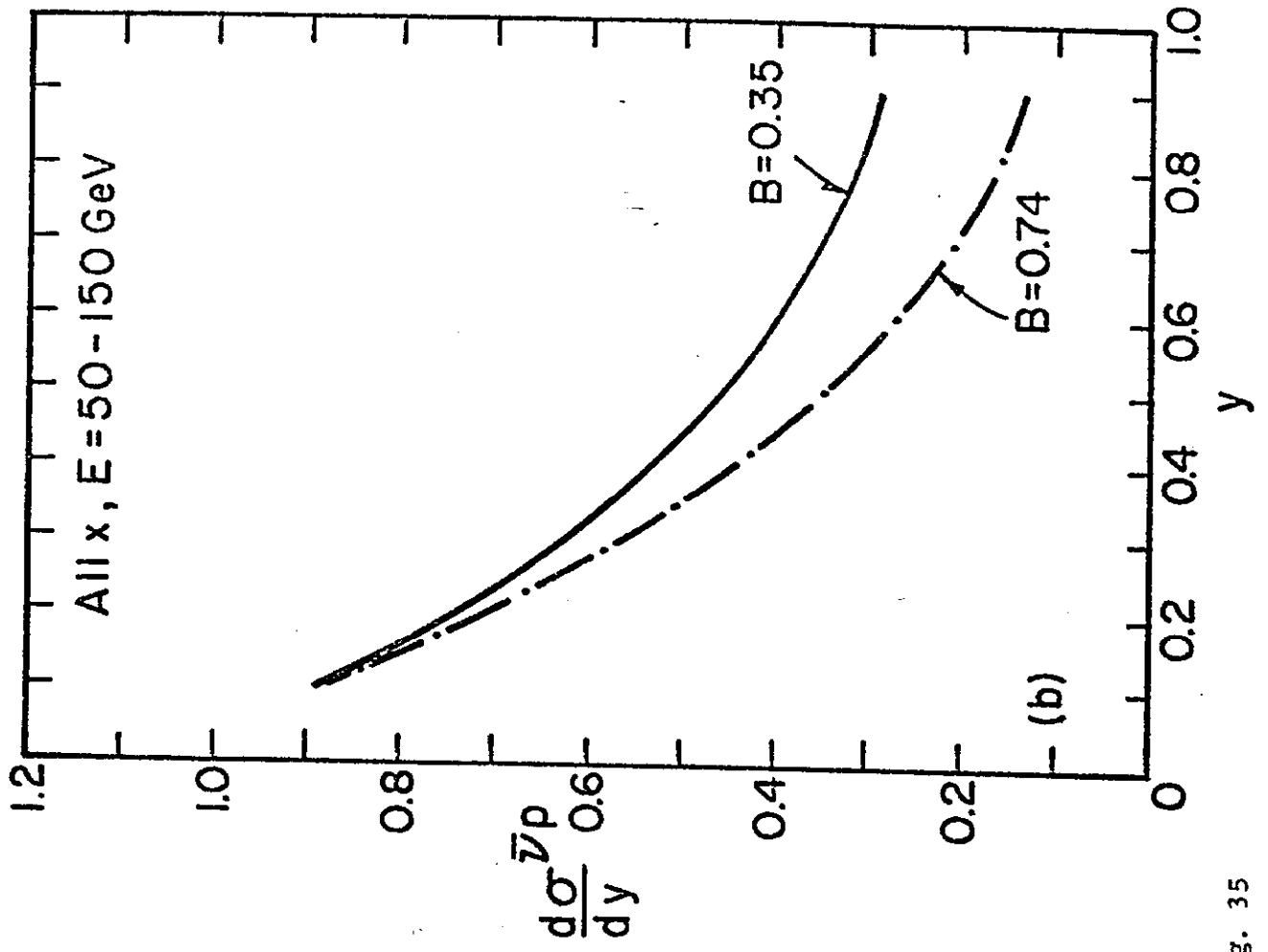
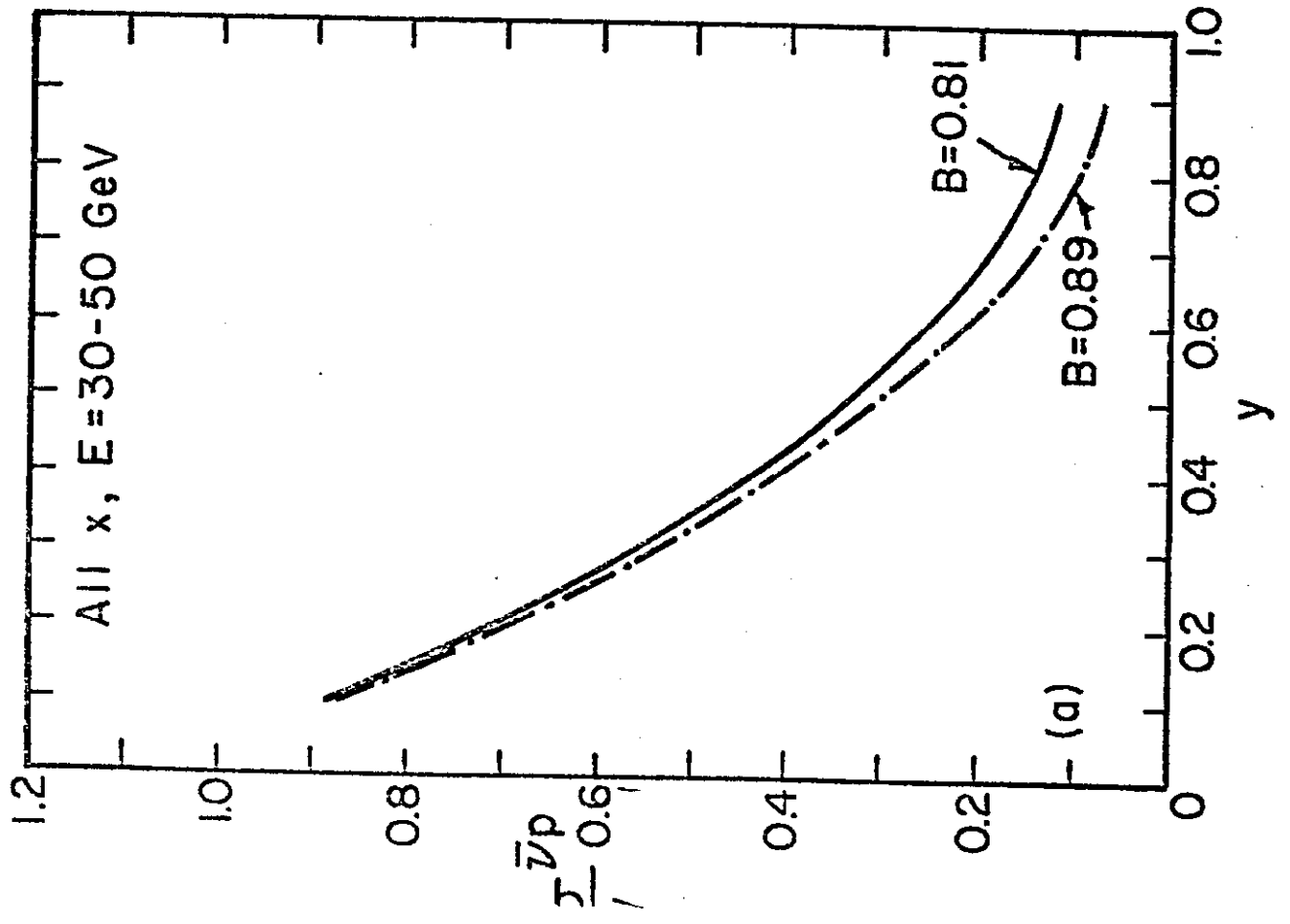


Fig. 35